THE UNIVERSITY OF

MICHIGAN

ENGINEERING COLLEGE INDUSTRY PROGRAM

Effect of Initial Velocity Distribution on Heat Transfer in Smooth Tubes

PETER HERMAN ABBRECHT

September 1956
IP-180

ANN ARBOR

THE UNIVERSITY OF MICHIGAN

INDUSTRY PROGRAM OF THE COLLEGE OF ENGINEERING

EFFECT OF INITIAL VELOCITY DISTRIBUTION ON HEAT TRANSFER IN SMOOTH TUBES

Peter Herman Abbrecht

This dissertation was submitted in partial fulfillment of the requirements for the degree of Doctor of Philosophy in the University of Michigan, 1956.

September, 1956

IP-180

ACKNOWLEDGEMENT

We wish to express our appreciation to the author for permission to give this thesis limited distribution under the Industry Program of the College of Engineering.

ACKNOWLEDGEMENTS

The author wishes to express his sincere appreciation to a number of individuals for their assistance during the course of this work and in particular to the following:

Associate Professor S. W. Churchill, chairman of the doctoral committee, for his continuous interest, encouragement, suggestions, and advice.

Professors D. L. Katz, A. M. Kuethe, H. A. Ohlgren, and Alex Weir for their suggestions and assistance.

Miss Anne Lampman for her assistance in the computational work.

The Department of Aeronautical Engineering of the University of Michigan for the use of their facilities for construction of hot-wire anemometers.

The Horace H. Rackham School of Graduate Studies of the University of Michigan for their grants of University Fellowships for the years 1952-54 and a tuition grant in 1955.

The Visking Corporation for their generous fellowship grant for the year 1954-55.

TABLE OF CONTENTS

TABLE OF CONTENTS (CONT.)

LIST OF TABLES

LIST OF FIGURES

LIST OF FIGURES (CONT.)

NOMENCLATURE

a = pipe radius, ft.

A' = constant in King's law equation.

B' = constant in King's law equation.

C_p = specific heat at constant pressure, Btu/lb °F.

C_f = local skin friction coefficient.

D = pipe diameter, ft.

f = friction factor, (sometimes function of).

f_{app} = local apparent friction factor = $\frac{-D}{2\rho(u_b)^2} \frac{dp}{dx}$.

G = mass flow rate, lb/hr sq ft.

g_c = conversion factor, 32.2 lb - mass ft/ lb - force sec^2.

h = heat transfer coefficient, $q/(t_w - t_b)$, Btu/hr ft^2 °F.

i = electrical current, amperes.

J = 778 ft - lb/Btu.

k = thermal conductivity, Btu/hr ft °F.

K = thermal diffusivity, $\frac{k}{\rho C_p}$

l = mixing length, ft.

L = length, ft.

Nu = Nusselt number, hD/k.

p = pressure, lb -force/sq. ft.

Pr = Prandtl number, $C_p \mu/k$

q = heat flux, Btu/hr sq ft.

q_ℓ = laminar heat flux, Btu/hr sq ft.

q_t = turbulent heat flux, Btu/hr sq ft.

Q = heat generation per unit length, Btu/hr ft.

r = radial distance, ft.

r_* = r/a.

R = electrical resistance, ohms.

R_a = wire resistance at air temperature, ohms.

R_o = wire resistance at °F, ohms.

Re = Reynolds number, D u_b/v.

Re_x = length Reynolds number, u_b x/v

S = distance between probe tips, ft.

t = temperature, °F.

t_b = mixed mean temperature, °F.

t_o = inlet temperature, °F.

t_s = stagnation temperation, °F.

t_w = wall temperature, °F.

u = mean axial velocity at a point, ft/sec.

u_b = average axial velocity, ft/sec.

u_m = maximum axial velocity, ft/sec.

u* = friction velocity, $\sqrt{\tau_o/\rho}$.

u^+ = dimensionless velocity, u/u*.

u' = root mean square of instantaneous velocity fluctuations in x direction.

U = ratio of mean local velocity to maximum velocity, u/u_m.

v = mean radial velocity toward wall, ft/sec.

W = weight rate of flow, lb - mass/ hr.

X = axial distance, ft.

y = distance from wall, inches.

y^+ = dimensionless distance from wall, u* y/v.

Z = dimensionless axial length, x/a, ft.

α = ϵ_c/ϵ_v, ratio of eddy diffusivities.

β = temperature coefficient of resistance, 1/°F.

γ = recovery factor.

ϵ_c = eddy conductivity, ft^2/sec.

ϵ_v = eddy viscosity, ft^2/sec.

Θ = dimensionless temperature $\frac{t - t_o}{t_w - t_o}$.

μ = viscosity, lb - force sec/ft^2.

ν = kinematic viscosity, ft^2/sec.

ρ = density, $lb_m/cu\ ft$.

τ = shear stress, lb - force / ft^2.

τ = laminar shear stress, lb - force/ft^2.

τ_t = turbulent shear stress, lb - force/ft^2.

$$\Phi = \int_0^{r_*} r_* U \frac{\partial \Theta}{\partial Z} d r_* .$$

ABSTRACT

The purpose of this study is to investigate the effect of initial velocity distribution on heat transfer to air flowing in a smooth tube. It is known that the geometric form of the inlet to a heat exchanger tube strongly influences the heat transfer coefficient in the inlet region. This effect is primarily due to the initial velocity distribution produced by the inlet. By measuring temperature and velocity profiles, and point heat transfer rates in the inlet region, it is hoped to gain a better understanding of the mechanism by which these effects occur.

Measurements were made for heat transfer to air flowing in a 1.52 inch inside diameter tube with the following geometric entrances: 1) a long tube which gave essentially fully developed turbulent flow, and 2) a bellmouth entrance which gave an initially flat velocity profile. Measurements were taken at distances of .453, 1.13, 1.75, 4.12, and 9.97 tube diameters downstream from the start of heating at Reynolds numbers of 15,000 and 65,000. Pressure drop measurements were also made in this region.

Longitudinal and radial temperature gradients, radial heat fluxes, and eddy diffusivities for momentum and heat transfer were computed from the measurements.

The ratio of eddy diffusivity for heat transfer to that for momentum transfer, α, was found not to be a function of length in the thermal inlet with fully developed flow. Over most of the tube cross-section the ratio was about 1.5. The ratio α was a function of length for the bellmouth inlet.

The radial heat flux was found to be essentially constant in the laminar and buffer zones and to vary linearly in the turbulent zone.

Pressure drop due to acceleration effects was found to be appreciable compared to wall friction losses in the bellmouth inlet.

It is concluded that theoretical analyses which postulate the same distribution of eddy conductivity in developing thermal boundary layers as for fully developed ones are valid for the case of fully developed hydrodynamic boundary layers in the thermal entrance region, but may be subject to large error when the hydrodynamic and thermal boundary layers develop simultaneously.

I. INTRODUCTION

Convective heat transfer to fluids flowing in circular tubes has been the subject of a large number of experimental and analytical investigations.

Until recently, by far the largest part of the research on heat transfer in pipes has been concerned only with the region far downstream from the pipe entrance where all effects due to inlet disturbances have vanished. Two factors have been responsible for this neglect of the consideration of inlet effects. In the first place, in most conventional tubular heat exchangers, the tubes are long enough so that the entrance region comprises only a small part of the total heat transfer area, and therefore has little effect on the heat transfer capacity of the unit as a whole. In the second place, because of the complexity of developing flow and temperature fields, mathematical treatment of the inlet region is difficult. The analysis is particularly complicated in the case of turbulent flow. Therefore, most of the early theoretical treatments of transfer processes in the inlet length, such as that of Graetz for heat transfer (19) and Schiller for momentum transfer (53), have been limited to laminar flow. However, the case of turbulent flow is by far the most important industrially.

Recent developments such as short tube nuclear reactors and aircraft heaters, in which most of the transfer area lies in the entrance region, have created a need for a more fundamental knowledge of the effect

of inlet conditions. The general impetus in the last few years in research in basic heat transfer phenomena has also heightened interest in the mechanism of heat transfer in the inlet region. Also, the advent of high speed mechanical and electronic computors has made numerical solution to several specific cases possible.

Data presented by Boelter (5) and others show that the heat transfer coefficient inside tubes directly downstream from a turbulence promoting inlet may be three times that obtained far downstream of the inlet where entrance effects have died out. This effect is probably due primarily to the initial velocity distribution and level of turbulence produced. For many cases, at least, the first factor is probably the most important. This is indicated by the fact that Boelter found in his work that the effect on the heat transfer coefficient of increasing the degree of turbulence by the addition of screens was negligible.

The purpose of this investigation is to study the mechanism by which the rate of heat transfer in turbulent flow in tubes is affected by the initial velocity distribution.

The fact that the initial velocity distribution influences heat transfer in the inlet region can be explained by a consideration of the hydrodynamic and thermal boundary layers. In all real (non-ideal) fluids flowing past a solid boundary, a boundary layer due to viscous shearing stress is present. The hydrodynamic boundary layer in the inlet length of a circular tube is shown in figure 1.

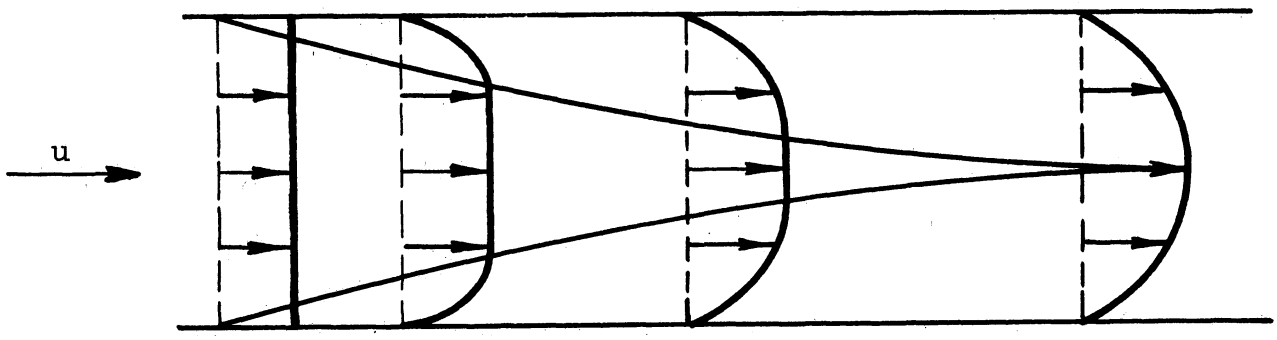

Figure 1. The Hydrodynamic Boundary Layer
in the Inlet Length of a Circular Tube

Here the fluid is considered to be moving with uniform velocity as it enters the tube. At the tube entrance there is a retardation of the fluid particles next to the wall because of frictional effects. A thin layer then exists in which the fluid velocity builds up from zero at the wall to the core velocity at the edge of the boundary layer. As the fluid moves down the tube, the thickness of the boundary layer gradually increases, until it merges at the center of the tube. There then exists the condition described as "fully developed flow." For a fluid with constant physical properties the shape of the velocity profile remains constant after fully developed flow has been attained. The above description is somewhat oversimplified since there is some change in the

shape of the velocity profile for a short distance downstream from the point where the boundary layer merges.

An analogous effect occurs when a fluid of uniform temperature flowing through a tube is suddenly subjected to a step change in wall temperature, as shown in figure 2.

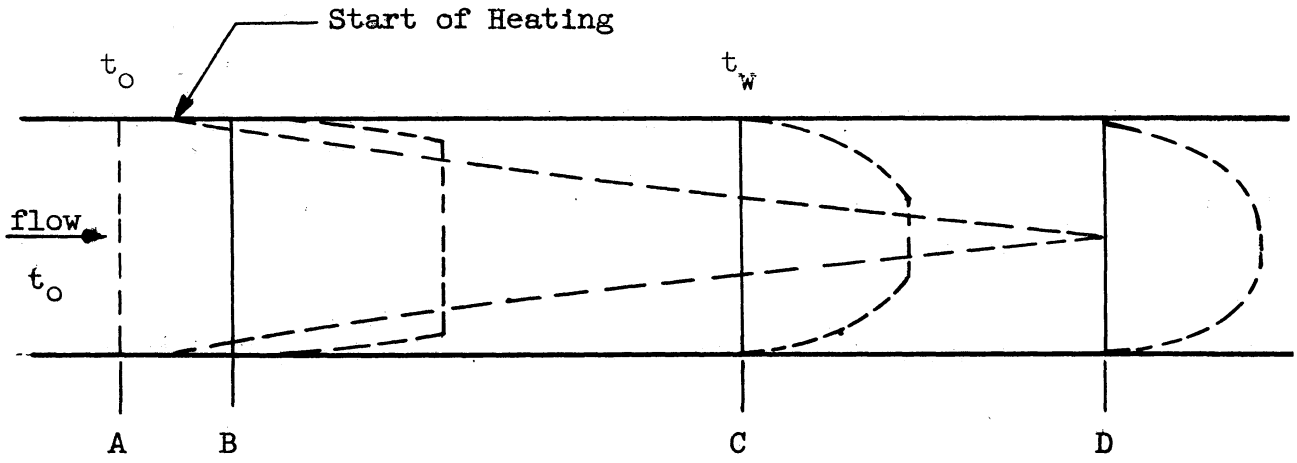

Figure 2. The Thermal Boundary Layer
after a Step Change in Temperature

The fluid and wall are initially at the same temperature t_o As the fluid enters the heated section the fluid particles next to the wall are heated. There is then a very thin layer in which the temperature decreases from t_w at the wall to t_o at the edge of the unheated core. At a sufficiently great distance down the tube the temperature boundary layer merges and the fully developed thermal boundary layer is attained. The distance required for the boundary layer to merge is known as the "thermal

inlet length." It is to be noted that with the boundary condition of constant wall temperature postulated here the shape of the temperature profile continues to change even after the thermal boundary layer becomes fully developed. If the heated tube were infinitely long, the fluid would emerge with a uniform temperature.

The above picture is also an idealized model, for a minute amount of heat might penetrate to the center even at B. This difficulty can be circumvented by defining the boundary layer as that layer bounded by the pipe wall in which the temperature increase over t_o is less than 2 % of $t_w - t_o$.

The thermal and hydrodynamic boundary layers may develop simultaneously, as when heating starts at the flow inlet; or the hydrodynamic boundary layer may be partially or fully developed at the point where heating starts.

As can be seen from figure 2, at a point in the fluid next to the step change in wall temperature, there is a finite temperature difference $t_w - t_o$ over an infinitesimal distance since the thermal boundary layer has not yet had a chance to develop. This implies that there is an infinite temperature gradient at this point. Since the heat flux at the wall is defined by:

$$q(x) = -k \left(\frac{\partial t}{\partial y}\right)_{y = 0} \qquad (1)$$

the heat flux at a step change in wall temperature would be infinite; and the heat transfer coefficient defined by:

$$h = \frac{q}{t_w - t_b} \tag{2}$$

would also be infinite.

Of course, in practice one does not obtain absolute step changes in temperature. However, very steep temperature gradients are obtained in the thermal entrance region and account for the much higher coefficients obtained there.

The temperature gradient is related to the velocity profile by the following partial differential equation which governs heat transfer in flow in a tube where both thermal and hydrodynamic boundary layers are developing.

$$u \frac{\partial t}{\partial x} + v \frac{\partial t}{\partial r} = \frac{\partial}{\partial x}\left[(K + \epsilon_c') \frac{\partial t}{\partial x}\right] + \frac{1}{r} \frac{\partial}{\partial r}\left[r(K + \epsilon_c) \frac{\partial t}{\partial r}\right] \tag{3}$$

Extensive experimental studies of the effect of two different initial velocity distributions upon heat transfer were made in this investigation. The first case was that where the velocity distribution is fully developed before heating begins. The second was that of uniform initial velocity distribution with both thermal and hydrodynamic boundary layers beginning at the same point. In both of these cases the boundary condition of uniform wall temperature was imposed.

The determination of temperature distribution and heat flux for these two cases has been accomplished by solving equation 3 after making certain assumptions.

One of these assumptions involves the functional relation for eddy conductivity ϵ_c. For the first case, this has been obtained by using the analogy between the transfer of heat and momentum, which states that the ratio of the eddy diffusivity for heat to that for momentum, α, is equal to unity. The eddy diffusivities for momentum (eddy viscosities) were obtained using generalized velocity distributions for turbulent pipe flow.

For the second case, either the analogy has been used or values of ϵ_c determined for fully developed flow and temperature fields have been considered to apply also to the developing boundary layer. Both these assumptions are particularly questionable for this case.

Values of α obtained in fully developed flow and temperature fields range from unity to 1.6, indicating that the analogy is not exactl correct. No data have been presented for eddy conductivities in the inlet region of a tube.

Other assumptions which must be made in the solution of equation 3 for the inlet conditions considered are the variation of heat flux radially (or $\frac{\partial t}{\partial x}$) and the form of the velocity distribution.

This investigation was made with the object of providing a better understanding of heat transfer in turbulent flow in inlet regions. By obtaining point temperature and velocity measurements the variation of such quantities as ϵ_c and ϵ_v, the radial heat flux, and temperature and velocity gradients were obtained as a function of radius and distance from the inlet.

This information should be of use in the prediction of the thermal transfer and temperature distribution in turbulent flow streams from a knowledge of the flow field and boundary conditions alone.

For this investigation, an apparatus was constructed to measure point heat transfer rates and temperature and velocity profiles within an air stream at varying distances downstream from the hydrodynamic inlet. Such data were obtained for a long tube entrance and a bellmouth entrance at Reynolds numbers of 15,000 and 65,000.

II. SURVEY OF PREVIOUS WORK

Empirical Correlations

An excellent review of the literature on turbulent heat transfer in tubes is given in "Heat Transmission" by McAdams (40). For design purposes empirical equations derived with the aid of dimensional analysis have found extensive application because of the ease and rapidity with which they may be used.

For fully developed flow in tubes dimensional analysis predicts the functional relationship:

$$\frac{hD}{k} = f\left(\frac{DG}{\mu}, \frac{C_p\mu}{k}\right) \qquad (4)$$

Dittus and Boelter (13) have presented the following equations for fully developed flow:

$$\frac{hD}{k} = .0243\ (Re)^{.8}\ (Pr)^{.4} \qquad \text{(heating)} \qquad (5)$$

$$\frac{hD}{k} = .0265\ (Re)^{.8}\ (Pr)^{.4} \qquad \text{(cooling)} \qquad (6)$$

For short tubes where entrance effects are important, the length to diameter ratio, $\frac{L}{D}$, must be included as one of the dimensionless groups in f of equation 4. From experiments of Burbach (6) in the range L/D = 10 to 400, Nusselt (44) concluded that h is proportional to $(D/L)^{1/18}$. He found this verified by experiments of Eagle and Ferguson (14) in about the same range.

Hausen (21) proposed the following relation which takes conditions in the intake region into account:

$$Nu = .116\,[(Re)^{2/3} - 125]\,(Pr)^{1/3}\,[1 + (\frac{d}{L})^{2/3}]\,(\frac{\mu_B}{\mu_W})^{0.14} \qquad (7)$$

where μ_B is the viscosity at bulk liquid temperature and μ_W the viscosity at tube wall temperature.

Experimental Investigations of Thermal Entry Length

The most extensive experimental investigations of heat transfer in the inlet region for turbulent pipe flow are those of Boelter, Young, and Iversen (5) and Hartnett (20). Boelter, et al., determined point heat transfer rates in the entrance region for a wide variety of hydrodynamic entrances, including long and short calming sections, bellmouths, orifices, and elbows. A steam jacket divided into a number of compartments along its length was used for heating, and heat transfer rates were determined from measurements of the amount of condensate from each compartment. For the long tube entrance the inlet region was found to vary from L/D of 10 at a Reynolds number of 27,000 to L/D of 15 at a Reynolds number of 53,000; for the bellmouth the inlet length was 9 L/D for Reynolds numbers between 26,000 and 56,000. For values of L/D greater than about five the average heat transfer coefficient could be approximated by the equation $h_{avg} = h_\infty\,(1 + P\,\frac{D}{L})$ where P is a constant for any given inlet.

Hartnett studied the flow of water and several oils in an electrically heated tube with a long calming section entrance. From heat-

flux and wall temperature measurements he calculated the Nusselt number at various distances downstream from the start of heating. His results are particularly valuable since they cover a wide range of Prandtl numbers. His results with water covered Prandtl numbers from 7 to 9 and Reynolds numbers from 16,900 to 89,200, while the oil runs covered Prandtl numbers from 61 to 480 and Reynolds numbers from 1580 to 46,600.

Al-Arabi and Davies (2) have studied several of the same entrances as Boelter, but used water as the fluid.

Cholette (7) utilized a small shell and tube heat exchanger so baffled that steam could be condensed in separate compartments to obtain average local coefficients of heat transfer in the inlet region. For an initially flat velocity distribution he found that the average Nusselt number was proportional to $(D/L)^{0.1}$

Heat transfer coefficients for the inlet region have also been reported by Aladyev (1) for water at uniform wall temperature; Johnson, Hartnett, and Clabaugh (29) for lead bismuth eutectic at uniform heat flux; and Hoffman (23) for molten sodium hydroxide at uniform heat flux.

Velocity Distributions

Careful experimental investigations of velocity distributions in fully developed turbulent pipe flow have been made by Nikuradse (43), Laufer (34), Deissler (10), and Sleicher (59). Measurements between parallel flat plates have been made by Laufer (35), Reichardt (48), and Corcoran et al., (9). Their results are applicable to pipe flow in the region close to the wall.

Various equations for correlating velocity distribution data have been proposed. These equations are described by Bakhmeteff (3), and Knudsen and Katz (30). The most commonly used correlation for turbulent velocity distributions near the wall is the Nikuradse-von Karman universal velocity distribution (30). In a review of Nikuradse's data, Ross (50) shows that for the region $0 < \frac{r}{a} < .85, u^+$ is not a single-valued function of y^+, but depends also on Reynolds number. For the inner 85% of the pipe radius he suggests the data be correlated by plotting $(u_{max} - u)/u^*$ against $1 - \frac{y}{r}$.

Rothfus and Monrad (51) have presented a modification of the u^+, y^+ relationship which does result in a unique correlation of the main stream velocity distribution in smooth tubes and extends the correlation to the case of flow between parallel flat plates.

Data for velocity distributions in the inlet region for the case of uniform initial velocity distribution have been reported by Deissler (10) and Weissberg (62). Both authors reported their values as u/u_{max} as a function of r/a, without attempting a general correlation. Ross (50) has recently published an analytical solution for the turbulent boundary-layer flow in the entrance region of a pipe.

Eddy Diffusivities

The relations for shearing stress and heat flux in laminar flow are:

$$\tau_\ell = \frac{\rho\nu}{g_c} \frac{\partial u}{\partial y} \qquad (8)$$

$$q_{\ell} = -k \frac{\partial t}{\partial y} \tag{9}$$

In an analogous manner, for turbulent flow one may write:

$$\tau = \frac{\rho}{g_c} (\nu + \epsilon_{\nu}) \frac{\partial u}{\partial y} \tag{10}$$

$$q = -\rho C_p \left(\frac{k}{\rho C_p} + \epsilon_c\right) \frac{\partial t}{\partial y} \tag{11}$$

where the second terms in the brackets on the right account for the contributions of turbulent action to the transfer process. Equations 10 and 11 may be considered to be the defining equations for the eddy diffusivity for momentum transfer and heat transfer respectively.

Reynolds (49) suggested that momentum and heat in a fluid are transferred in the same way and that $\epsilon_v = \epsilon_c$.

Prandtl (47) proposed a theory for turbulent heat and momentum transfer based on the concept of mixing length. He postulates a model (figure 3) in which a turbulent eddy travels from one layer of fluid at y through a distance ℓ (the mixing length) to another layer $(y + \ell)$ of different velocity and temperature. The eddy is considered to retain the mean temperature and velocity of the original layer during its flight and to dissipate them into the second layer when it arrives there.

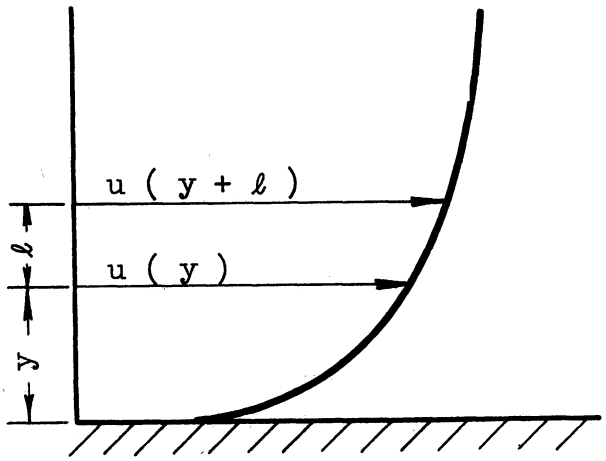

Figure 3. Portion of Turbulent
Velocity Profile Showing Mixing Length

The difference between the eddy's old and new velocity is $u_m(y + \ell) - u_m(y)$ or approximately $\frac{\partial u}{\partial y}$. The mass exchange across plane a per unit area due to eddy exchange is equal to ρv. Prandtl makes v to be of the same order of magnitude as the difference in velocities u_m $u_m(y+\ell) - u_m(y)$. The shear between the layers due to eddy motion is the product of the mass exchange per second and the difference in velocities of the two layers:

$$\tau_t = \frac{\rho}{g_c} \left(\ell^2 \frac{du}{dy}\right) \frac{du}{dy} \tag{12}$$

a similar analysis for heat transfer yields:

$$q_t = C_p \rho \left(\ell^2 \frac{du}{dy}\right) \frac{dt}{dy} \tag{13}$$

If ϵ_ν is substituted for $\ell^2 \frac{du}{dy}$ in (12) and ϵ_c for $\ell^2 \frac{du}{dy}$ in (13), we obtain the expressions for turbulent transfer in (10) and (11).

Jenkins (27) modified the mixing length theory by allowing the eddy to transfer some of its heat and momentum during its time of travel over the mixing length. His results predict that the ratio of eddy conductivity to eddy viscosity, α, should be a function of the turbulence and physical properties of the system, rather than being equal to unity as in Prandtl's analysis. In particular, one would expect α to vary in cases where the turbulent flow field is still developing such as in the inlet region of tubes or behind immersed bodies.

Experimental values for eddy diffusivities for momentum and heat transfer have been reported for several different flow systems. Reichardt (48), using measurements of velocity and temperature profiles for pipes by Lorenz (37) and for flat plates by Elias (16), computed values of α of 1.4 and 1.5 respectively.

From their experimental velocity and temperature distributions in a smooth heated tube, Seban and Shimazki (56) determined a maximum value of 1.2 for α ocurring in the region adjacent to the buffer layer.

Isafoff and Drew have determined eddy diffusivities for momentum and heat in turbulent flow of mercury. They found that the ratios $\frac{\epsilon_\nu}{(\epsilon_\nu)_{max}}$ and $\frac{\epsilon_c}{(\epsilon_c)_{max}}$ are functions of radius but not Reynolds number. For the maximum values of ϵ_ν and ϵ_c at a given Reynolds number, they obtained the relations:

$$(\epsilon_\nu)_{max} = 6.3 \times 10^{-5} (Re)^{.83} \qquad (14)$$

$$(\epsilon_c)_{max} = 29 \times 10^{-8} (Re)^{1.29} \qquad (15)$$

and present their data in a generalized plot of $\frac{\epsilon_c}{\epsilon_\nu}(Re)^{-.46}$ vs. $\frac{r}{a}$

Corcoran, et al., (19) computed eddy diffusivities between heated flat plates. Because of some uncertainty in their data as to the variation of α with radial position, they present average values of α for the whole channel as a function of Reynolds number. These data indicate an increase in α with Reynolds number. However, in a more recent paper (8) they report that for a slightly different level of turbulence the reverse trend appears to be true at Reynolds numbers above 20,000.

Careful temperature measurements of Sheppard (58) made with the object of establishing the ratio between ϵ_c and ϵ_ν, yield a value of about 1.6 for this ratio. Other authors who have reported eddy diffusivities for tube flow are Sleicher (59) for heat and momentum, and Deissler (12) for momentum.

For flow behind heated cylinders it appears that the value of α is 2 (61). Prandtl (46) suggests that this difference between the value of α in boundary layer flow and that in free turbulence may be due to a difference in the orientation of the axis of the eddies with respect to the direction of flow.

Analytical Solutions for Heat Transfer in Pipes

The energy equation for a fluid of constant properties in turbulent flow in the entrance region of a smooth pipe, neglecting heating

due to pressure changes and frictional dissipation, is (18)

$$\frac{\partial}{\partial x}\left[(K + \epsilon_c')\frac{\partial t}{\partial x}\right] + \frac{1}{r}\frac{\partial}{\partial r}\left[r\,(K + \epsilon_c)\frac{\partial t}{\partial r}\right] = u\frac{\partial t}{\partial x} + v\frac{\partial t}{\partial r} \qquad (3)$$

where the prime mark indicates that the diffusivities in the x and r directions are not necessarily equal.

In the solution of this equation the first term on the left is generally neglected, since the amount of heat transferred longitudinally by conduction is small compared to that transferred by flow. This assumption appears to be validated by the analyses of Deissler (12) and Poppendiek (45). At a Reynolds number of 21,000 Deissler found the ratio of axial conduction to bulk transport to be .008 at x/D = 0.8 and .002 at x/D = 3.1.

For fully developed turbulent pipe flow the mean radial velocity, v, is equal to zero and the second term on the right vanishes. Equation 3 then becomes:

$$\frac{1}{r}\frac{\partial}{\partial r}\left[r\,(K + \epsilon_c)\frac{\partial t}{\partial r}\right] = u\frac{\partial t}{\partial x} \qquad (16)$$

Several solutions to equation 16 have been obtained for the case of fully developed thermal and hydrodynamic boundary layers. Martinelli (39), Lyon (38), and Deissler (11) considered the case of constant heat flux at the wall, for which $\frac{\partial t(r)}{\partial x} = \left(\frac{\partial t}{\partial x}\right)_b$=constant. They based their analysis on the analogy between heat and momentum transfer and used $\alpha = 1$ in their numerical calculations.

Martinelli assumed that u is a constant and equal to the mean velocity. On this basis he used a linear distribution of heat flux

radially, except in the laminar and buffer layers, where he assumed the heat flux equal to that at the wall. He used the generalized von Karman-Nikuradse velocity distributions to determine eddy viscosity.

Lyon and Deissler retained u as a function of r and integrated the equation numerically. Lyon used the smoothed data of Nikuradse for his determination of u and ϵ_ν, while Deissler developed an empirical equation for ϵ_ν from his velocity data. In his solution the heat flux is considered constant across the tube.

Seban and Shimazaki treated the case of fully developed velocity and temperature distributions with constant wall temperature. They assumed that a generalized temperature distribution which is invariable in the direction of flow exists such that $\frac{\partial}{\partial x}\left(\frac{t_o - t}{t_o - t_b}\right)=0$. Momentum diffusivities for the turbulent core were obtained from the Prandtl-Nikuradse velocity distribution. Numerical solutions were obtained by use of an iterative method.

Latzko (33) obtained analytical solutions for heat transfer in the entrance region for three cases: (1) hydrodynamic and thermal states fully established, (2) hydrodynamic state fully established, uniform initial temperature distribution, (3) uniform initial temperature and velocity distributions. Using Prandtl's and von Karman's equation for shearing stress and velocity distribution and the equivalence of eddy diffusivities for momentum and heat transfer, he wrote equation 16 as follows:

$$\frac{\partial}{\partial r}\left[r\left(\frac{a^2 - r^2}{2a}\right)^{6/7}\frac{\partial T}{\partial r}\right] = M\, r\left[1 - \left(\frac{r}{a}\right)^2\right]^{1/7}\frac{\partial T}{\partial x}$$

where $M = \frac{8}{7} \frac{u_b^{1/4} (2a)^{3/28}}{.199\, \nu^{1/4}}$. By a method of approximation he obtained a three term solution for case (1) which also applies to case (2) when x approaches ∞ . For the third case he used an integral method for computing boundary layer buildup. Boelter et al., (5) have succeeded in simplifying Latzko's equations considerably.

Deissler (12) has also obtained a solution for the case of initially uniform temperature and velocity distributions using integral methods for computing velocity and temperature profiles. He assumes that expressions derived for eddy diffusivities in fully developed boundary layers apply also to developing boundary layers. Further assumptions included in his analysis are that $\alpha = 1$ and that variations of shear stress and heat flux across the flow and thermal boundary layers have a negligible effect on velocity and temperature distributions.

Berry (4) and Sleicher (59) have obtained solutions of equation 16 for the thermal inlet region by the method of separation of variables. Sleicher obtained numerical solutions for the case of fully developed flow with a step change in temperature by means of an electronic analog computor.

Sanders (52) has obtained a general turbulent flow solution for pipe entrance regions with uniform wall temperature by transforming the turbulent core to a laminar core of equivalent thermal resistance. Levy (36) presents a method by means of which transient heat conduction solutions can be used to determine temperature distribution of fluids

flowing in pipes, annuli, and between flat plates. Poppendiek and Harrison (45) have reviewed several pipe solutions that are not limited to an established temperature distribution.

III. APPARATUS

In this chapter is described the equipment which was constructed to obtain temperature and velocity profiles, point wall heat transfer rates, and pressure drop data in the hydrodynamic entrance region. Discussion of the hot-wire instrumentation is deferred till Chapter IV in order to make the discussion of experimental procedure more readily understandable.

The hydrodynamic entrances chosen for study were (1) a long straight tube which produced essentially fully developed turbulent flow and (2) a bellmouth entrance which gave a uniform initial velocity distribution.

Figures 4 and 5 show photographs of the apparatus with the long tube and bellmouth in place. A flow diagram of the apparatus is shown in figure 6. The components of the system may be classified into six divisions: air supply filtration and regulation, hydrodynamic entrance, heating section, calorimeter, traversing mechanism, and exhaust section.

The air from the supply main, after filtration, passes through an entrance section in which the initial velocity profile is established. It then passes through a heated tube where the temperature profile is developed and then through the calorimeter, where measurements of thermal flux and temperature and velocity profiles are made. In order to investigate the thermal and hydrodynamic boundary layers at different distances from the inlet, several interchangeable heating tubes of different

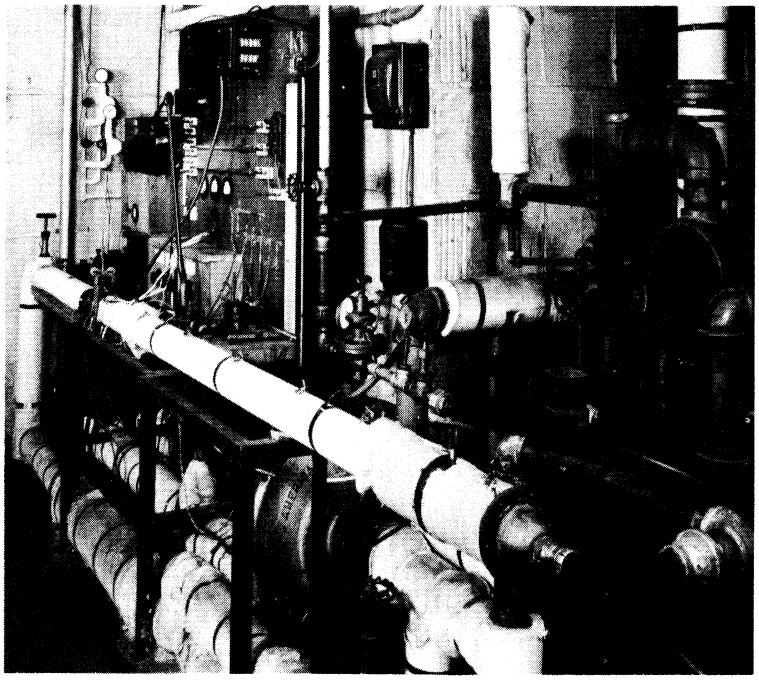

Figure 4. Experimental Apparatus with Long Tube Entrance

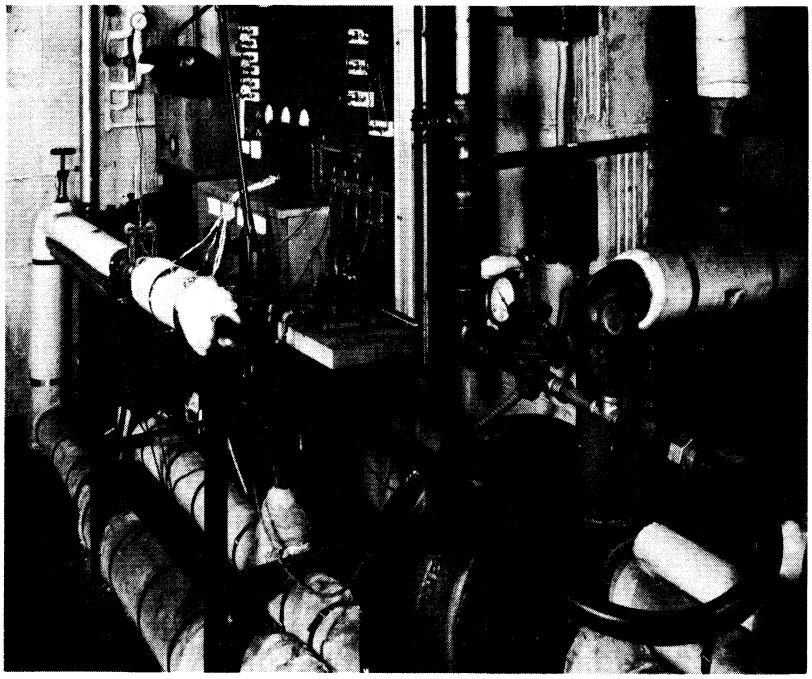

Figure 5. Experimental Apparatus with Bellmouth Entrance

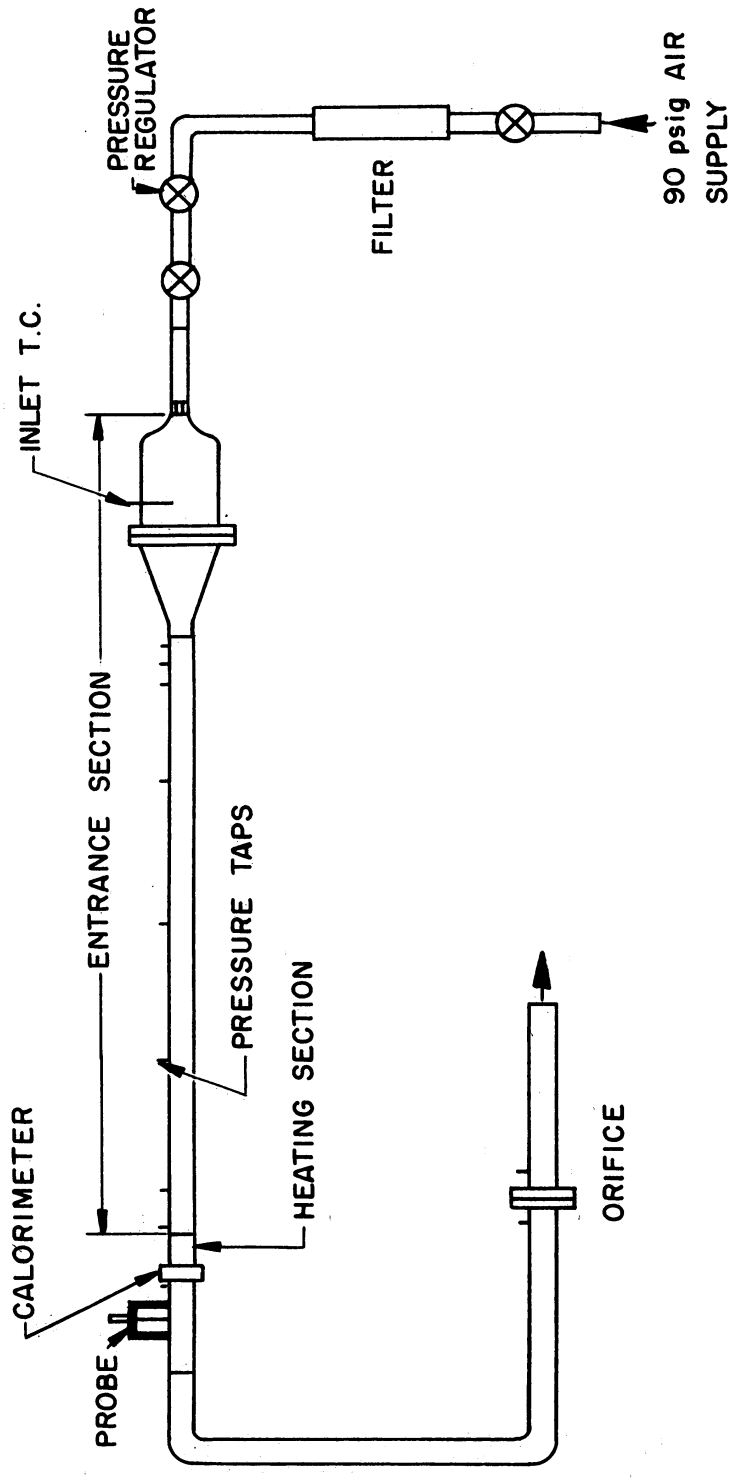

Figure 6
Flow diagram of apparatus

length were used. From the calorimeter the air flowed through an exhaust section in which the flow rate was determined by an orifice meter, after which it was vented to the outside of the building. The various components of the flow system are described below.

Air Supply

Air from the 90 psig laboratory supply main was passed through a cylindrical filter containing screens, glass wool, cotton wool, and activated carbon. A pressure control regulator downstream from the filter was used to maintain a constant line pressure at a point ahead of the final throttling valve. By maintaining a constant pressure at the inlet of the test section a constant flow rate was obtained, since differences in air density in the test section during a run due to changes in atmospheric pressure and temperature were negligible. After throttling, the air was conducted to the test section in a one-inch flexible hose. This arrangement permitted entrance sections of different lengths to be installed without complicated changes in piping.

Hydrodynamic Entrances

1) Bellmouth

To remove turbulence effects and non-symmetry in flow generated by the pressure regulating system and hose, a calming chamber was placed before the bellmouth. The hose from the throttling valve was coupled to a diverging nozzle which expanded the area for flow up to the four inch diameter of the calming section. The calming chamber consisted of an eight inch length of four inch diameter Carlon pipe.

A small electrical heater consisting of two layers of 30 gage enameled constantan wire criss-crossed on a plastic disk was placed at the entrance of the calming section. The purpose of this heater was to control the temperature of air entering the test section, primarily for probe temperature calibration as will be described below.

Power input to the heater was regulated with a Powerstat auto-transformer. The capacity of the heater was such that it was possible to raise the temperature of the incoming air by about 10°F at the highest flow rate. Because of the small thermal capacity of the fine wire, temperature changes in response to changes in heater power were very rapid and fine control was possible.

Two 1/16-in. mesh monel screens were placed in the calming section downstream from the heater. The purpose of these screens was to break up any large eddies that might still be present and to smooth the temperature distribution produced by the preheater. Available correlations for the decay of turbulence behind screens (32) indicate that most of the fine scale turbulence produced by the screens would be dissipated before the fluid left the calming chamber.

A thermocouple to measure the temperature of air entering the test section was placed in the calming section downstream of the last screen. The couple was placed in a thermal well which consisted of a piece of 3/32-in. stainless steel tubing which extended to the center of the chamber. To prevent disturbance of the initial velocity profile, the well was withdrawn during the taking of velocity and temperature profiles.

The bellmouth entrance was flanged directly to the calming section. It consisted of a converging nozzle machined from aluminum such that the inside diameter was reduced from 4 to 1.520 inches in a length of about 5 inches. Because of the system of flanging used, it was necessary that the nozzle be constructed with a straight run $1\frac{1}{2}$ inches long at its outlet end. This is somewhat unfortunate, since the hydrodynamic boundary layer thus starts building up slightly before heating begins. However, since there is some boundary layer buildup in the converging portion of the nozzle, the complication introduced is only a matter of degree.

Preliminary investigations of velocity and temperature profiles both with and without the calming section preheater in operation showed that the nozzle produced uniform temperature and velocity fields except for a thin boundary layer next to the wall.

Besides its use as a distinct entrance, the bellmouth preheater combination was also installed upstream of the long tube entrances in all runs in which it was used. The purpose for this was to insure a uniform and definable velocity distribution before the long tube entrance.

2) Long Tube Entrance

The long entrance consisted of a 66 inch long thick-walled copper pipe 1.520 inches inside diameter and 1.900 inches outside diameter. This length of 43.5 L/D was sufficient to give essentially fully developed turbulent flow. The required values usually recommended for attaining fully developed turbulent pipe flow vary from 50 to 100 pipe diameters. No set

value can be determined, however, for the critical L/D depends on the smoothness of entry as well as the Reynolds number. Velocity distributions taken at various distances downstream from the long tube entrance showed that flow was fully developed near the wall, although there was still some development occuring in the center portion of the tube.

The long tube entrance was also equipped with pressure taps at distances of 1, 3, 5, 15, 30, 44.5, 61, and 65 inches from the starting end. Pressure taps consisting of 1 inch lengths of thick walled 1/8 inch O. D. stainless steel hypodermic tubing were soft soldered to the copper tube.

The pressure tap holes were formed by first drilling a 1/32 inch hole through the copper tube wall, and then counterboring partway through from the outside to form a hole into which the stainless steel tubing could be driven before soldering. Burrs on the inside of the tube were removed by the honing process described below. To reduce the possible influence of one static hole upon the one downstream from it, azimuthal positions of the holes were staggered on two different generating lines of the pipe located about ten degrees apart.

Heating Sections

(1) Steam Jackets

Four different heating sections with lengths of 1.025, 1.975, 3.540, and 14.45 inches were used to obtain different heated L/D's. Only one of these sections was used at a time. Each section was machined from the same dimension pipe as the long tube entrance.

For the longer heating sections , steam appeared to be the most satisfactory medium. This choice was based on the fact that with condensing steam the outside coefficient would be on the order of several thousand while the inside coefficient would be about one-hundredth as large. Thus the inside coefficient would be controlling,and little longitudinal temperature gradient would be expected along the tube.

The two longest heating sections consisted of steam jackets constructed as shown in figure 7. Copper rings 1/8 inch thick were machined so that they would slip over the thickwalled copper pipe and fit inside the outer jacket, which was made from standard three inch copper pipe. The steam jackets were assembled with solder. One-eighth inch brass nipples were soldered to the jacket to provide a steam inlet, condensation outlet, and a tap for a manometer line.

Five thermocouple holes were drilled in each jacket, two in the upstream end and three in the downstream end. The holes were .020 inches in diameter and drilled at an angle so that they came within .020 inches of the inside wall at a point about 1/4 inch from the end of the jacket. Thirty-six gage chromel constantan thermocouples were inserted to the depth of the holes and secured with porcelain cement. The purpose of these thermocouples was to estimate the degree of uniformity of the wall temperature distribution both radially and longitudinally.

All thermocouples used in the apparatus were made from 36 gage chromel constantan wires. The two wires were twisted together and then

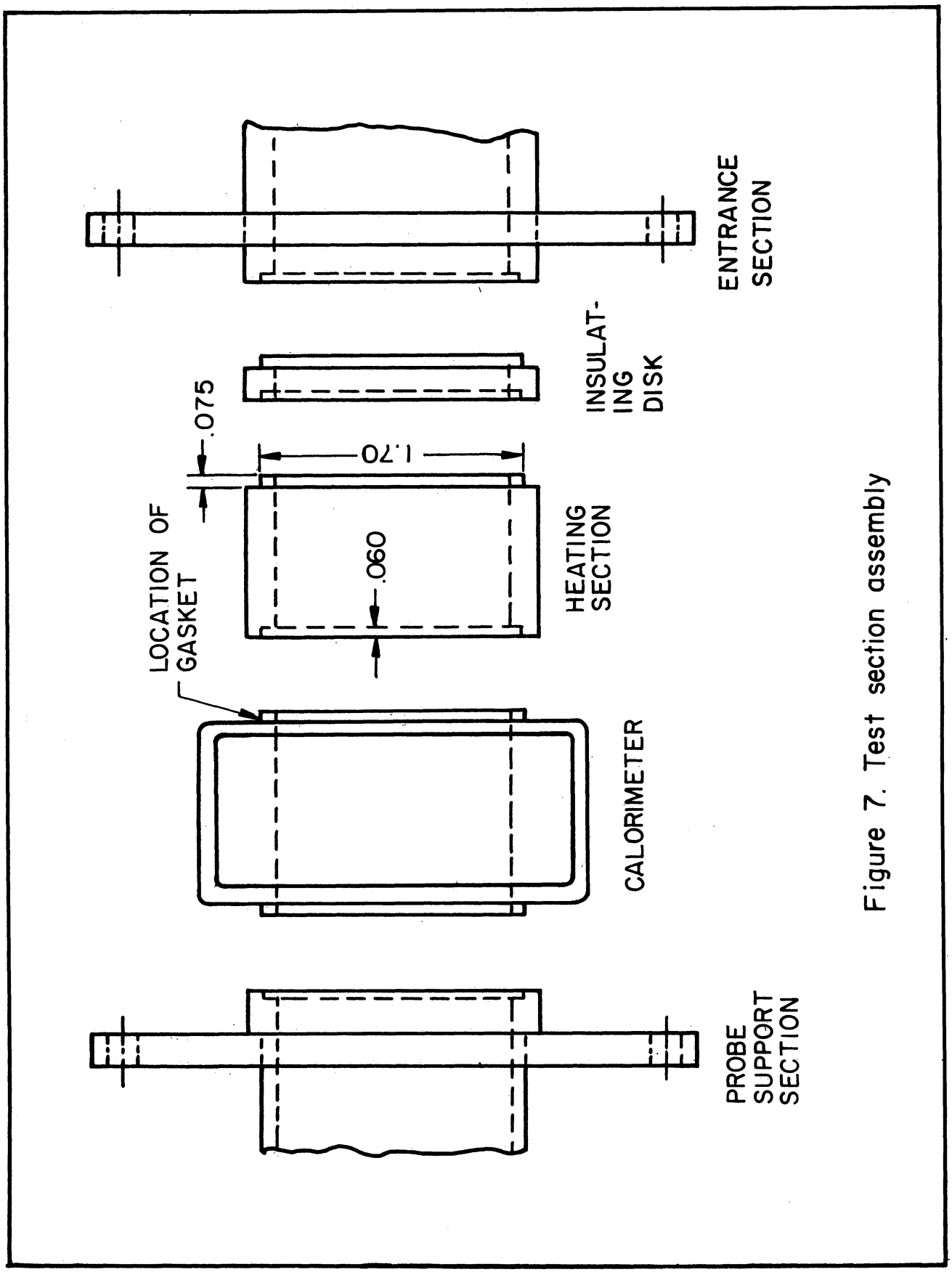

Figure 7. Test section assembly

fused in an acetylene flame. The length of the bead was trimmed to about .02 inches and the tip painted with microstop electroplating lacquer.

The thermocouple cold junction was immersed in purified kerosene in a thin glass tube which was placed in melting ice in a well-insulated thermos bottle.

The thermocouple and cold junction leads entered a well insulated wooden box which was lined with copper to assure its being isothermal. For thermocouples in the heating-lengths this connection was made by multi-conductor connectors so that only the heating length being used was connected. The box housed four Leeds and Northrup 2-pole, 12-position selector switches, type 31-3.

Copper wires connected the switches to a Leeds and Northrup type K-2 potentiometer. The error signal from the potentiometer was fed to a Liston-Becker model 14 D. C. breaker amplifier, whose output was fed to a Brown Electronik potentiometer used as an indicating galvanometer. It is estimated that the precision of temperature measurement was about .03°F.

Two thermocouples were calibrated in a constant temperature bath against a platinum resistance thermometer calibrated by the Bureau of Standards. A calibrated Leeds and Northrup Mueller bridge was used to measure the thermometer's resistance. The thermocouple calibration is shown in figure 35 . It agrees closely with that given by General Electric (17) for their chromel-constantan couples.

The rest of the thermocouples in the apparatus were then calibrated against the standardized couples under isothermal conditions.

Steam from the 120 psig supply main was throttled down in three stages to the pressure in the jacket. Since the desired wall temperatures were usually in the range of 100 to 110°F, corresponding to saturation pressures of 2 to 2.6 inches mercury, it was necessary to exhaust the condensate under vacuum. This was accomplished by a vacuum pump drawing through an ice trap and then a dry ice trap. An air bleed was provided on the pump as a means of fine pressure adjustment. At the low steam flow rates required, there was a tendency toward surging due to accumulation of condensate in the supply lines. This was overcome by drawing a considerable amount of vapor through the steam jacket and condensing it in the ice trap. The total amount of steam condensed during a six hour run usually amounted to about a gallon.

(2) Electrically Heated Sections

Because of the difficulties involved in controlling minute quantities of steam, electrical heating was used on the two shortest heating sections. The outer side of the thick walled copper pipe was painted with electroplating enamel and then wrapped with tissue paper to provide a non-conducting surface. The insulated pipe was then wound with 1/8 inch wide chromel ribbon with about 1/16 inch spacing between turns. Heating current was supplied by an adjustable autotransformer operating from a 220 volt source which was smoothed by a Sola constant voltage transformer.

Thermocouples were located at the same positions as in the steam jackets, except that with the electrical heaters it was possible to drill the holes perpendicular to the tube wall rather than at an angle.

Calorimeter

The details of construction of the calorimeter are shown in figure 8. Essentially it consisted of a one inch segment of thick-walled copper pipe, electrically heated by a closely wound 1/8 inch wide by .0126 inch thick chromel ribbon and surrounded by a heated guard to prevent external heat losses. The dead air space between calorimeter and guard was filled with loosely packed cotton to reduce convection. The calorimeter segment and guard, also of copper, were electrically insulated from their resistance windings as described above for the electrical heating sections. The outside of the guard was wrapped with 36 gage chromel wire and heated with current from an Adjustavolt autotransformer. The calorimeter and guard heater resistances were approximately 1.35 and 140 ohms respectively.

The guard heater was insulated thermally from the adjacent sections of the guard by disks of Continental-Diamond grade xx-13 paper-base laminated phenolic plastic (thermal conductivity approximately .25 BTU/hr ft^{o}F.) The thermal expansion coefficient of this material is almost identical to that of copper, thereby reducing the possibilities of unequal expansion. The calorimeter segment, plastic disk, and guard

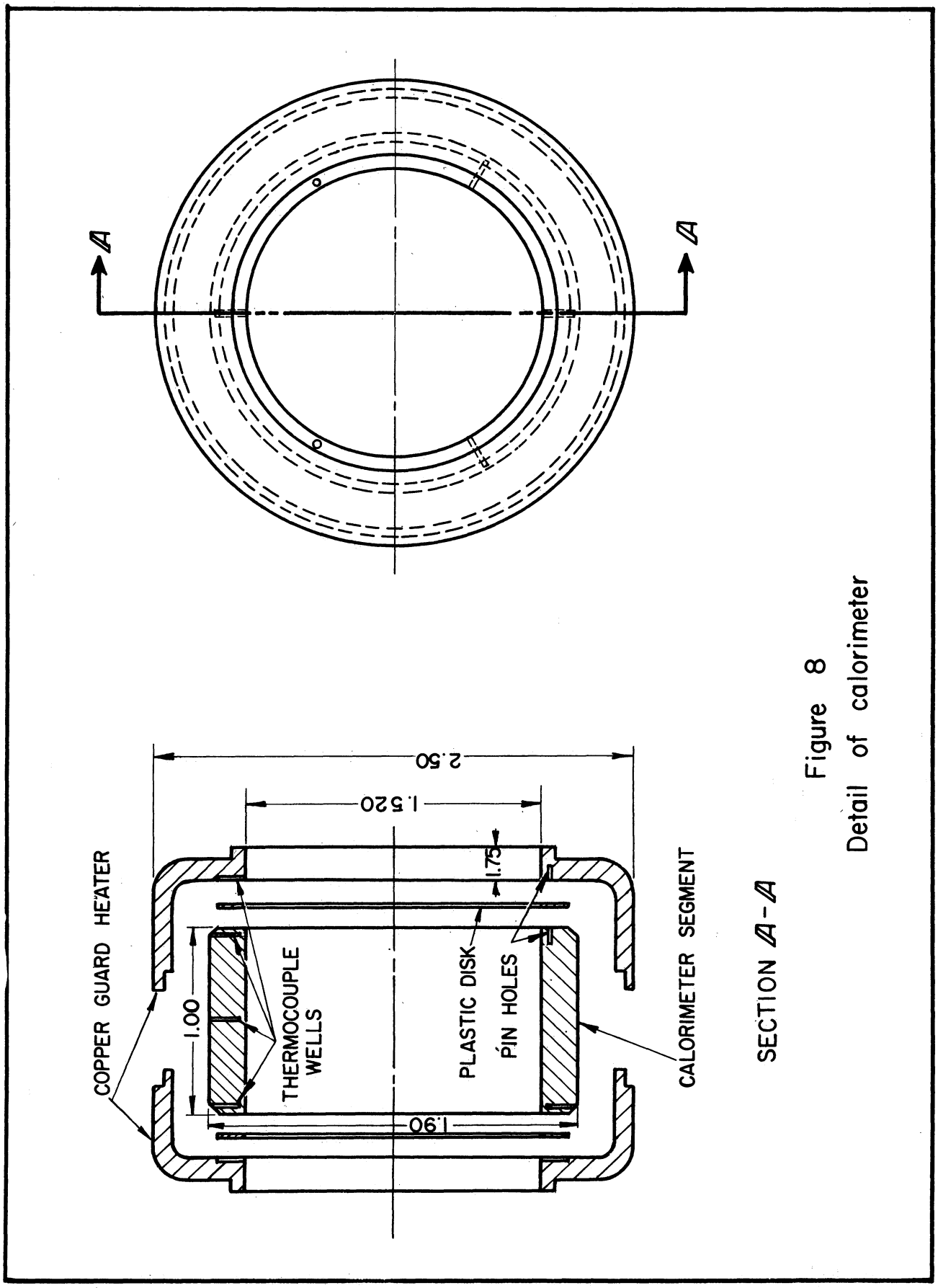

Figure 8
Detail of calorimeter

heater segments were held in alignment by means of .025 inch diameter chromel pins, as shown in the diagram.

Thermocouples were located in the ends of the calorimeter segment and at corresponding points in the guard so that by adjustment of guard and calorimeter heater currents, it was possible to maintain calorimeter wall temperature and guard wall temperature very close to each other. Under such isothermal conditions there was no loss from the calorimeter to the surroundings and the total heat input to the calorimeter could be considered to flow through the pipe wall into the air stream.

Current for the calorimeter heater was obtained from two 6-volt storage batteries connected in parallel. A battery charger was floated on the line during operation to reduce the drain on the batteries and provide a more constant current. Calorimeter current was controlled by a resistance network consisting of several fixed resistors with shunting switches and a slidewire for fine adjustments.

Power input to the calorimeter was obtained from measurement of the voltage across the calorimeter winding terminals with a calibrated D. C. voltmeter and measurement of current was done by determining the potential drop across a calibrated .01 ohm resistance with a Leeds and Northrup student type potentiometer.

Alignment of calorimeter, heating section, and entrance section was accomplished by means of male and female joints as shown in figure 7. All sections were carefully honed to a 30 micro-inch finish to ensure smoothness of surface and avoid steps in the inside wall surface at joints

between sections. The maximum step found between sections was estimated to be on the order of .001 inch.

The components of the test section were held together with 3/16 inch machine screws acting upon steel flanges .20 inches thick with six .20 inch holes located on a 3 1/2 inch bolt circle. The system was so designed that no flange was connected directly to the calorimeter or the thickwalled copper pipe of the heating sections. This was necessary since any flange mounted on the heat transfer surface would have disturbed the wall temperature distribution.

For runs using electrically heated sections, the entire assembly was held together by one set of tie bolts running across the heating section and calorimeter from a flange on the entrance section to one on the traversing mechanism. With the steam jackets, intermediate flanges soldered on each end of the outer wall of the jackets were used.

Thin gaskets of soft polyethylene sheeting were inserted between sections as shown in figure 7. The thickness of gasket used was somewhat greater then the width of the gasket space. The tie bolts were drawn up till the mating metal surfaces were in contact (as evidenced by visual inspection of the inside wall surface). This compressed the gaskets sufficiently to prevent leakage. Lock washers were used on all tie bolts.

A carefully machined .20 inch thick disk of glass fibre laminated phenolic plastic (thermal conductivity .29 BTU/hr ft^{o}F) was inserted between the hydrodynamic entrance section and the heating section in all cases. The purpose of this disk was to reduce end loss and more

nearly approximate the condition of a finite step in wall temperature at the start of the heated length.

Exhaust Section and Gross Flow Measurement

To obtain the gross flow rate a sharp edged orifice was located in the exhaust system used to vent the heated air from the test section to the outside of the building. The orifice was located in a 2 1/2 inch pipe and had a hole diameter of 1 1/2 inches. Pressure taps were made by drilling a 1/16 inch hole in the pipe wall, counterboring the outside, and silver-soldering a short piece of 1/4 inch copper tubing in the hole. Vena contracta taps were used. Orifice temperature was measured by a mercury-in-glass thermometer located downstream from the vena contracta.

The orifice installation was designed in accordance with the specifications for meter runs and orifice plates suggested in Stearns (60). However, since space limitations made it necessary to use a meter run somewhat shorter than that recommended by Stearns, a calibration was made of the orifice in place. A series of critical flow orifices was used as the standard. Excellent agreement was obtained between results obtained for different critical flow orifices for the ranges in which they overlapped. The calibration obtained agreed within three per cent with the theoretical predictions from Stearns. The slight deviation was probably due to the shortened meter run.

Pressure Measurement

Two manometers were used for measurements of orifice pressure difference, static pressures, and pitot heads. Meriam red oil (sp. gr. = .817 at 85°F) was used as the manometer fluid in both instruments.

Pressure differences under .70 inch of meriam red oil were measured on a micromanometer which read directly in thousandths of an inch of meriam red oil.

A U-tube manometer was used for greater pressure differences. Differences in manometer fluid level were measured with a cathetometer which read to .01 cm.

Tygon tubing was used for the pressure lines from the orifice and test section static taps and the total head tube. A manifold consisting of several three-way glass stopcocks connected with tygon tubing allowed pressures in different points of the system to be read on either manometer without disconnecting pressure lines.

The Temperature-Velocity Probe and Traversing Mechanism

Radial temperature and velocity profiles in the flowing stream were made with a hot wire anemometer probe. A photograph of the probe is shown in figure 9. It consisted of a piece of 1/8 inch stainless steel tubing of 1/32 inch wall thickness bent to the shape shown.

Before bending, two insulated copper wires were passed through the tube and soldered to steel sewing needles. The needles were then lacquered except at the tips, bound with thread to the tubing, and covered with successive layers of Saureisen cement.

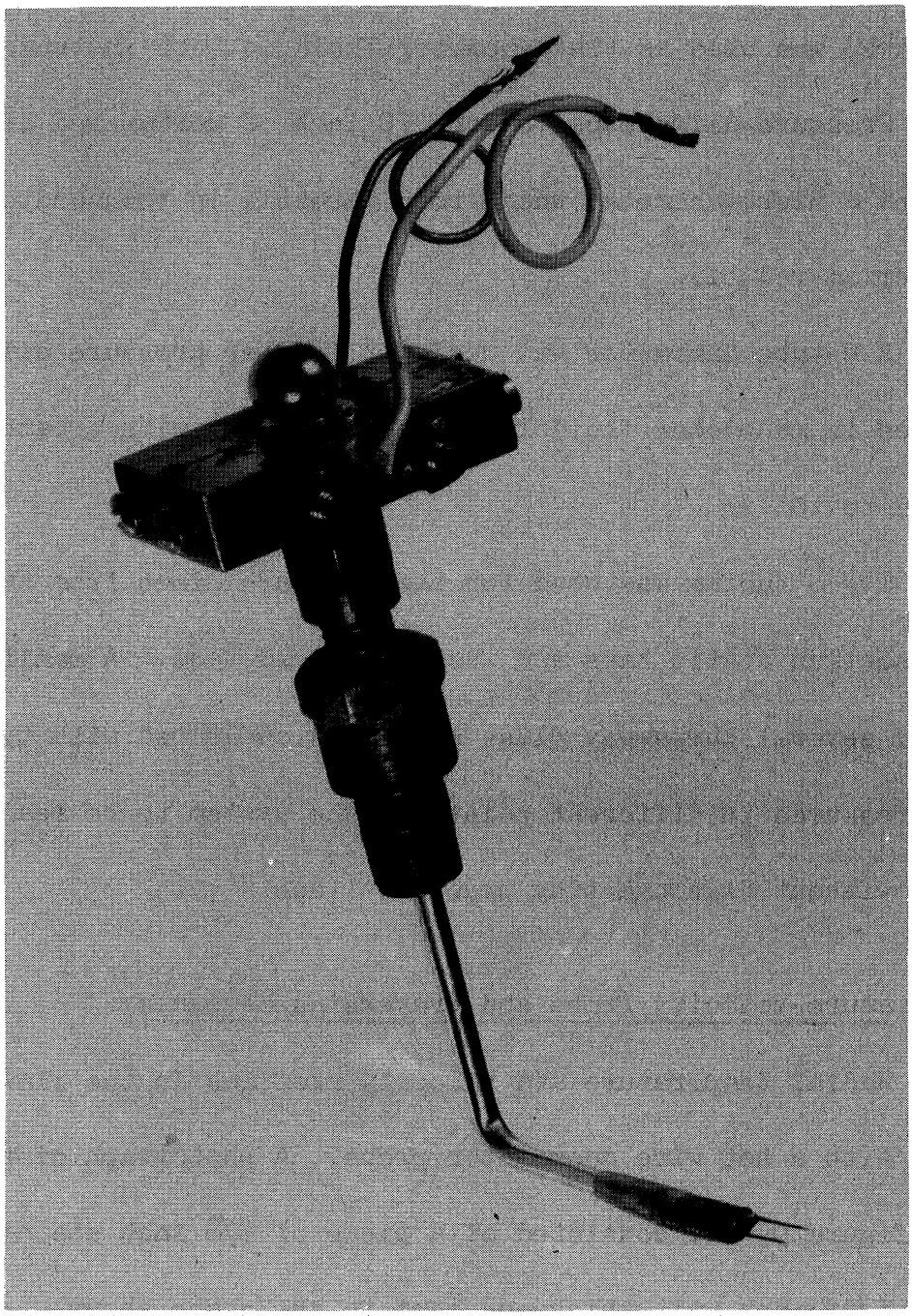

Figure 9. Velocity-Temperature Probe

During this process the needles were bent so that, when the shaft of the probe was held in a vertical position, the tips of the two needles would lie in the same horizontal plane. The Saureisen coating was sanded to a smooth streamlined shape and lacquered. This technique produced a stiff probe which could not vibrate in a rapidly flowing air stream.

The actual sensing element of the probe consisted of a fine platinum wire soldered across the tips of the needles. Platinum wire .0003 inches in diameter is obtained imbedded in the center of silver wire .003 inches in diameter (Wollaston process). A short length of this wire is placed across the needle tips and one end soldered to one of the tips. Then, under a very slight tension, the wire is soldered to the other needle. The wire must be at right angles to the probe tips and horizontal with respect to the shaft axis. The surplus wire on either end is trimmed off with scissors.

The silver is then etched off the center portion of the wire with a jet of dilute nitric acid solution through which a small current is passed. Completion of the etching process is indicated by a very sharp drop in the etching current. The amount of tension under which the wire is soldered is quite critical, since with too small tension the wire will not be straight, while with too much tension it will break. The etched portion of the wire was usually about .04 inches long, while the distance between needles was .14 inches.

The probe was installed in a section of plastic pipe adjacent to the downstream end of the calorimeter. A shaft bearing for the probe was constructed by filling a 1/8 inch close pipe nipple with brass and then carefully boring it out to a tight fit. The nipple was screwed into a high pressure tubing-to-pipe connector, the tip of which was filled with graphite-string packing and which served as a packing gland. This assembly is shown in figure 9.

The connector was screwed into a tapped hole in the plastic pipe. The probe extended upstream so that the tip was located at the center (in the axial direction) of the calorimeter.

The mechanism for traversing the tube radially is shown in figure 10. It consisted of a micrometer barrel rigidly mounted above and on the same axis as the hole into which the probe bearing assembly was screwed. The barrel bore down on a 3/8 inch steel ball fixed to the top of the probe. The probe was held up against the micrometer spindle by small steel cables on each side which ran over pulleys and on which weights were hung.

A pointer was attached near the top of the probe shaft so that the probe could be turned around the shaft axis. This pointer was secured to a moveable guide mounted on the rear flange of the plastic section. With this arrangement it was possible to align the probe tips parallel to the tube axis.

A total head tube assembly was mounted in the side of the plastic section 90 degrees around the tube from the hot wire probe.

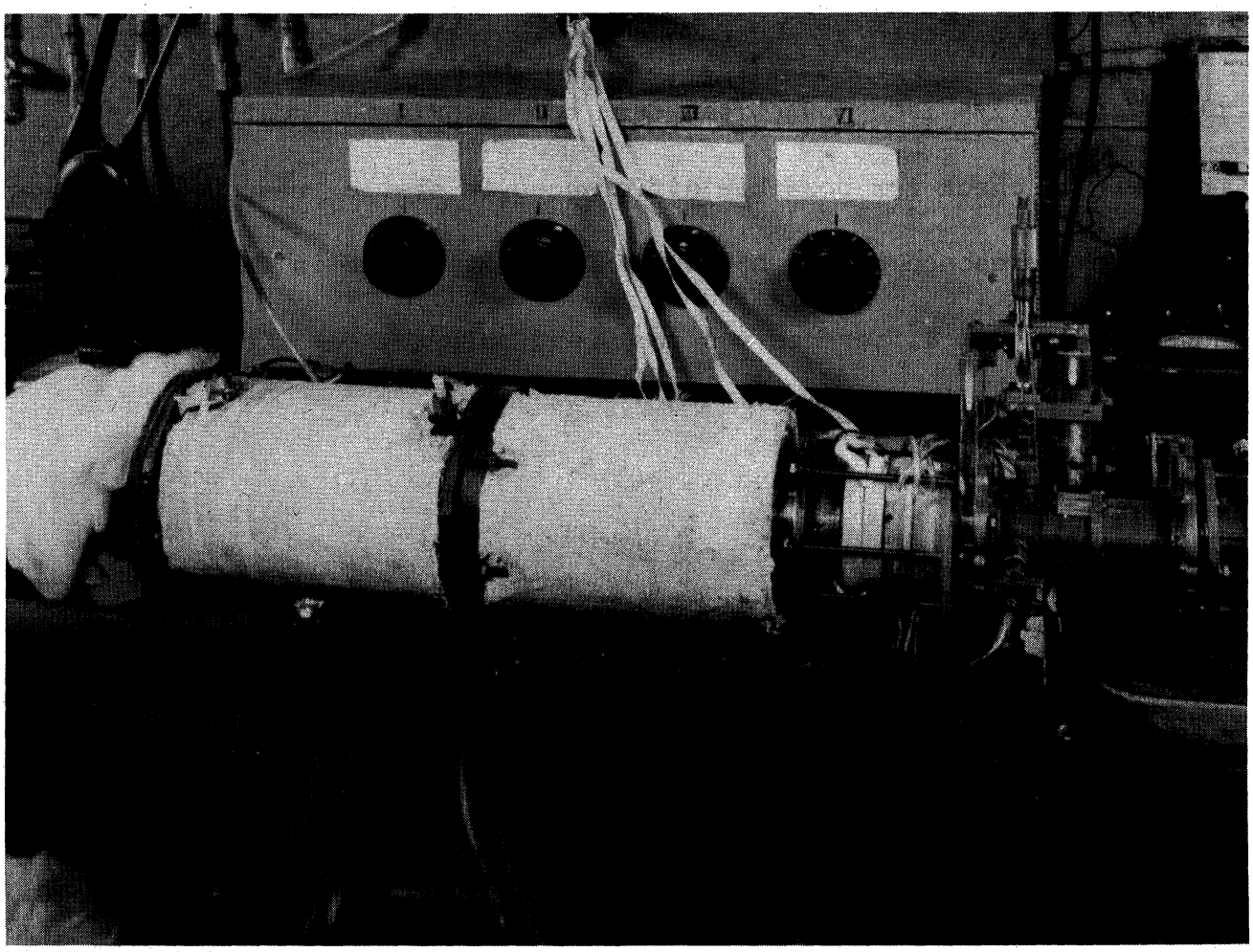

Figure 10. Traversing Mechanism

This probe extended forward into the calorimeter to a point about 1/8 inch downstream from the hot wire probe tip. The total head tube was used for calibrating the hot wire for velocity and was mounted in a packing gland so that it could be retracted against the wall when not in use. Three static pressure taps were equally spaced around the plastic tube 1/4 inch downstream from the calorimeter so that it was possible to check for possible differences in static pressure readings due to the presence of the hot wire and pitot probes in the calorimeter. However, no such difference was found and only the top tap was used during the experimental work.

IV. EXPERIMENTAL AND CALCULATION PROCEDURES

Velocity Profiles

Excellent reviews of the theory and techniques of hot wire anemometry have been presented by Kovásznay (31) and Willis (63). The operation of a hot wire for determination of mean local speed depends on the relation between the rate of cooling of a small electrically heated wire placed in a gas stream, and the local velocity of the stream. For a heated wire placed normal to the stream, the relation between the rate of electrical heat production in the wire and the rate of loss to the stream for steady state can be expressed by the equation

$$i^2 R = (A' + B' \sqrt{u}) (T_w - t) \qquad (17)$$

where t denotes fluid temperature, T_w the wire temperature, R the wire resistance and A' and B' are constants depending on the dimensions of the wire and the physical properties of the fluid. The resistance of the wire is given by

$$R = R_o (1 + \beta T) \qquad (18)$$

where β denotes the temperature coefficient of resistance of the wire and R_o is wire resistance at 0°F.

Combining (17) and (18) yields

$$i^2 \frac{\beta R R_o}{R - R_a} = A' + B' \sqrt{u}$$

where R_a is the wire resistance at the air temperature t. Thus, if i is kept constant and the quantity $R/R - R_a$ determined for several known velocities, a plot of $\sqrt{u}$ against $R/R - R_a$ should give a straight line calibration.

The hot wire circuit is shown in figure 11. . Current was supplied by a 24 volt storage battery. With the double pole, double throw switch "A", it was possible to send either a large current (about 65 ma.) for measuring velocity or a small current (about 1.5 ma.) for measuring air temperature through the 10 ohm precision resistor and the hot wire. With the large current, the equilibrium temperature of the wire was from 100°F to 250°F above the temperature of the air stream, depending upon the point velocity. The resistance determined at this temperature was used as R in equation 19.

The wire resistance measured with the 1.5 ma. current passing through it was used as R_a in equation (19). Adjustment of either current within rather wide limits was possible with the variable resistors included in each branch of the parallel circuit.

The voltage drop across either the hot wire or the 10 ohm precision resistor was measured with the K-2 potentiometer and amplifier-galvanometer system mentioned above in connection with determination of thermocouple EMF.

The current flowing through the hot-wire was determined from the potential drop across the 10 ohm resistor; this together with the potential drop across the wire allowed the hot wire resistance to be computed. A small correction was applied for hot-wire lead resistance.

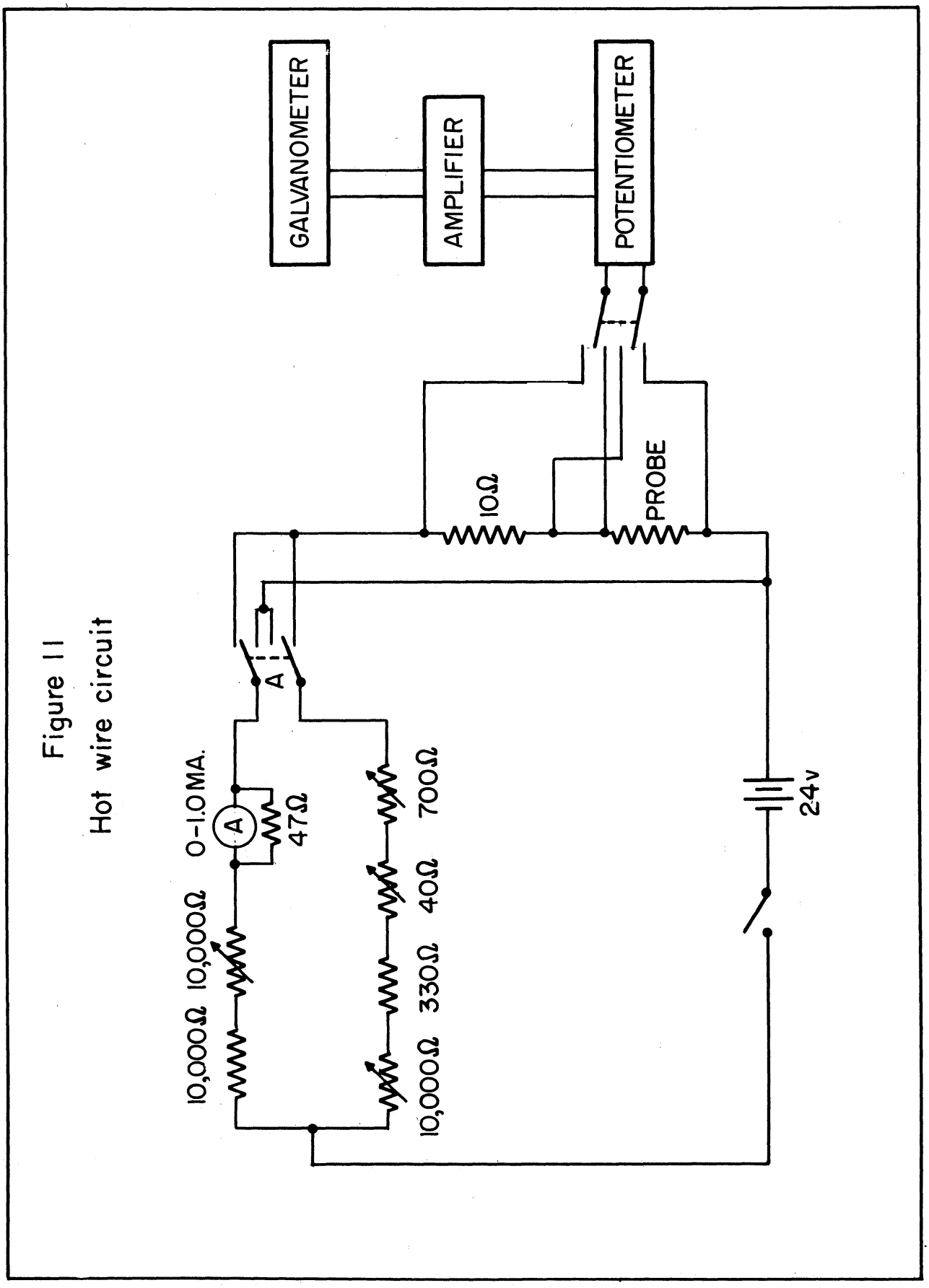

Figure 11

Hot wire circuit

Because of the presence of fluctuating velocity components due to turbulence it was necessary to include an R-C damping circuit to obtain readings of mean velocity. These fluctuations were generally small in the center of the stream, went through a maximum with increasing radius and then diminished as the wall was approached. This trend closely resembled that found for the eddy diffusivities.

Wire velocity calibrations were made using the total head tube mounted at right angles to the hot-wire probe. The center velocity was determined by the total head tube; it was then retracted and the hot-wire probe moved into the center and readings taken. The procedure was repeated for several velocities over the range to be investigated and the results plotted as $\sqrt{u}$ against $\frac{R}{R - R_a}$. This plot gave a straight line except at very low velocities, where there was a slight curvature probably due to a change in the flow regime of the air over the wire.

In computing velocities from total head tube readings, the impact tube coefficient was considered equal to unity and a small correction applied for the pressure drop along the tube between the points where the total and static pressure were measured. The accuracy of velocity measurement varied from 0.5% at moderate velocities to 5% at 6 ft 1 sec.

In the region very close to the wall errors are introduced due to non-linearity of the wire response to fluctuating velocity components and heat transfer from the wire to the wall. These effects are discussed in the next chapter.

Mean flow rates were computed by graphical integration of the velocity profiles using the relation:

$$u_b = \frac{2}{a^2} \int_0^a u \, r \, d \, r \qquad (20)$$

Mean flow rates computed by equation (20) agreed within 3% with those determined from orifice measurements.

Temperature Profiles

Temperatures in the air stream were measured by using the hot-wire anemometer as a resistance thermometer. This technique has been described by Schlinger (54) and Sleicher (59). The experimental procedure was the same as that described for obtaining the wire resistance at air temperature, R_a, described under Velocity Profiles. Since the resistance of the wire is a function of temperature, the wire temeprature can be calculated from its resistance after calibration.

Actually, because of aerodynamic and electrical heating effects the wire is at a temperature slightly higher than the static temperature of the stream. These effects were not important in the determination of R_a for velocity measurements since they were taken in account by the calibration procedure. However, corrections for them must be applied for accurate temperature measurement.

The stagnation temperature of a flowing stream of gas is given by:

$$t_s = t + \frac{u^2}{2g_c \, JC_p} \qquad (21)$$

The wire with no current actually comes to a temperature less than t_s given by:

$$T_w = t + \gamma \frac{u^2}{2g_c JC_p} \qquad (22)$$

where γ is the "recovery factor". Hottel and Kalitinsky (24) experimentally determined an average value of $\gamma = .66$ for a range of velocities similar to that employed. They found that for small wires γ was nearly independent of diameter. The correction due to aerodynamic heating was calculated from equation 22 using $\gamma = .66$.

A correction is also necessary for heating of the wire caused by the current used to measure its resistance. This correction can be computed from generalized correlations for the heat-transfer coefficients of cylinders in cross-flow as given by McAdams, p (40). For wires with length to diameter ratios of the magnitude used here (about 130 to 1) end losses from the wire must also be considered. The fine wire is heated by the current, but the heavier supporting silver wires may be assumed to be close to T_w, the temperature assumed by an adiabatic wire. Some of the heat generated in the wire is thus conducted from the platinum wire at its ends.

The latter two corrections may be combined in a manner described by Sleicher (59). The differential equation describing the temperature of a wire with uniform heat generation per unit length, Q; uniform heat-transfer coefficient h along its length axis x; and ends and surroundings at t = o is:

$$\frac{\partial^2 T_w}{\partial x^2} - \frac{4h}{k_w D} T_w + \frac{4Q}{k_w \pi D^2} = 0 \qquad (23)$$

$$t\,(0) = 0$$
$$t\,(\infty) = \text{finite}$$

The solution of the equation 23 is:

$$T_w = \frac{Q}{\pi k_a Nu}\left[1 - e^{-\psi \frac{X}{D}}\right] \qquad (24)$$

$$\psi = 2\sqrt{Nu}\,\frac{k_a}{k_w}$$

Integrating equation 24 over the wire length L gives the average wire temperature as:

$$(T_w)_{avg} = \frac{Q}{\pi k_a Nu}\left[1 - \frac{2e^{-\psi X/D}}{\psi X/D} - \frac{1}{\psi X/D}\right] \qquad (25)$$

where the term in brackets is the correction to account for conduction cooling at the ends. This correction, which increases with decreasing velocity, amounted to 16.5% at a velocity of 10 ft/sec.

Radiation corrections were found to be negligible. The temperature corrections are plotted as a function of velocity in figure 12.

The turbulent velocity fluctuations mentioned in the section on Velocity Profiles caused corresponding fluctuations in temperature. The K-2 potentiometer was balanced by estimating by eye the setting at which the mean of the galvanometer settings was zero. Settings were reproducible to $\pm$ .25 microvolt or better, which corresponded to a maximum error in temperature of $\pm$ .08 F.

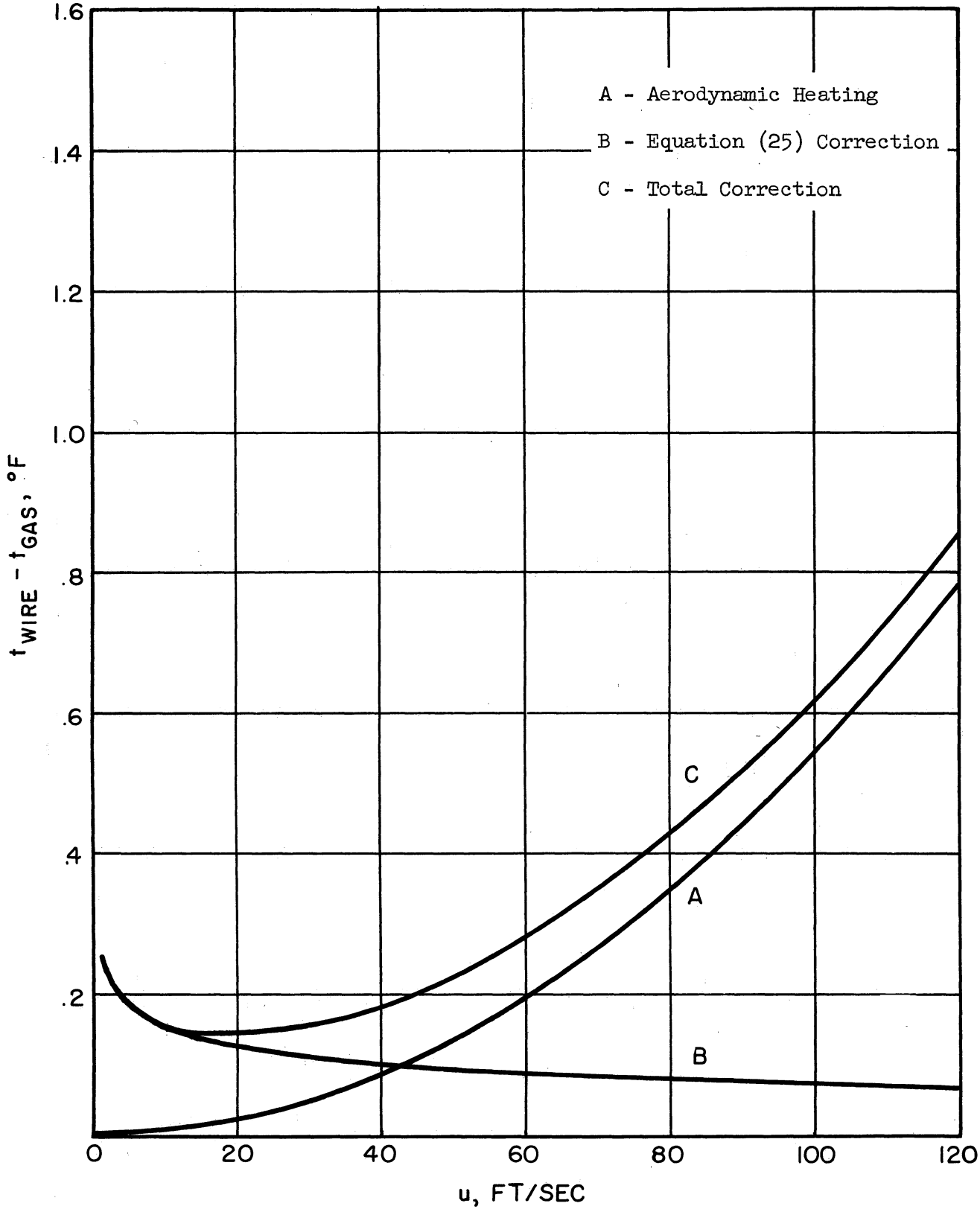

Figure 12. Temperature Corrections for .3 mil Platinum Wire .0482 inches long

The temperature probe was calibrated against a thermocouple located in the center of the tube downstream from the probe. The installation of this thermocouple was discussed in the chapter on apparatus.

The preheater in the calming section was used to heat the air stream to several different temperatures covering the range to be employed in the test run.

Since the calibration couple was left unshielded in order to ensure rapid response it was subject to aerodynamic heating effects. It was assumed that the recovery factors for couple and wire were equal. Although this assumption is not absolutely true, little error was introduced on account of it because of the fact that temperature calibrations were made at a low speed (about 10 ft per sec.) where aerodynamic heating effects only amounted to .02°F.

The wire was calibrated for temperature and velocity before every run and several check points were taken after the run. In a few instances the calibration changed markedly during the run, probably due to a stretching of the wire by a small particle in the air stream.

Location of

The point at which the hot-wire probe tips made contact with the upper wall was determined electrically by measuring the resistance between the probe and the wall. Before each run a check was made to see that the probe needles were aligned with the axis of the tube (the mean flow direction.) This was done in the following manner: The probe was brought to within a few thousandths of an inch of the estimated position of the

wall. The probe tip was then rotated about its axis so that first one side of the probe tip touched the wall, and then the other. The approximate center position was noted and the probe raised slightly. This procedure was continued until the angular position of the probe was found that would result in both sides of the probe touching the wall simultaneously as the probe was raised. This position was maintained by locking the probe pointer guide.

The dimensions of each hot-wire were determined by measurement under a microscope equipped with a calibrated traveling diaphragm. Figure 13 is a view of the probe with the probe tips in contact with the wall, as it would appear to the stream of air in the tube.

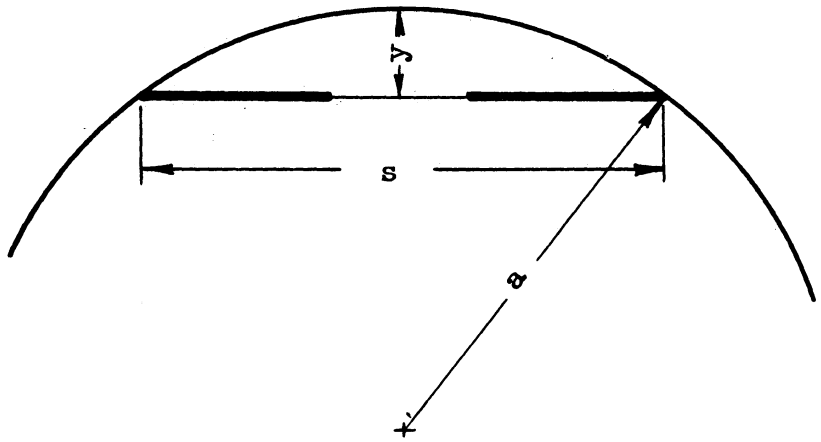

Figure 13. Dimensions of Hot-Wire Probe

The distance y of the middle of the fine wire from the wall is given by the relation:

$$y = a\left(1 - \sqrt{s^2/4a^2}\right) \tag{26}$$

This distance was considered to be the distance of the wire from the wall when the probe and wall were in electrical contact. Although not all parts of the wire were at the same distance from the wall, this was a good approximation, since the sensing element consisted only of the center third of the wire.

Experimental Procedure

The cold junction was filled at least an hour before the start of the run to ensure its being at 0°C. Before the run the hot-wire probe was calibrated for both temperature and velocity.

The flow rate was then set and the inlet temperature determined. The heaters and steam jacket (if used) were then turned on. Careful adjustment of heater inputs and steam flow rates was made until all parts of the equipment were at the proper temperature level. Special effort was made to get temperatures at adjacent points in the calorimeter and guard as nearly equal as possible. The average difference between adjacent points was less than .1°F. This procedure of equalizing temperatures generally took two to three hours.

The probe zero position was then checked and a temperature traverse started from the center of the tube and carried to the wall. A velocity traverse was then taken at the same points as the temperature

traverse. Although the temperatures could have been computed from the wire cold resistances obtained as part of the velocity traverse, it was considered more satisfactory to complete the temperature measurements as rapidly as possible after thermal equilibrium was established.

Wall and inlet temperatures, flow rate, and probe calibrations were checked at the conclusion of the run. The maximum difference between initial and final inlet temperature was .3°F, or a little over 1% of the operating Δt, while initial and final flow rates agreed within 1%.

For each entrance and L/D ratio-runs were made at Reynolds numbers of 15000 and 65000.

Physical Properties of Air

Values of the density, viscosity, specific heat at constant pressure, and thermal conductivity of air were required for calculations from the experimental data.

The density was computed from the perfect gas law. Other physical properties were obtained from the "Handbook of Supersonic Aerodynamics" (28).

V. DISCUSSION OF RESULTS

In this investigation velocity and temperature distributions and point heat transfer rates were obtained in the entrance region for air flowing in a 1.520 inch inside-diameter heated pipe. The two hydrodynamic entrances investigated were 1) a straight tube 66 inches (43.3 pipe diameters) long which gave essentially fully developed turbulent flow and 2) a bellmouth entrance which produced an initially flat velocity distribution. Temperature and velocity profiles and point heat transfer rates were taken downstream from the long tube entrance at length-to-diameter ratios of .543, 1.13, 4.12, and 9.97 after the start of heating and after the bellmouth at X/D's of .543, 1.13, 1.75, 4.12, and 9.97 after heating began. For each entrance and X/D, runs were made at Reynolds numbers of 15,000 and 65,000. The upper limit of Re = 65,000 was the maximum flow rate that could be obtained with good control from the air supply system. The lower limit was chosen to give as wide a range as possible, and yet ensure turbulent flow in the fully developed hydrodynamic boundary layer. Pressure drop measurements in the entrance region were taken for these flow rates.

As mentioned in the discussions of equipment and experimental procedure above, only one X/D could be investigated during each Thus, for a given entrance and Reynolds number, there were small differences in initial temperatures, wall temperatures, and flow rates between runs taken at different X/D's.

In order to put profiles taken at different X/D's on a comparable basis and to permit the calculation of longitudinal gradients, the following dimensionless quantities were introduced:

$$\Theta = \frac{t - t_o}{t_w - t_o}$$

$$Z = \frac{x}{a}$$

$$r_* = \frac{r}{a}$$

$$U = \frac{u}{u_m}$$

Gross values for the heat transfer runs are reported in Table I of Appendix B while point values for velocity and temperature profiles are given in Table II of Appendix B. The results given in these tables and the pressure drop studies are discussed below.

Pressure Drop

The pressure gradient as a function of length is shown in figures 14 and 15 for the long tube with bellmouth entrance. These data were taken with the 15 inch steam jacket in place so that the total length over which data were taken was 82 inches or 54 X/D. Pressure drops were measured differentially, with all differences being taken between adjacent taps. This was done since a very small change in flow rate could cause very large errors in pressure gradients computed from integral measurements, while having little effect on differential measurements. It also permitted the differenced data to be plotted directly and a smooth, equal area curve drawn through the increments.

Pressure differences between the closely spaced taps in the inlet region were relatively small and difficult to determine

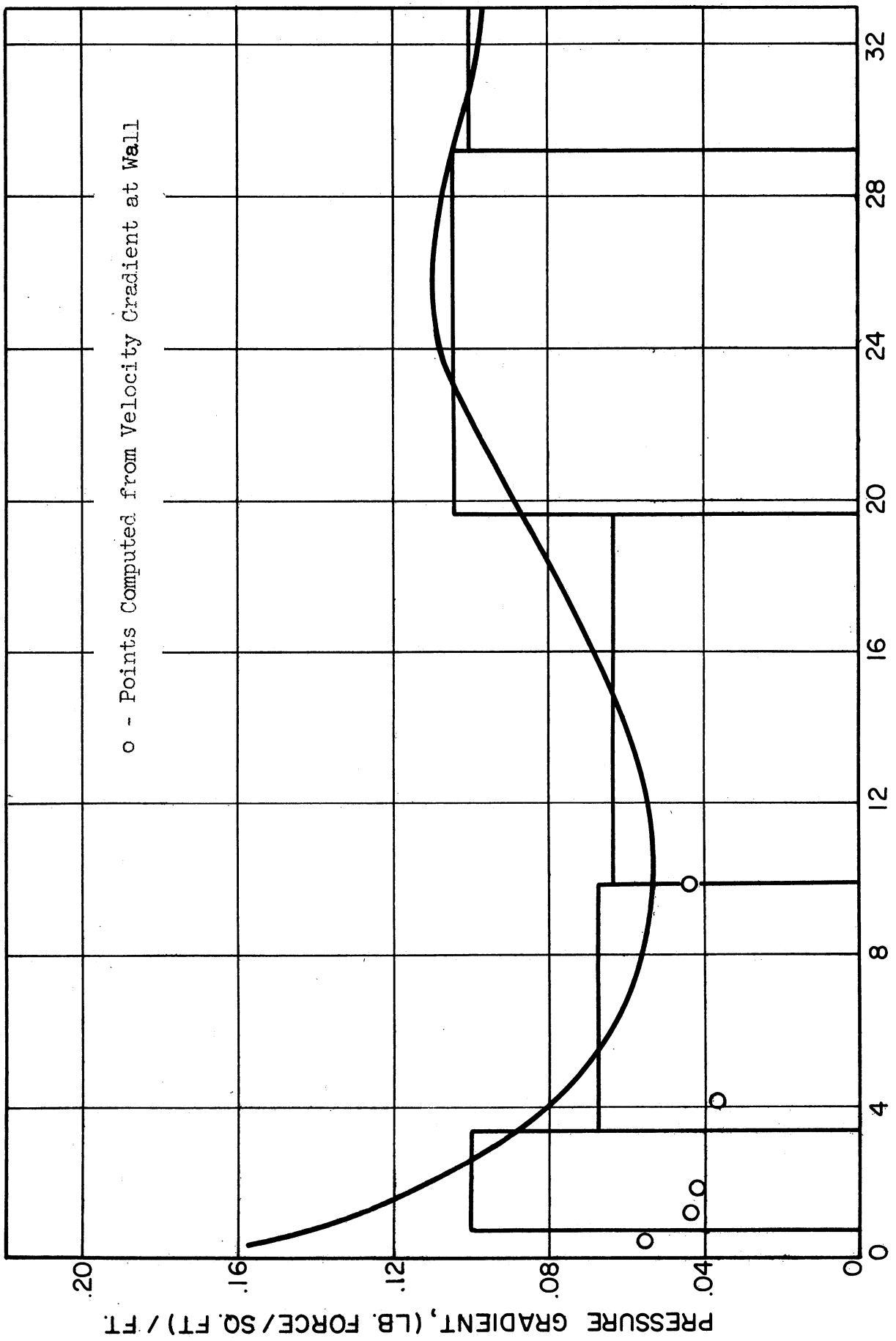

Figure 14. Pressure Gradient in the Inlet Region after Bellmouth Entrance for Re = 15,000

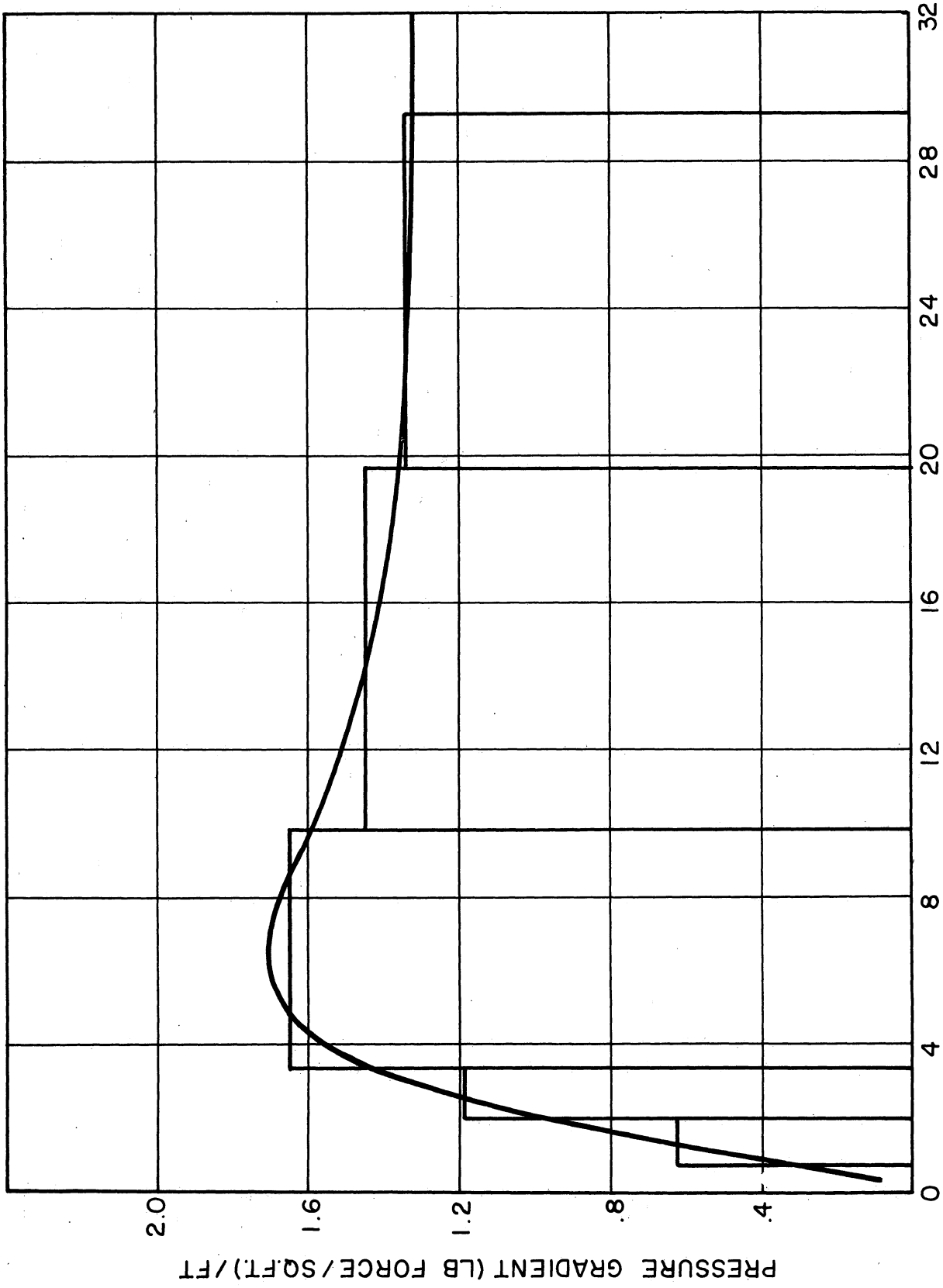

Figure 15. Pressure Gradient in the Inlet Region after Bellmouth Entrance for Re = 56,000

accurately. For the first three taps at the lower flow rate there were periodic fluctuations in manometer readings of about .001 inch magnitude, compared to measured pressure differences of about .0035 to .005 inches. However, these readings were reproducible within limits of less than 10 percent, while uncertainty in measurements located further downstream where taps were spaced further apart was about 3 percent.

The pressure gradient became essentially constant at an L/D of 45 for Re = 15,000 and L/D of 25 for Re = 65,000.

The average values of friction factors computed from several runs in the region of constant pressure gradient were very close to those reported by Moody[42] for fully developed flow in smooth pipes. It should be noted here that the point at which the pressure gradient becomes constant is not the same as that at which the velocity profile becomes stabilized, since slight changes in the center of the profile occur without measurably influencing the pressure drop.

From figure 14 it is seen that for the Reynolds number of 15,000 the pressure gradient first decreases with length, then rises, goes through a maximum, and diminishes to its asymptotic value. This can be explained by the fact that, even for high Reynolds numbers for which the fully-developed flow is turbulent, a laminar boundary layer is formed at the entry of the tube. This layer increases in thickness along the length of the tube and at some distance from the entrance undergoes transition and becomes turbulent. The point at which transition takes place depends on the Reynolds number, the entrance condition of the fluid, and the condition of the tube.

Pressure gradients based on wall shear stress and computed from velocity gradients at the wall are also plotted in figure 14.

These points lie considerably below the smoothed equal area curve obtained from wall static pressure measurements. This fact can be explained by a consideration of boundary layer momentum forces.

The pressure drop in the tube entry is equal to the sum of two terms, the pressure loss due to skin friction plus a term representing the longitudinal rate of increase in momentum flux. The latter effect is associated with the developing velocity profile. As the boundary layer thickness increases, the frictionless core of the flow outside the boundary layer undergoes a contraction in cross-sectional area and is therefore accelerated. The increasing core velocity produces a pressure gradient along the pipe.

Shapiro, et al.,[57] on the basis of their experimental results, have proposed the following relation for the local apparent friction factor in a laminar tube entry:

$$f_{app} = 1.72 \sqrt{Re_x} \tag{27}$$

where f_{app} is the friction factor computed from wall pressure drop measurements. For laminar flow over a flat plate with zero pressure gradient the local skin friction coefficient has been found to be[18]

$$C_f = 0.664 \sqrt{Re_x} \tag{28}$$

Thus the local apparent friction factor for a pipe entry is 2.59 times as great as the local skin friction coefficient for a flat plate.

Theoretical analyses[57] show that, although there is a pressure gradient in a tube whereas there is none for a flat plate, the boundary layer behavior in a tube entry is substantially identical with that on

a flat plate. Consequently, the actual skin friction coefficients (based on wall shear stress) are the same for the tube entry and the flat plate.

From these considerations it is seen that in the laminar tube entry the pressure drop due to momentum changes is 1.59 times as large as the pressure drop due to wall friction, or 39 percent of the pressure drop in the tube entry is caused by wall friction while the remaining 61 percent is caused by momentum changes. These figures are only valid near the entrance where the boundary layer thickness is small compared with the pipe radius.

The total apparent friction factor and the skin friction coefficient, based on velocity gradient at the wall, are shown in generalized form in figure 16. Points for the apparent friction factor were computed using pressure gradients read from the smoothed curve of figure 14. The skin friction coefficient near the entrance is seen to run from about 27 percent to 30 percent of the total apparent friction factor, then gradually approaches the apparent friction factor at further distances downstream.

Equation 27 , as proposed by Shapiro, is also plotted on figure 16. Although the slopes of the two curves for apparent friction factor are the same, Shapiro's line lies somewhat above that of the present investigation. This is apparently caused by a difference in the entrance condition of the fluid. This is indicated by the fact that Shapiro found transition occurring at a length Reynolds number of 5×10^5, while in the present study transition occurred at Re_x of about 1×10^5. This was probably due to the fact that in this case the entrance was not intentionally constructed so as to encourage the laminar

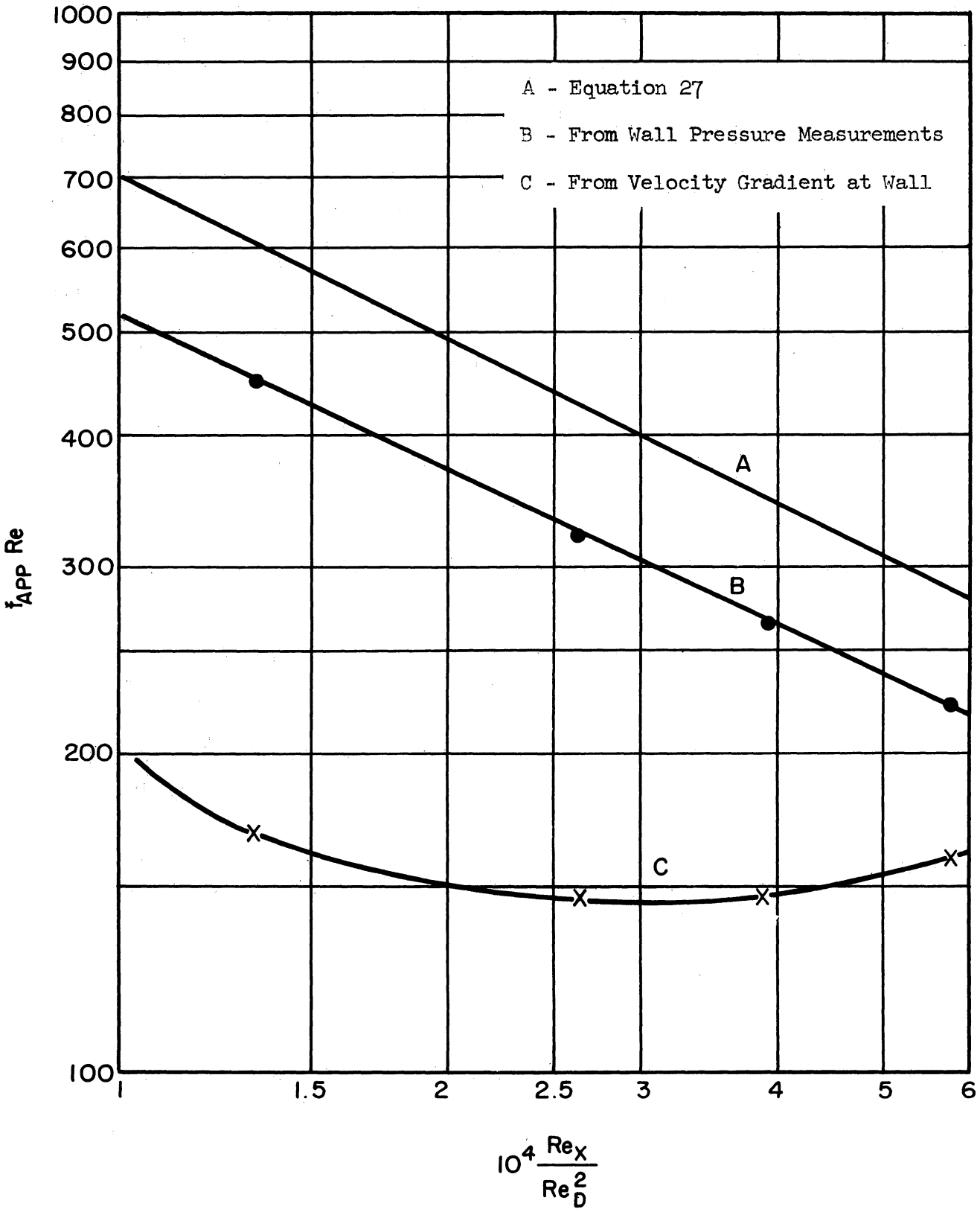

Figure 16. Friction Factor in Inlet Region after Bellmouth Entrance for Re = 15,000

flow regime. The net result appears to have been a shifting of the curve of figure 16 to the left.

As can be seen from figure 15, for the Reynolds number of 65,000, the transition to turbulent flow appears to have taken place very close to the entrance. It was not possible to compute skin friction coefficients in this case since the velocity gradients near the wall were still increasing and the gradient at the wall could not be accurately defined.

Point Heat Fluxes

Heat fluxes were computed from measurements of power input to the calorimeter, determined from voltage and current measurements. Two corrections were applied to these values.

First, a correction was applied for conduction losses through the plastic insulating disks between the calorimeter segment and the adjoining sections of the guard heater due to small non-uniformities in temperature as determined by calorimeter and guard thermocouples. These corrections were in no case over 3 percent.

A second correction was necessary since even with the calorimeter segment and adjacent sections of the guard at uniform temperature, there was some temperature non-uniformity in the shell of the guard. An approximate correction was obtained for this by determining the heat input with no flow and uniform wall and guard temperatures at different levels above ambient temperature. This correction is plotted in figure 17.

The corrected heat fluxes were plotted differentially as $\frac{\Delta q}{\Delta x}$ vs. x and a smooth equal area curve drawn through the increments. Point

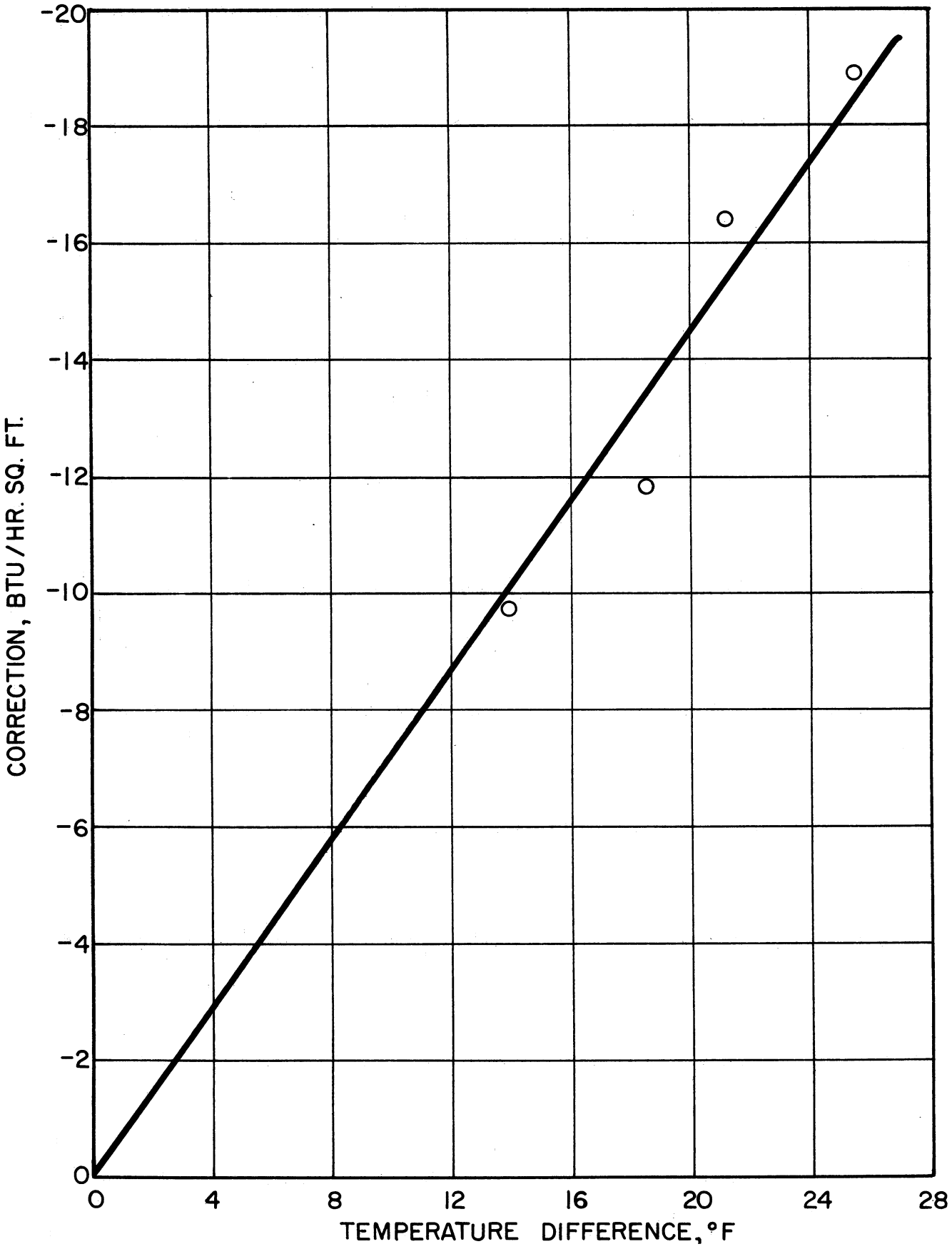

Figure 17. Heat Flux Correction for Calorimeter Measurements as Function of Wall to Room Temperature Differences

values of heat flux were read from the curves and Nusselt numbers computed.

Figure 18 shows Nusselt numbers as a function of X/D for the long tube entrance. Also plotted on figure 18 are values obtained by Sleicher[59] at three X/D's for the same entrance. The data of Boelter[5] (extrapolated) for his long calming section entrance are also shown. Agreement between the three sets of data is excellent. For both Reynolds numbers the Nusselt numbers start out high and gradually decrease with distance downstream.

The Nusselt number appears to have attained very close to its asymptotic value at X/D of 10. For the lower Reynolds number the Nusselt number is 2.8 percent above that computed from the Dittus-Boelter equation, while for the higher Reynolds number it is slightly below (-.35 percent) the computed value.

Nusselt numbers as a function of X/D for the bellmouth entrance are shown in figure 19. Extrapolated results of Boelter for a bellmouth entrance without screens are also shown. Agreement between the two sets of data is good. For the lower Reynolds number a minimum in the Nusselt number is observed at an X/D of about 7. The Nusselt number then starts to rise again. This effect is due to the transition from laminar to turbulent flow as mentioned under Pressure Drop above. At an X/D of 10 the Nusselt number is still rising sharply and has only reached 51 percent of the value predicted by the Dittus-Boelter equation. At a Reynolds number of 65,000 the Nusselt number diminishes uniformly, its value at X/D of 10 being 2 percent above the computed asymptotic value. The Nusselt number for the bellmouth at X/D = .453 was 32 percent below that obtained for the long tube entrance at Re = 15,000, and 17 percent lower at Re = 65,000.

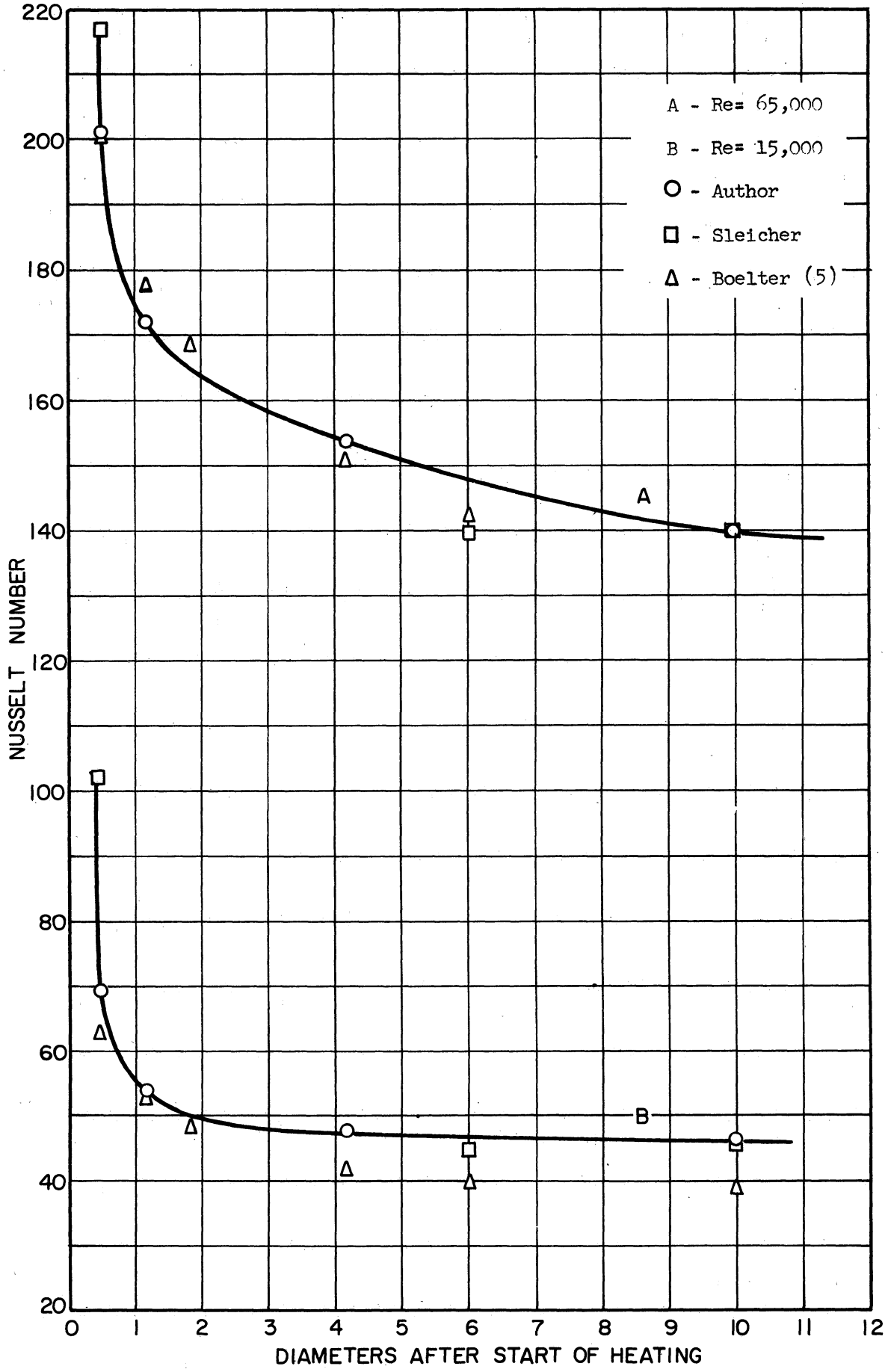

Figure 18. Variation with Length of Point Nusselt Number for Long Tube Entrance

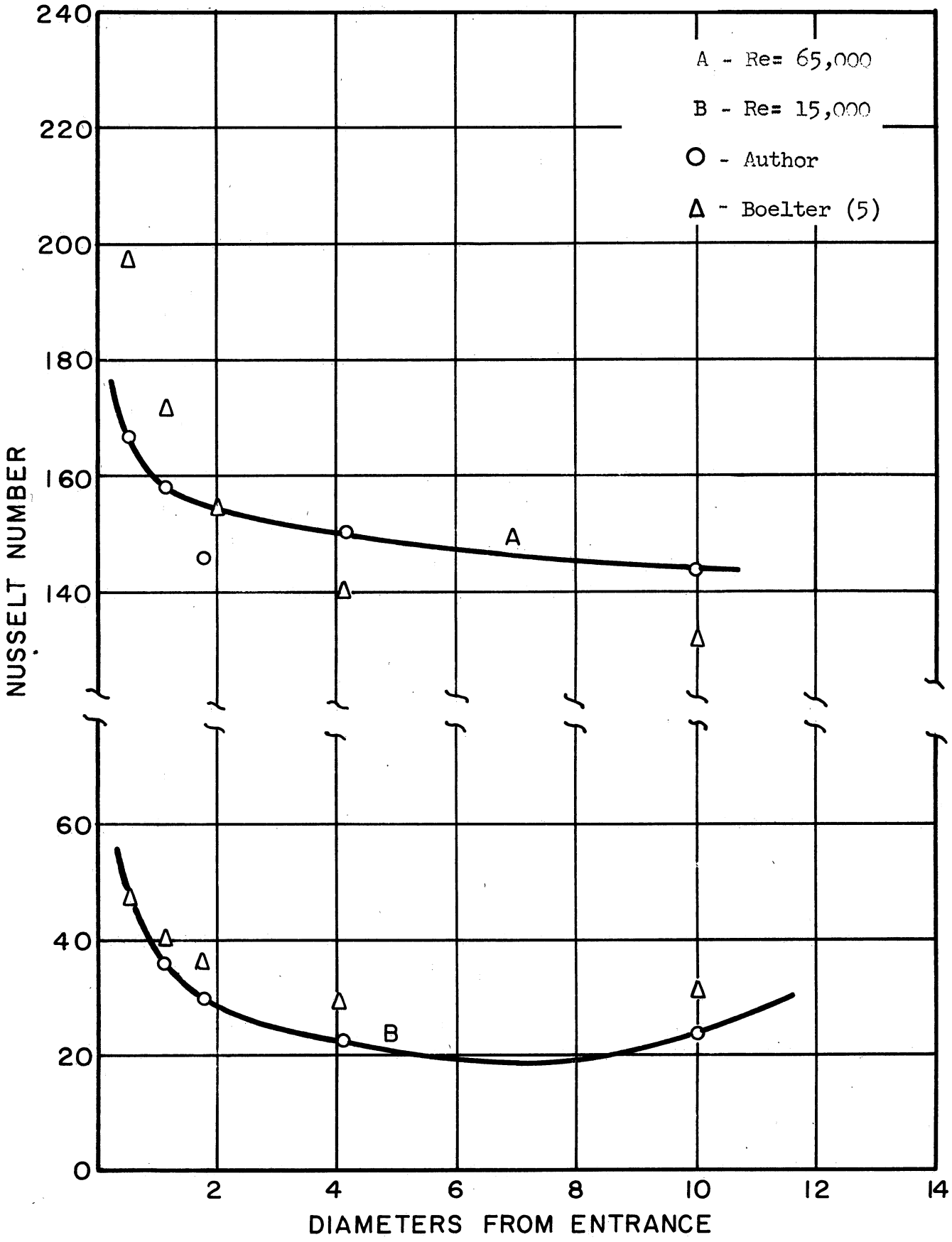

Figure 19. Variation with Length of Point Nusselt Number for Bellmouth Entrance

A check of wall heat fluxes was made by comparing the mixed mean temperature from integration of the temperature profile at the calorimeter with the mean temperature obtained by integration of the wall heat flux using the relation

$$\ln \frac{t_w - t_o}{t_w - t_b} = \frac{2}{C_p \rho a u_b} \int_0^Z h \, d \, Z \qquad (29)$$

Heat balances computed by these two methods generally agreed within better than 10 percent, except for the L/D of .453 where the combination of rapidly changing Nusselt number and small total heat addition due to short heating length caused larger percentage errors.

A further rough check on point heat fluxes was made by comparing heat fluxes computed from radial temperature gradients at the wall with fluxes computed from calorimeter measurements. This method is not very accurate since radial gradients were still changing rapidly as close to the wall as it was possible to obtain readings. However, wall slopes computed from calorimeter measurements and plotted on the temperature profiles appeared reasonable and indicated at least that no gross error in wall heat flux was present.

Velocity Profiles

Values of u/u_m vs. r/a for the long tube entrance are plotted in figure 20. These are average values of profiles taken in the range of 44 to 53.5 pipe diameters downstream from the tube entrance.

At a given Reynolds number, there is a slight variation in the shape of the reduced velocity profiles obtained at X/D's of 44, 44.5, 47.5, and 53.5 pipe diameters. This is due to the fact that there is still some development of the hydrodynamic boundary layer occurring in

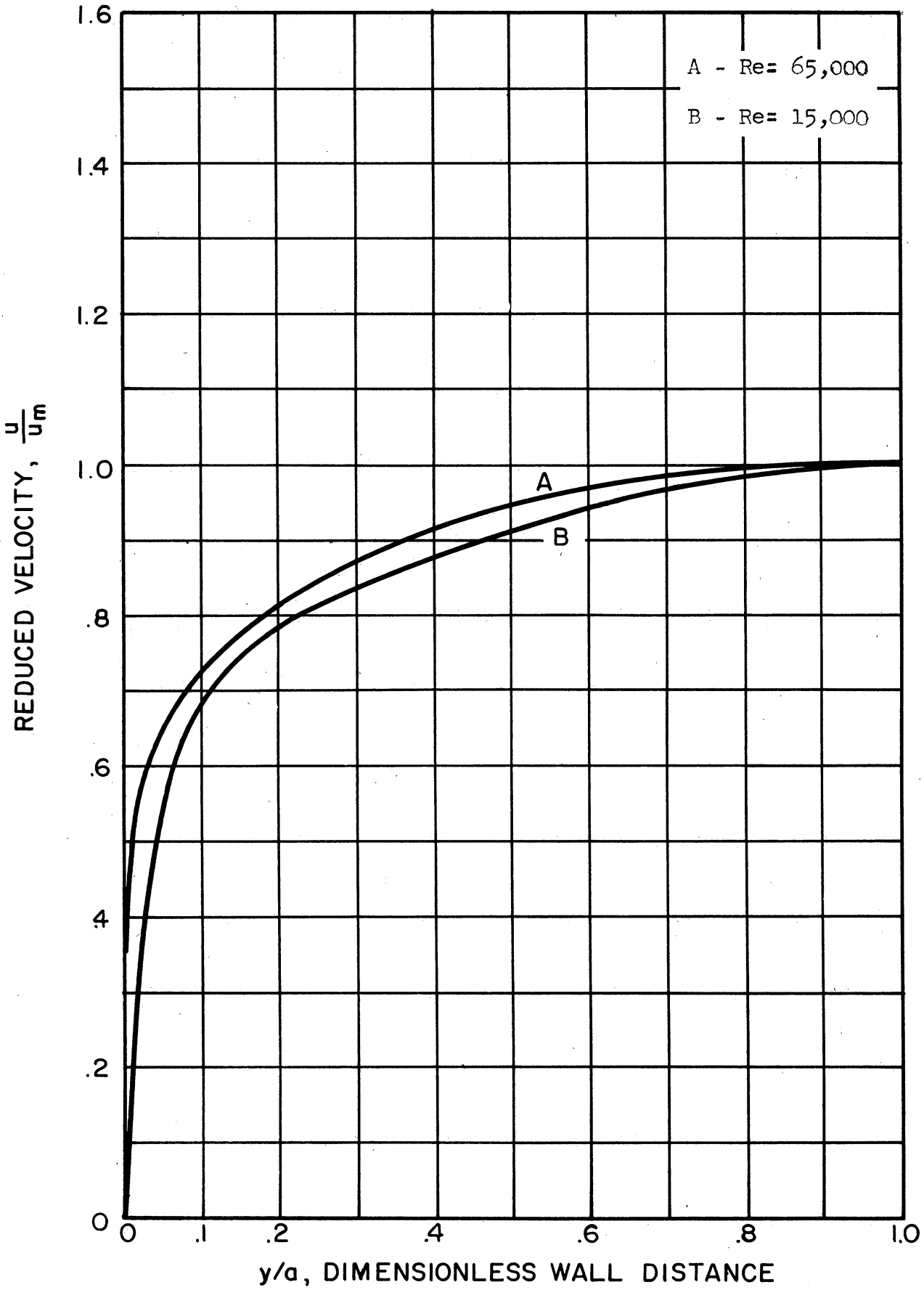

Figure 20. Variation with Flow Rate of Reduced Velocity Distribution for Long Tube Entrance

the center of the tube, although the boundary layer has already merged. This effect is more pronounced at the higher Reynolds number, due to the fact that for higher Reynolds numbers a longer X/D is required to obtain fully developed pipe flow.

The fact that the boundary layer is still developing in the center of the tube can be clearly seen from velocity deficiency curves for the Reynolds number of 65,000 at X/D's of 44.0 and 53.5 plotted in figure 21. Also plotted in figure 21 is the velocity deficiency curve given by Bakhmeteff[3] for fully developed turbulent flow. This type of correlation is particularly sensitive to changes in velocity profile near the center, since it involves taking very small differences in velocities.

The velocity data taken after the long tube entrance are plotted as the universal velocity distribution u^+ vs. y^+ in figure 22. The results of several investigations of velocity distribution in turbulent pipe flow are given in figure 23. Each of the lines is a mean through the data points of the author except the line labeled "Reichardt", which is a mean line through the points of Nikuradse, Reichardt-Motzfeld, and Reichardt-Schuh as reported by Reichardt.[48] All of the lines except Laufer's are in close agreement. However, Laufer's work was done with extreme care in a large diameter pipe. The reason for the discrepancy in his results is not apparent, but it appears that his results near the wall are not very reliable.

The results of the present investigation lie slightly below the others in the region $3 < y^+ < 15$. This is probably due to the fact that near the wall, where the mean axial point velocity is small, the ratio of the fluctuating components to the mean point velocity, u'/u,

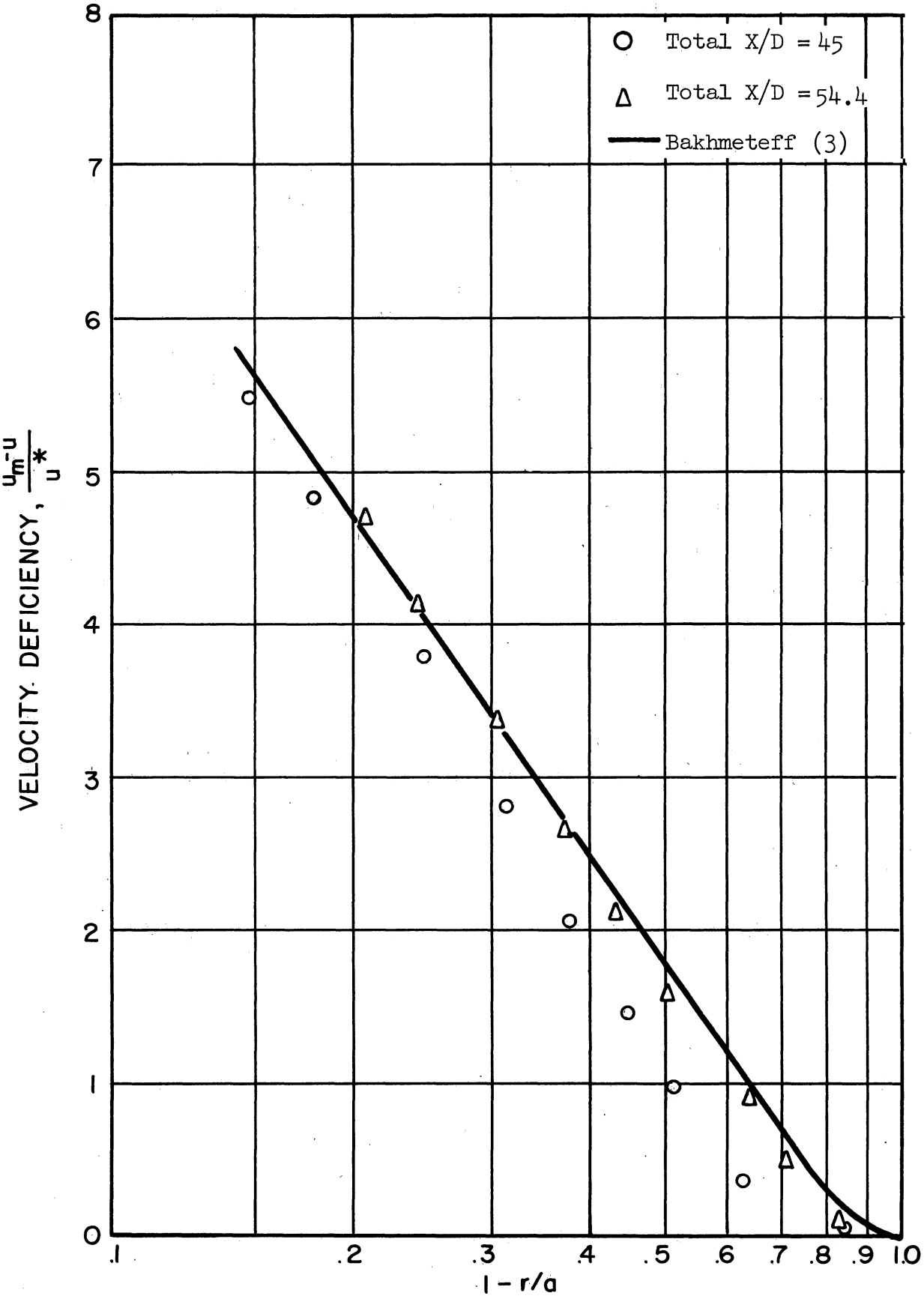

Figure 21. Velocity Deficiency after Long Tube Entrance for Re = 65,000

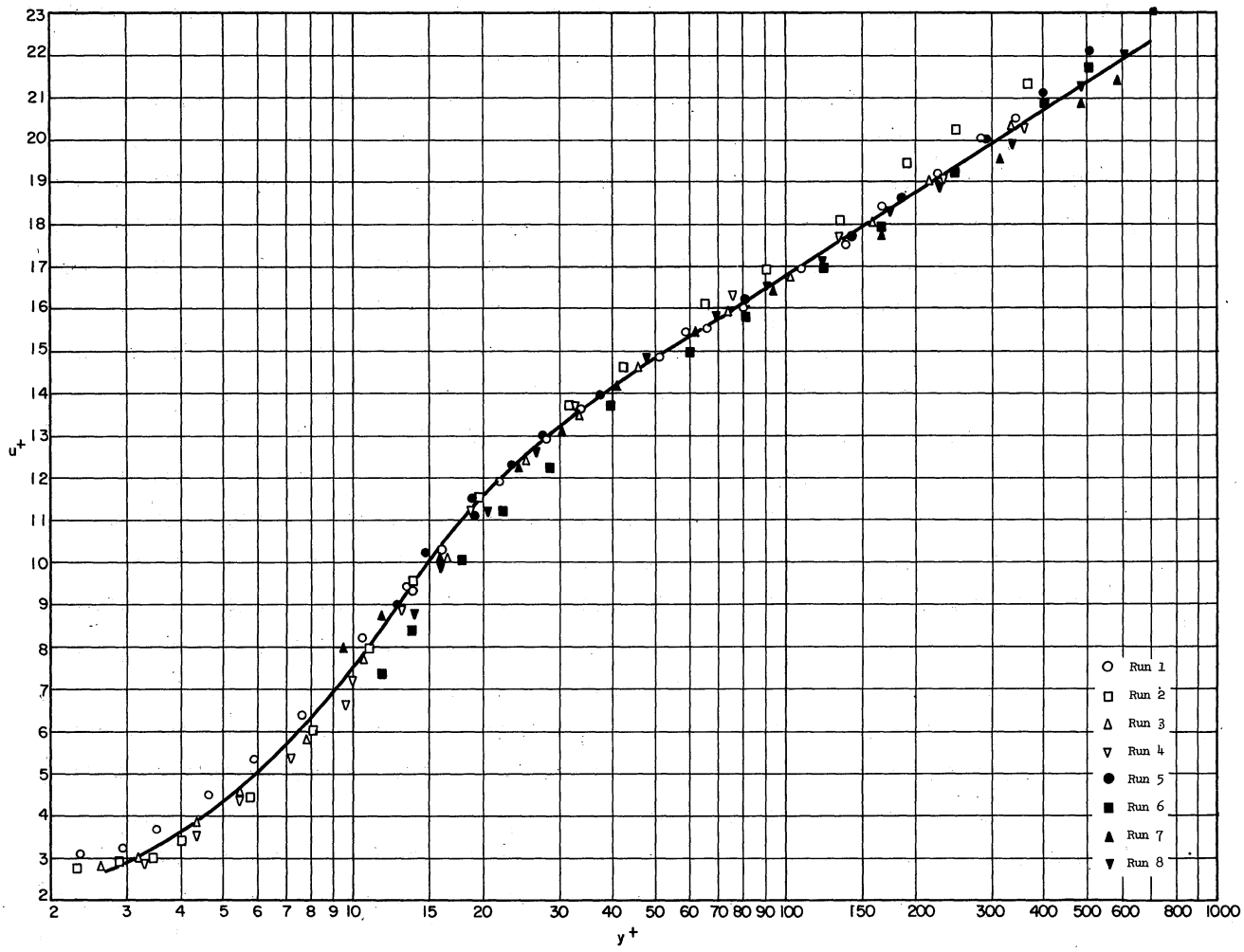

Figure 22. Universal Velocity Distribution for Long Tube Entrance

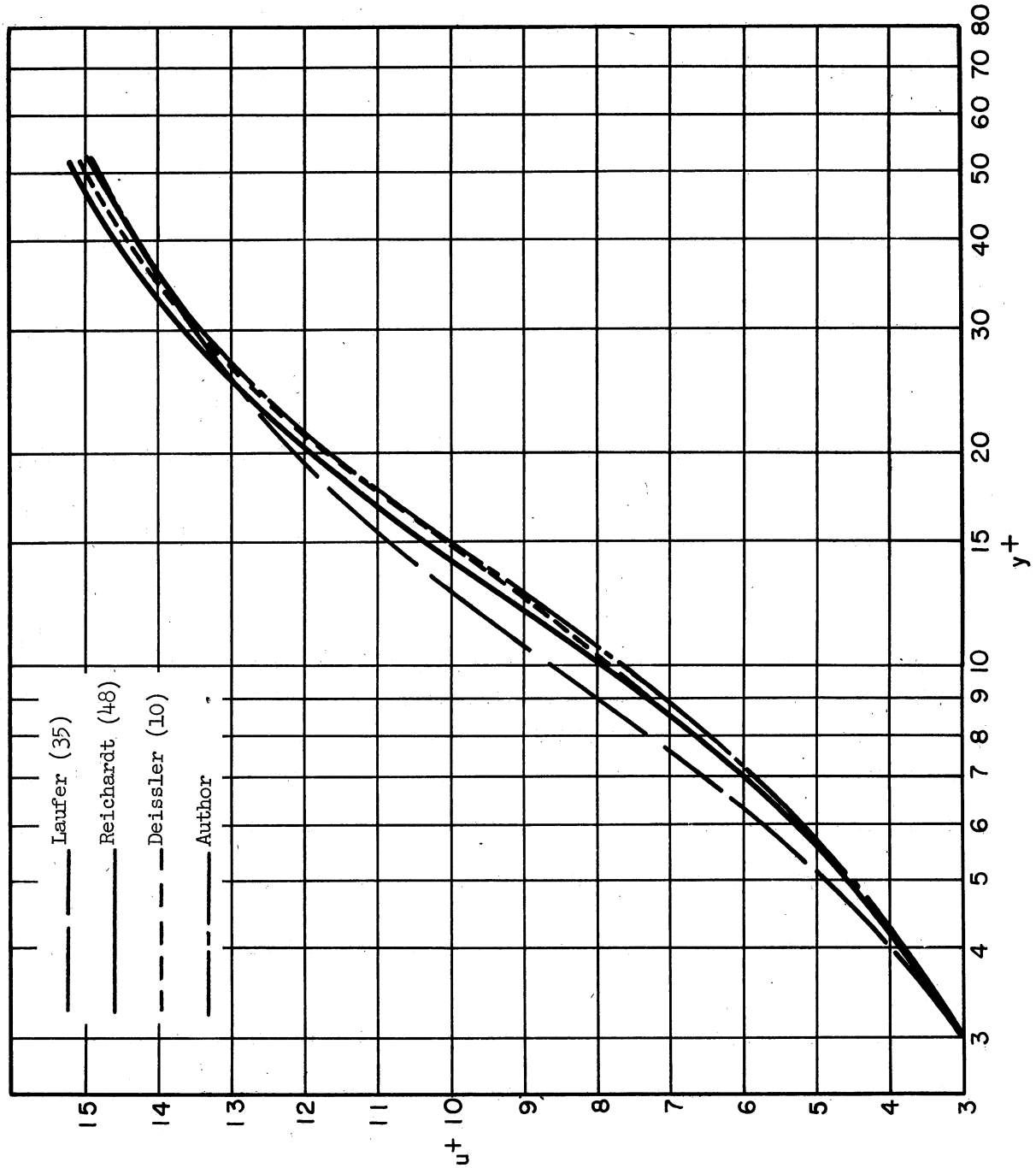

Figure 23. Comparison of Velocity Profiles near a Pipe Wall

becomes large. Equation (19) is valid only for the case where u'/u is negligible compared to unity; in other words, with large velocity fluctuations near the wall the behavior of the wire becomes non-linear. Sleicher[59] derived a correction for this effect of the form

$$u = u_1/[1 - 1/8\ (u'/u)^2]^2 \qquad (30)$$

while Weissberg[62] used the correction

$$u = u_1\ [\ 1 + 1/4\ (u'/u)^2] \qquad (31)$$

Here u_1 is the point velocity computed from the hot wire calibration. Sleicher used the measurements of velocity fluctuations reported by Laufer to compute his correction and found that the maximum correction was 4 percent. A few points calculated for the worst conditions of this investigation indicated that the largest correction would be about 3 percent. Since this is well below the accuracy expected of velocity measurements near the wall, and the profiles appeared to be extrapolating to zero velocity at the wall without the correction, it was not applied here.

As seen in figure 22, for $y^+ < 3$, there is an apparent increase in velocity as the wall is approached. This is due to heat transfer from the heated wire to the wall when they are separated by short distances. Attempts have been made to correct for this effect (Willis[63] and Weissberg[62]); however, the accuracy of the corrections is questionable and none was made here.

No significant difference was found between velocity profiles taken during heating and non-heating runs.

Reduced velocity profiles in the inlet region after the bellmouth entrance are shown in figures 24 and 25. For the Reynolds number of 15,000 the velocity profiles are practically linear for a considerable distance from the wall. It is possible to fit a cubic parabola, characteristic of laminar boundary layers, to these curves (excluding the region outside the hydrodynamic boundary layer.)

In figure 24 it is seen that the slopes at the wall progressively decrease with distance downstream until the X/D of 9.97 is reached. The gradient at this last position is greater than at the one preceding it, indicating that the transition to turbulent flow in the entrance boundary layer is taking place.

For the higher Reynolds number velocity measurements could not be taken close enough to the wall to accurately define the gradient at the wall.

Radial velocity gradients wer

ferencing and drawing smooth equal area

Temperature Profiles

Dimensionless temperature profiles for the long tube entrance are shown in figures 26 and 27, and for the bellmouth in figures 28 and 29. These temperatures were then cross-plotted to obtain the longitudinal temperature profiles, such as those plotted for the long section at Re = 15,000 in figure 30. The points reported by Sleicher for the same entrance at an X/D = 31 have been included.

Longitudinal temperature gradients were determined by differencing the longitudinal profiles and drawing smooth equal area curves. Slopes of the longitudinal profiles were also taken graphically and plotted on the equal area charts as an aid to drawing the

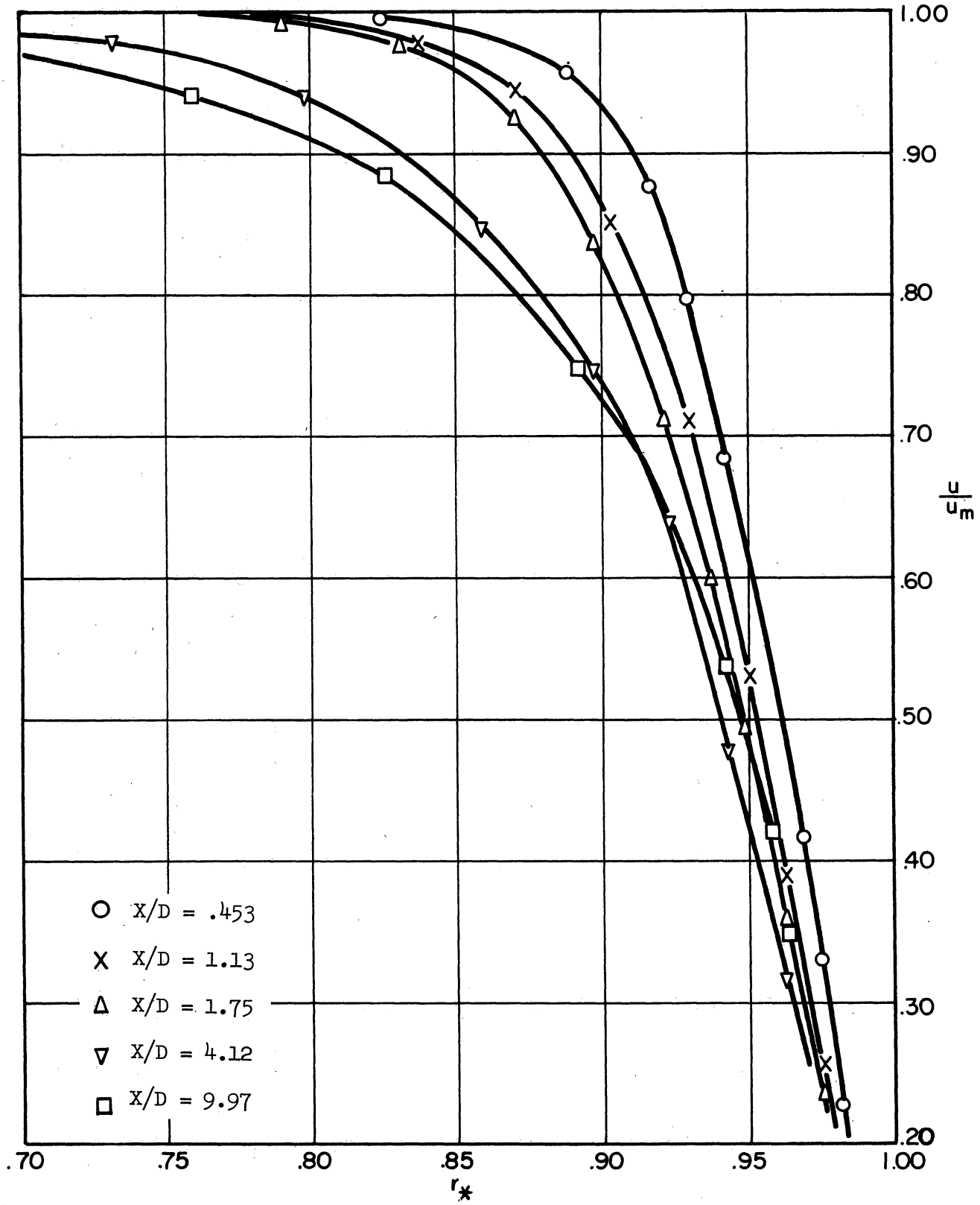

Figure 24. Dimensionless Velocity Distribution after Bellmouth Entrance for Re = 15,000

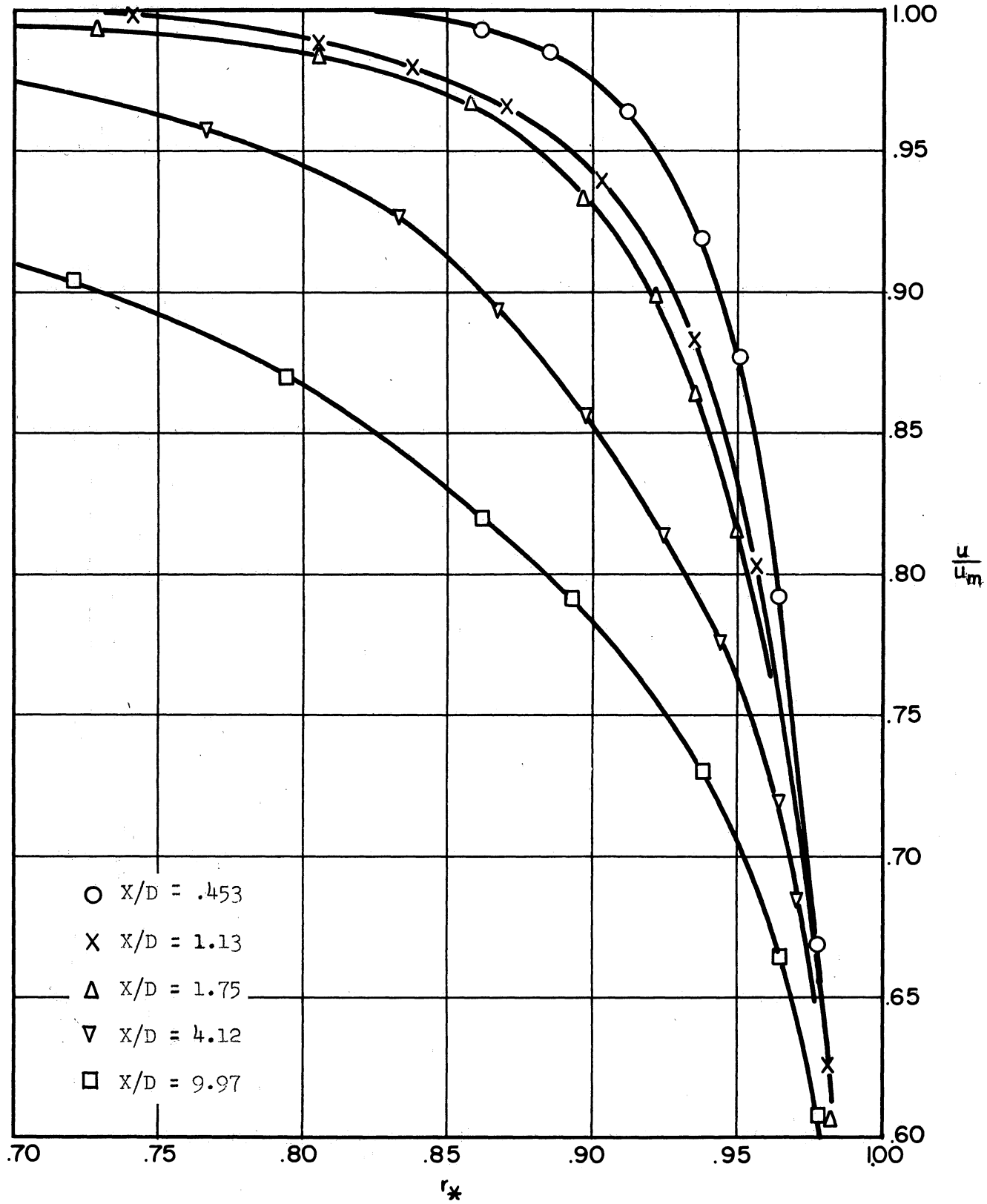

Figure 25. Dimensionless Velocity Distribution after Bellmouth Entrance for Re = 65,000

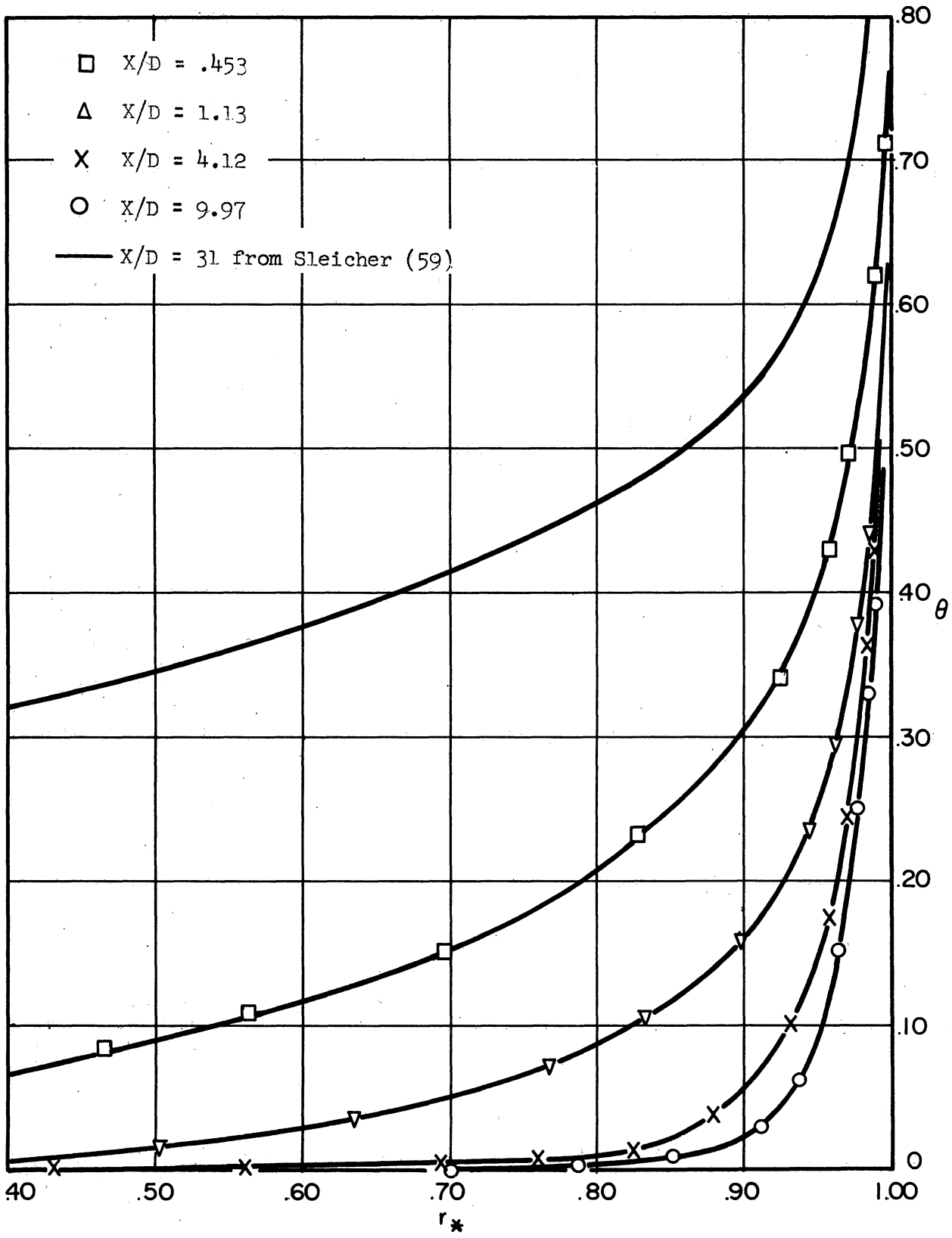

Figure 26. Dimensionless Temperature Distribution for Long Tube Entrance for Re = 15,000

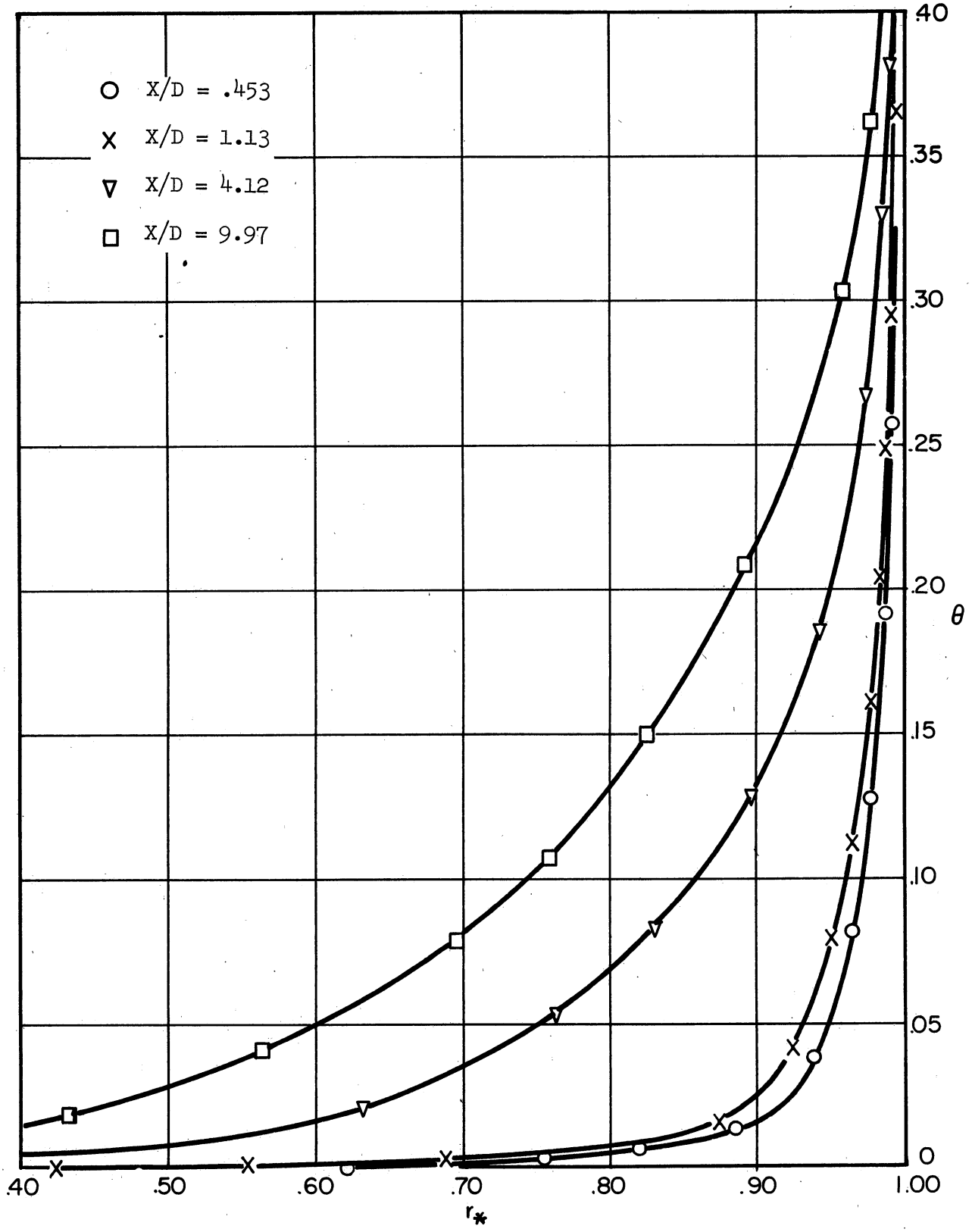

Figure 27. Dimensionless Temperature Distribution for Long Tube Entrance for Re = 65,000

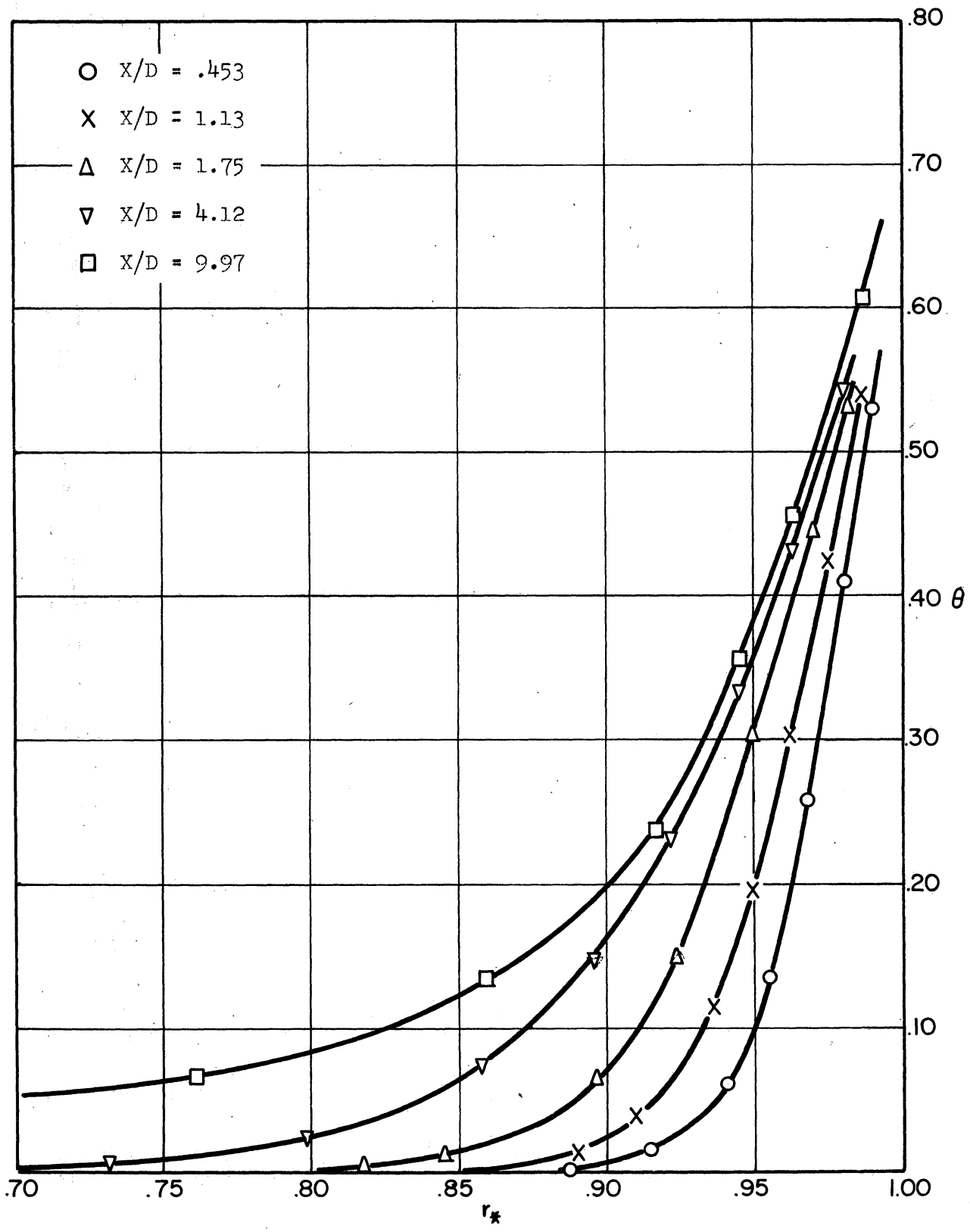

Figure 28. Dimensionless Temperature Distribution for Bellmouth Entrance for Re = 15,000

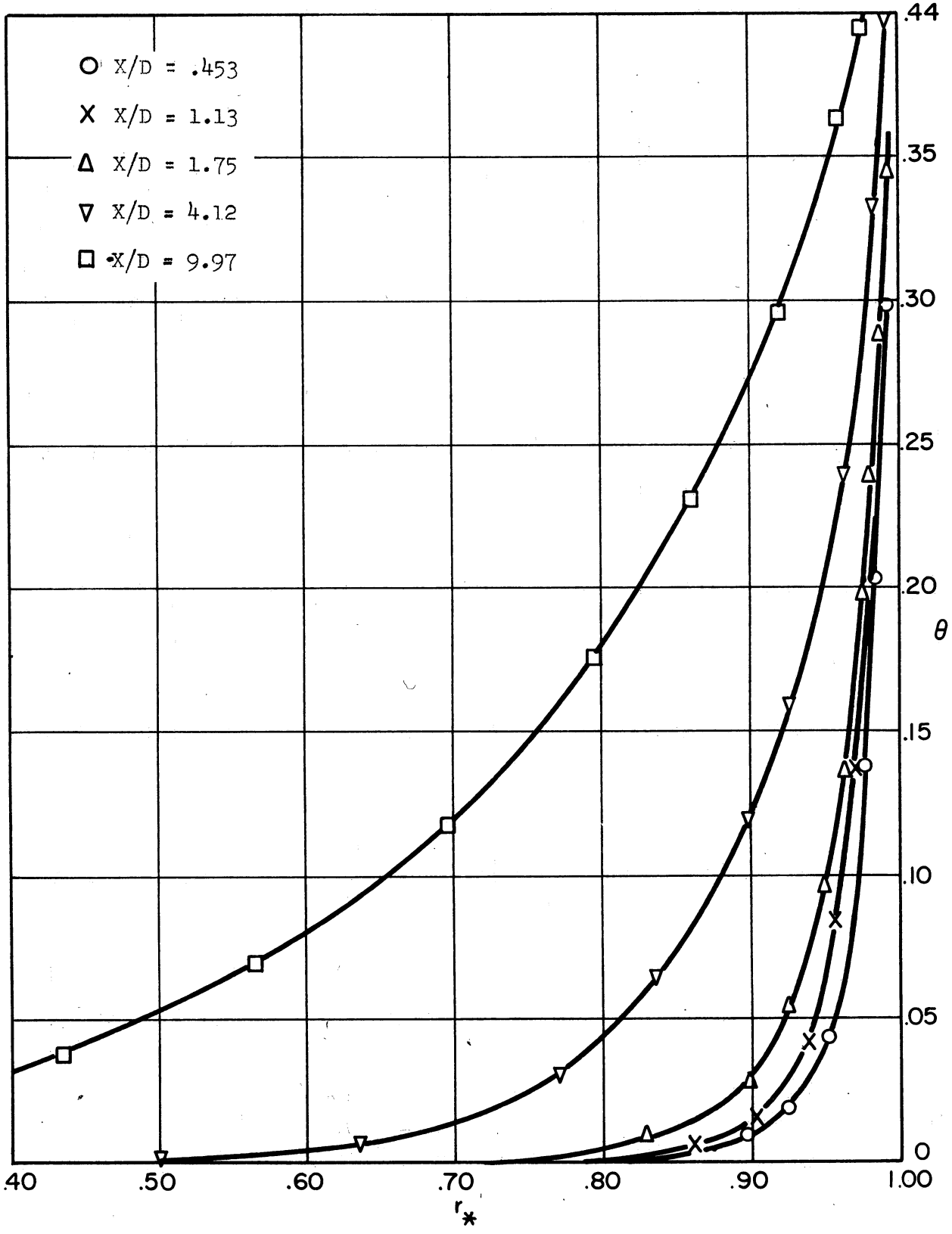

Figure 29. Dimensionless Temperature Distribution for Bellmouth Entrance for Re = 65,000

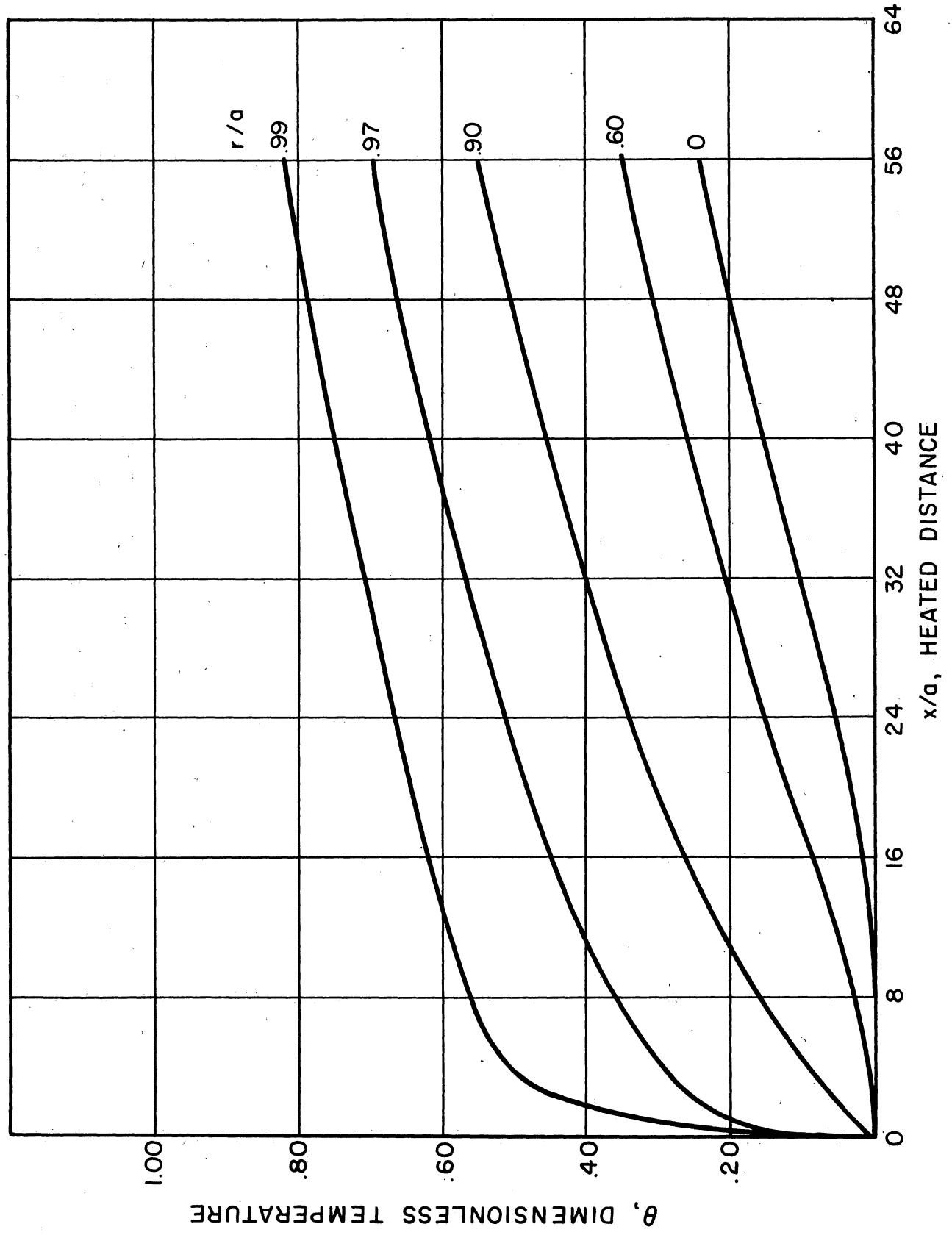

Figure 30. Longitudinal Temperature Distribution for Long Tube Entrance for Re = 15,000

curve. Curves drawn through these points generally gave good equal area fits.

The longitudinal temperature gradients as a function of x/a with r_* as a parameter for the long test section at Re = 15,000 are shown in figure 31. Also plotted is the longitudinal gradient of the mixed mean temperature

$$\frac{d\,\Theta_b}{dZ} = 2\,\frac{Nu}{Pr\ Re}\,\frac{t_w - t_b}{t_w - t_o} \tag{32}$$

where the Nusselt number is obtained from the calorimeter heat flux measurements.

It is seen that far downstream the assumption that the longitudinal temperature gradient at any radius is equal to the mean gradient is quite good, except very near the wall, since for constant wall temperature the longitudinal gradient at the wall is zero. However, near the entrance the assumption is very bad. Of course, in the unheated core outside of the boundary layer in the inlet region the longitudinal temperature gradient is still zero.

For a step change in wall temperature, the longitudinal temperature gradient at the wall would be infinite at x/a = 0 and zero for x/a > 0. From figure 31 it is seen that this condition is approached as one gets very close to the wall (large values of r_*).

In figure 32 the data of figure 31 have been cross-plotted to show the longitudinal temperature gradient as a function of r_*, with x/a as the parameter.

Radial temperature gradients were computed by numerically differencing the data and drawing smoothed equal area curves. A typical curve is shown in figure 33 for run 4.

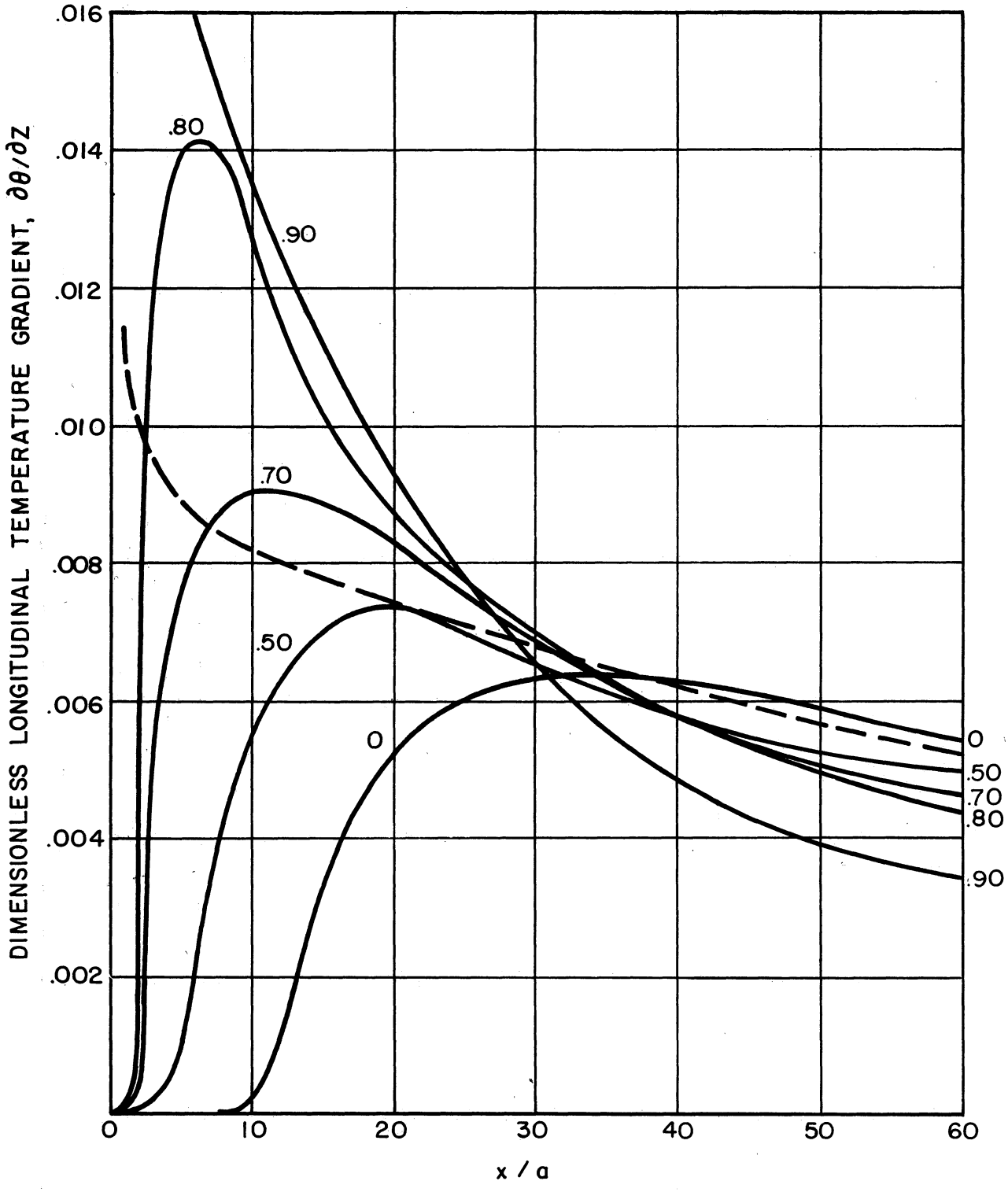

Figure 31. Variation with Length of Longitudinal Temperature Gradient for Long Tube Entrance

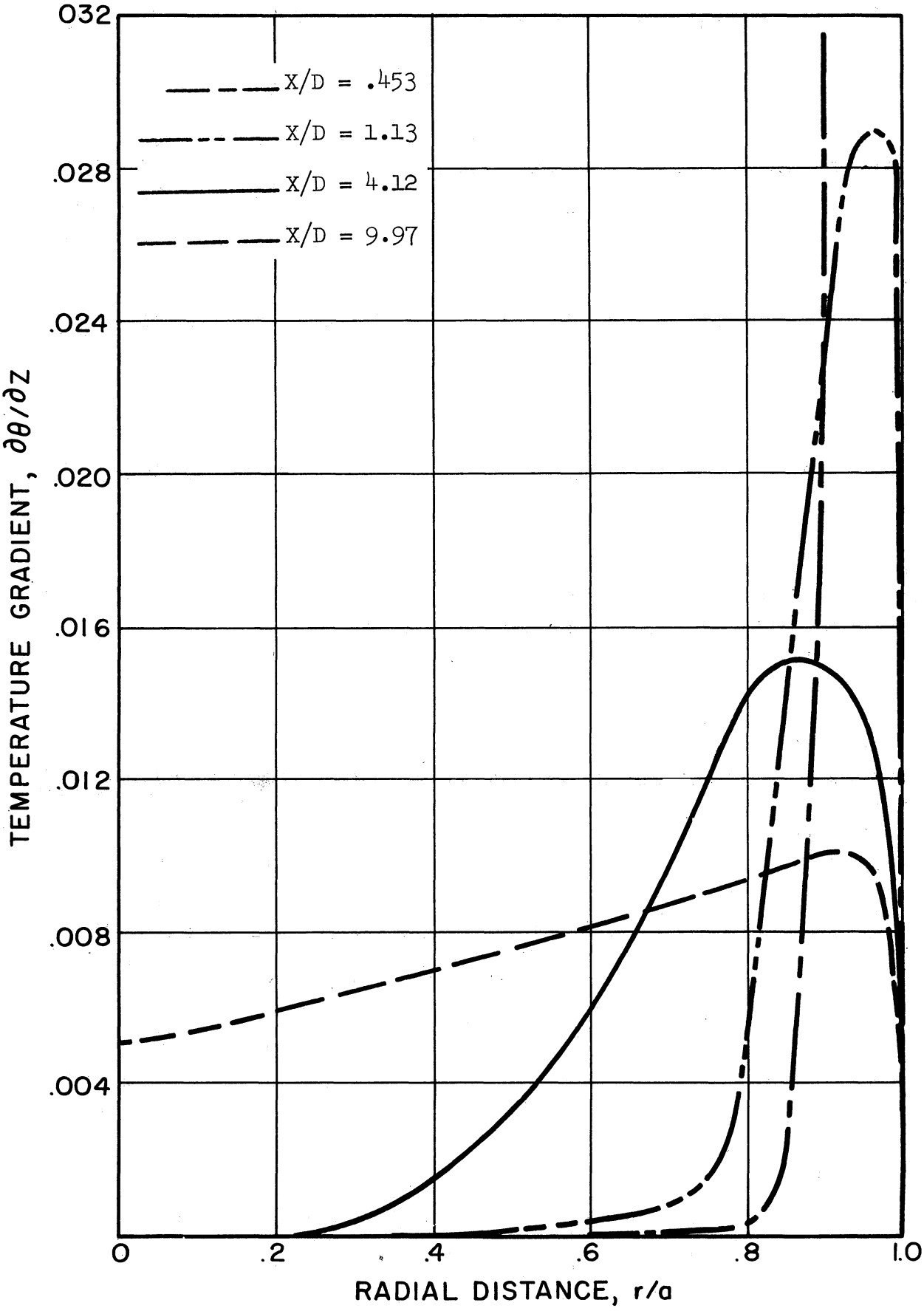

Figure 32. Variation with Radial Distance of Longitudinal Temperature Gradient for Long Tube Entrance for Re = 15,000

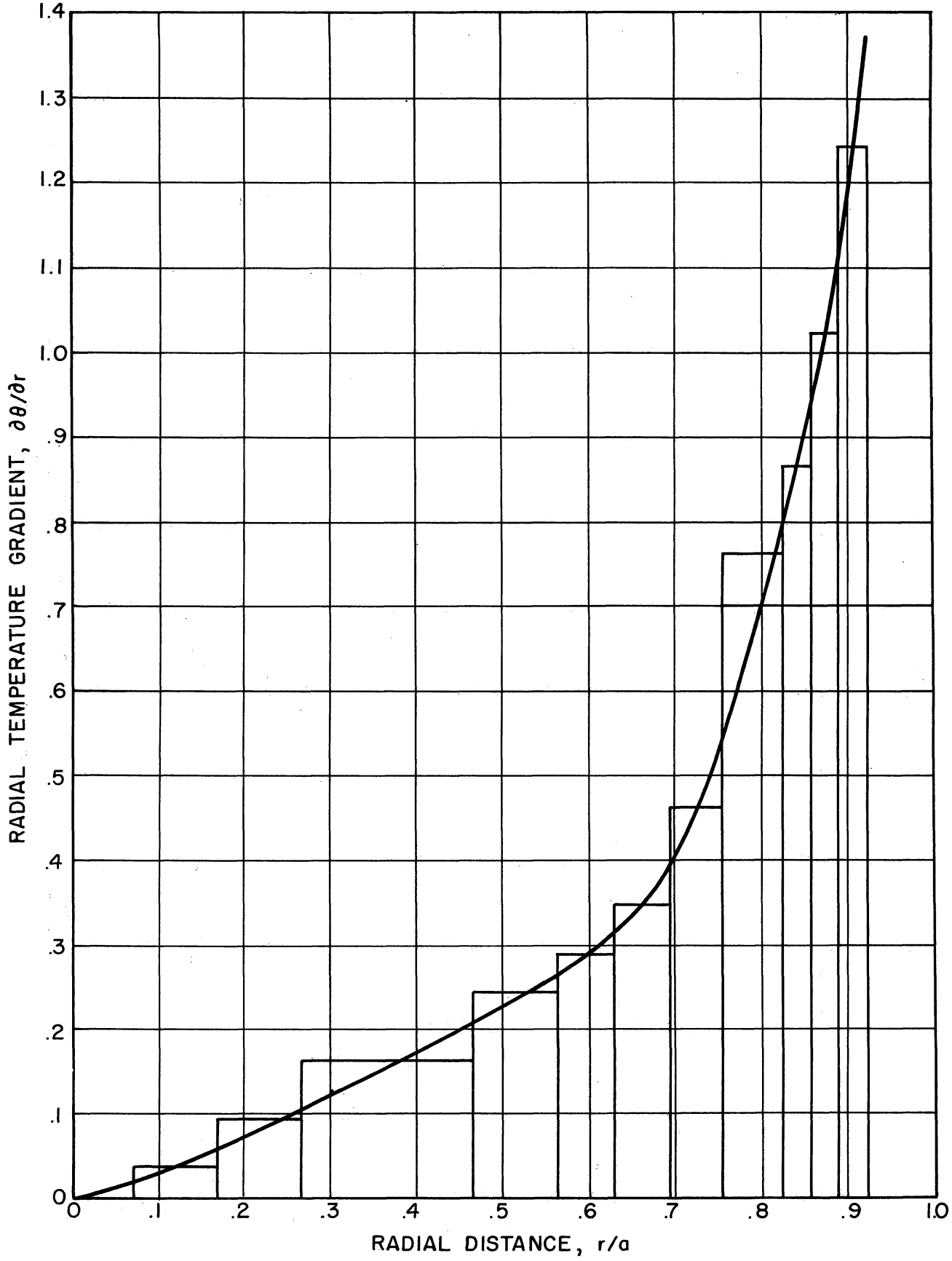

Figure 33. Graphical Differentiation of Radial Temperature Distribution for Run 4.

Eddy Diffusivities

For the long tube entrance eddy diffusivities for momentum transfer were computed from equation (35) and eddy diffusivities for heat transfer from equation (42). The derivation and use of these equations is given in Appendix A. The values for the diffusivities for the long tube entrance are listed in Table II, runs 1 through 8.

For fully developed turbulent flow with constant properties, the velocity profile and the longitudinal pressure gradient are constant, therefore ϵ_ν should not be a function of length. As mentioned under the discussion of velocity profile results, the flow in the thermal inlet region following the long tube entrance was still developing slightly. This caused a slight variation with length of the eddy viscosity distribution in the center of the tube. The maximum deviation (between profiles taken at total L/D's of 44.5 and 54) was about 7 percent. This occurred near the center of the stream. Calculated values of eddy diffusivities are subject to larger error in this region than near the wall because of the very low radial gradients in the tube center. Errors due to this factor may account for most of the variation.

If the turbulent transfer processes for heat and momentum transfer are similar, the eddy conductivity also should not be a function of length for fully developed flow. The values obtained here for ϵ_c at heated X/D's of .453 and 9.97 agreed within 5 percent except for the region next to the unheated core, where radial temperature gradients were very small.

The eddy diffusivities appear to drop off rapidly near the tube center. The same effect was found by Schlinger, et al.[54] and Corcoran[8] for uniform flow between flat plates. Values of eddy

viscosities near the wall agree closely with those obtained by Sleicher[59] for the same entrance.

The variation with radius ϵ_ν/ν and ϵ_c/ν in the thermal inlet region following the long tube entrance is shown for Reynolds numbers of 15,000 and 65,000 in figures 36 and 37 respectively. These values are average values for the X/D's studied.

The variation with radius of the ratio $\alpha = \epsilon_c/\epsilon_\nu$ is shown in figure 41. Values near the center are not plotted, since the temperature gradients in the tube center at the largest X/D were small and the calculated diffusivities were therefore subject to error.

The ratio α increases sharply near the wall, as reported by Corcoran.[9] For the region $.5 < r/a < .9$, the value of α appears to be about 1.5. The effect on α of Reynolds number in the range investigated appears to be small, except for the region close to the wall.

Eddy conductivities for the bellmouth entrance were computed from equation 42 (Appendix A). They are shown as a function of radial distance with X/D as a parameter in figures 38 and 39.

From figure 39 it is seen that ϵ_c increases rapidly with distance downstream in the inlet region. This is because of changes in velocity distribution due to the developing hydrodynamic boundary layer and the transition from laminar to turbulent flow.

Since for Re = 15,000 the bellmouth boundary layer starts out laminar, the eddy conductivity near the inlet would be expected to be equal to zero. As shown in figure 38, ϵ_c is very small at the lowest X/D and increases with distance down the tube as the transition to the turbulent boundary layer occurs.

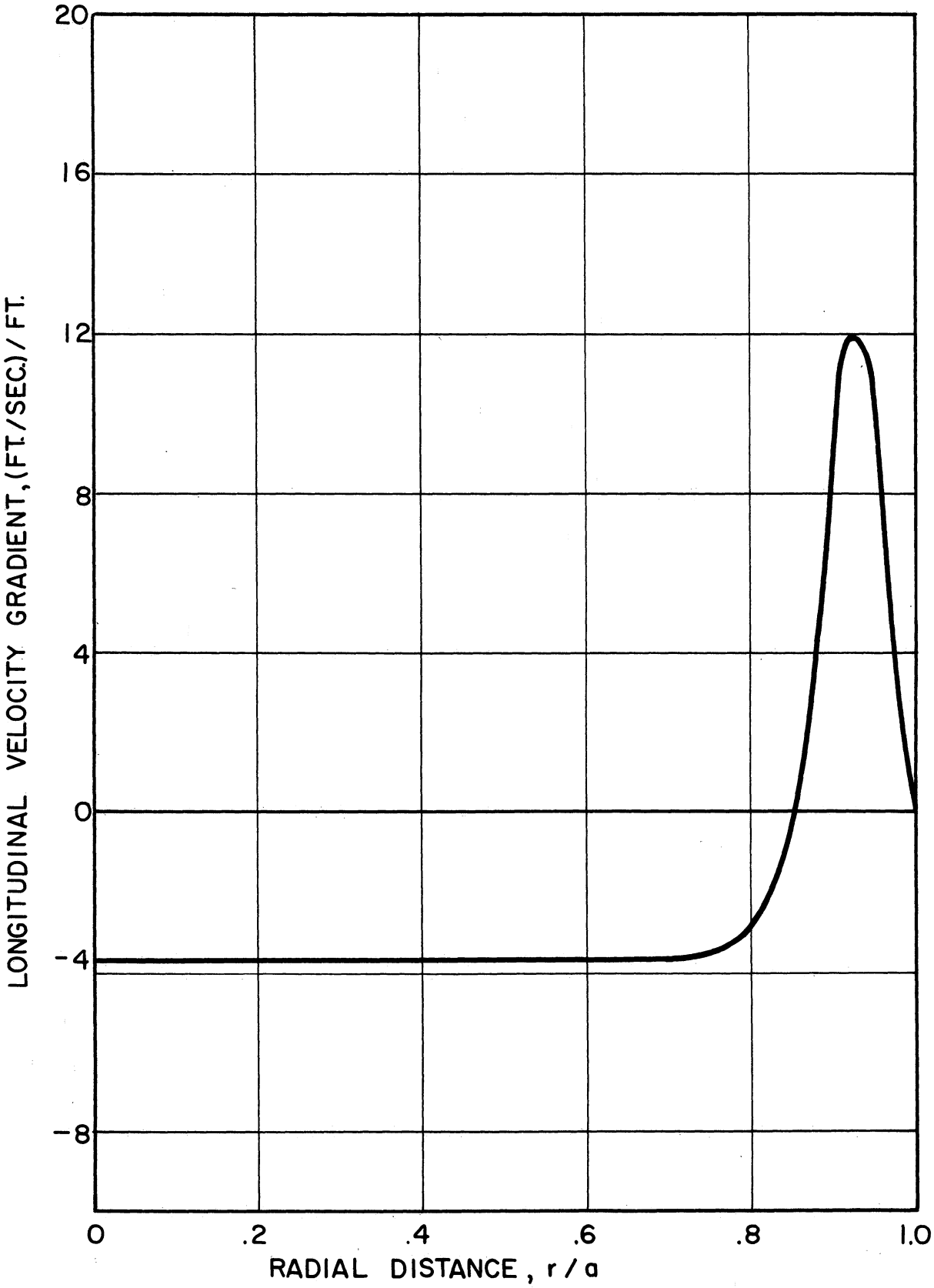

Figure 34. Longitudinal Velocity Gradient 1.5 Diameters after Bellmouth Entrance for Re = 15,000

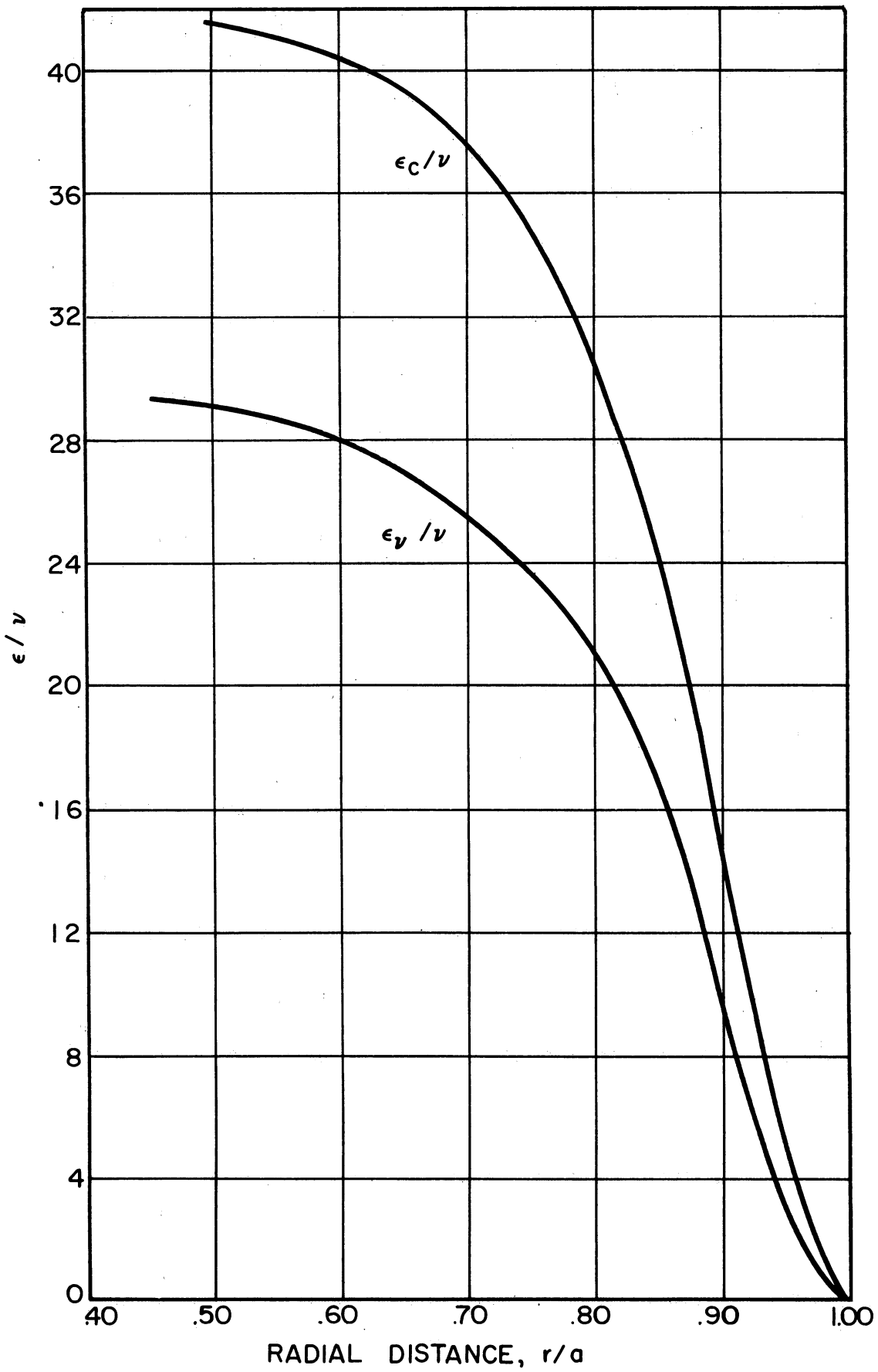

Figure 36. Variation with Radius of Eddy Diffusivities for Long Tube Entrance for Re = 15,000

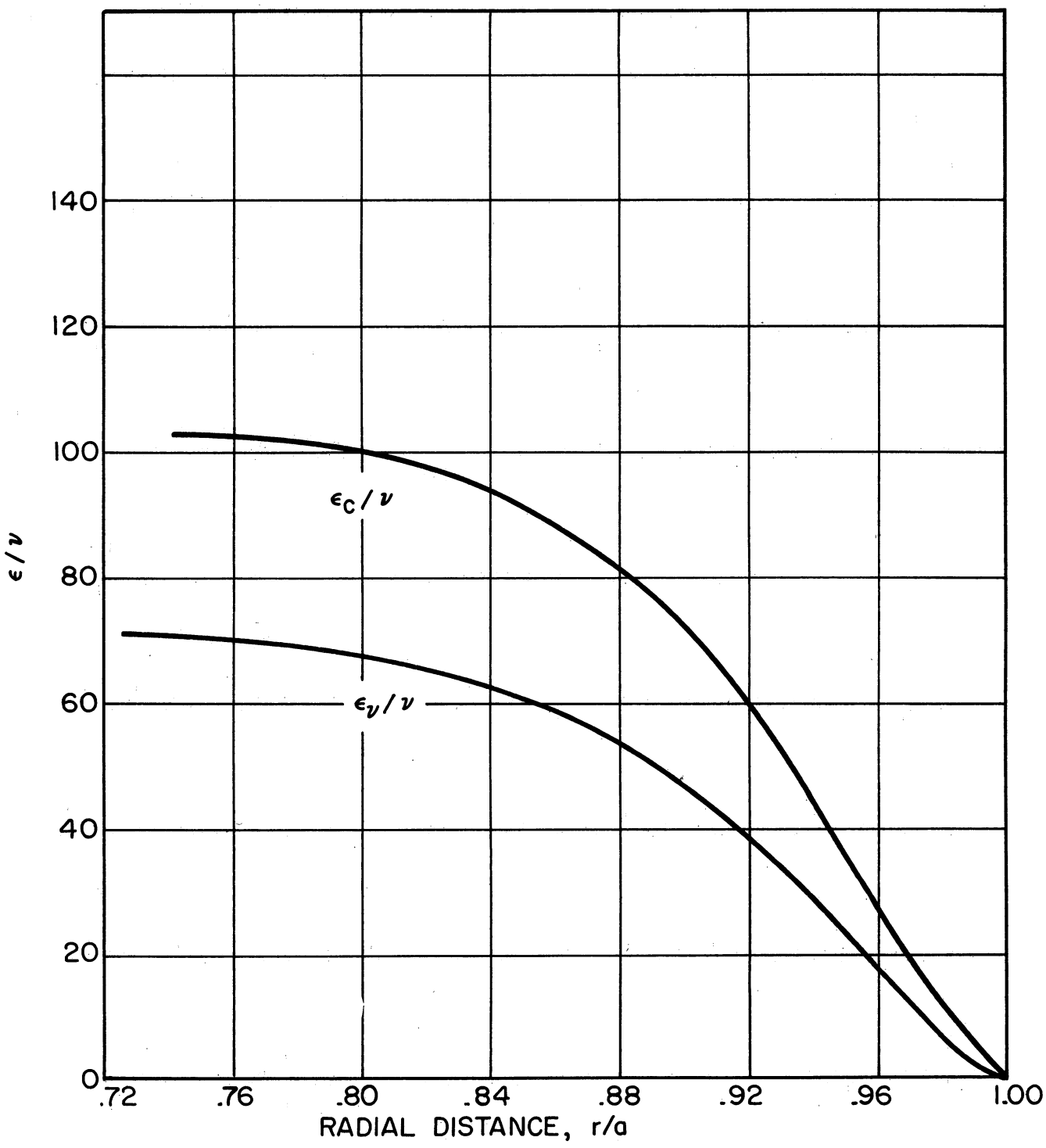

Figure 37. Variation with Radius of Eddy Diffusivities for Long Tube Entrance for Re = 65,000

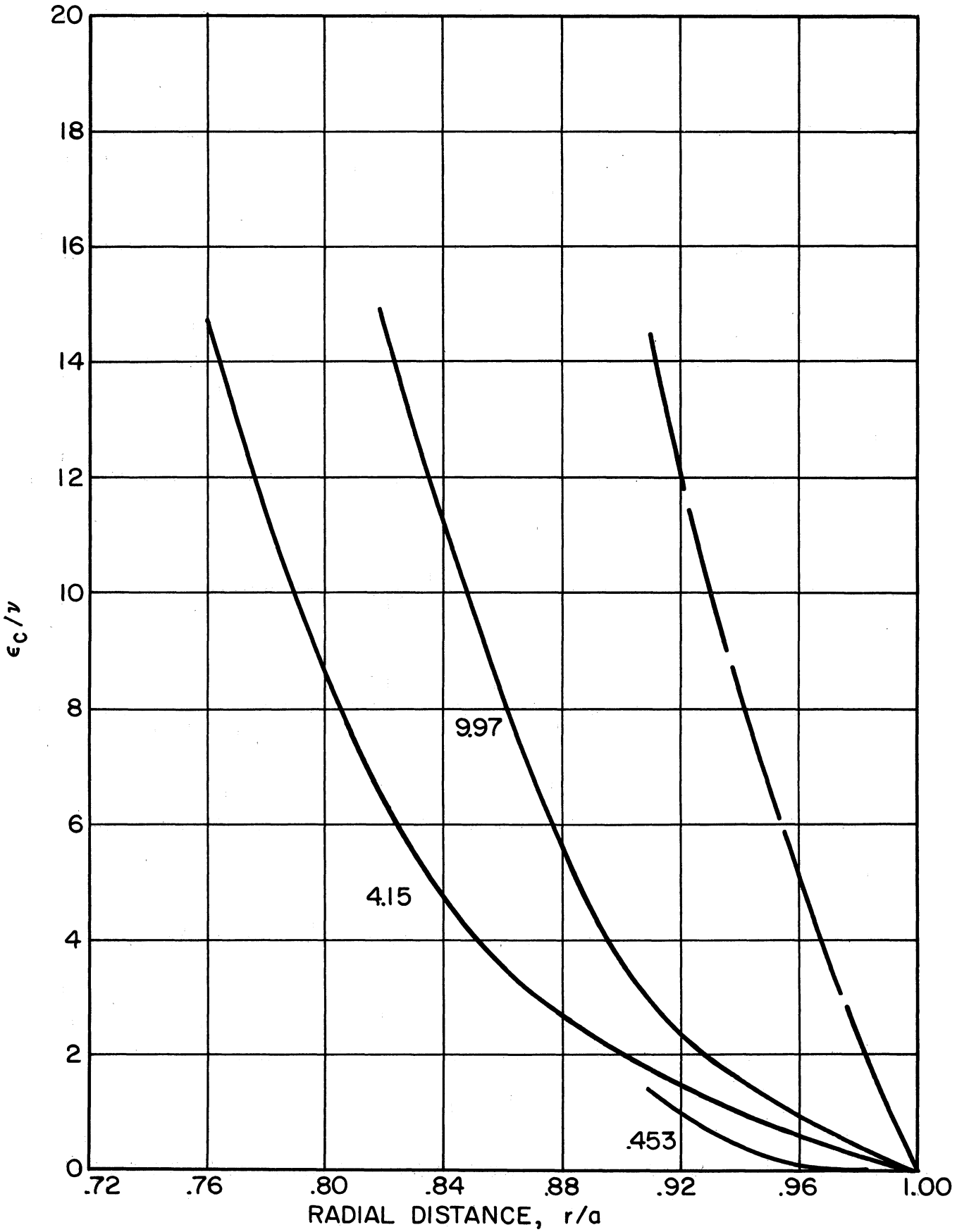

Figure 38. Radial Distribution of ϵ_c/ν in Inlet Region for Bellmouth Entrance for the X/D's Shown (Broken Line for Long Tube Entrance). Re = 15,000

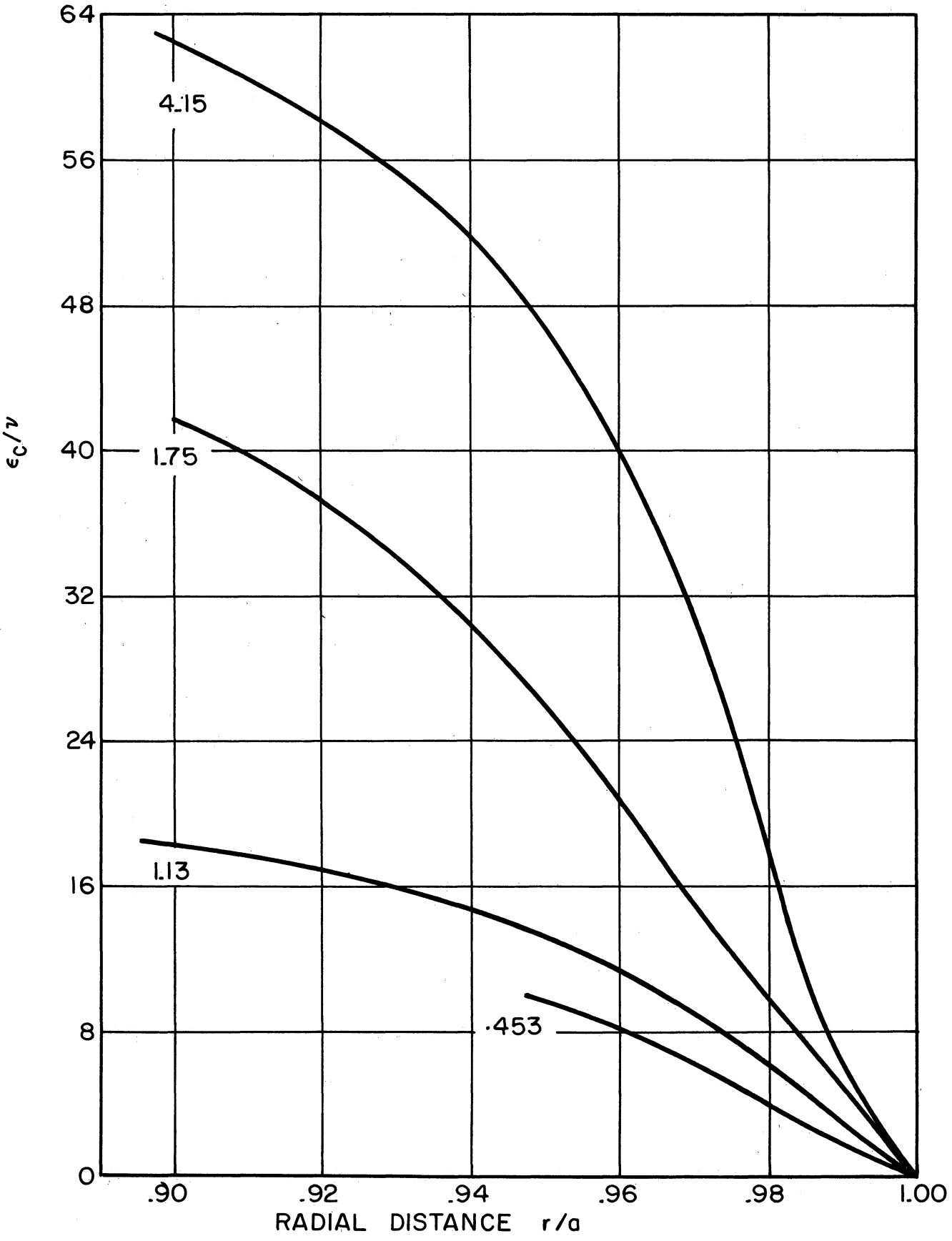

Figure 39. Radial Distribution of ϵ_c/ν in Inlet Region for Bellmouth Entrance for the Four X/D's Shown. Re = 65,000

As discussed in Appendix A, eddy viscosities in the bellmouth inlet region for laminar flow computed from equation 35 are inaccurate, since this equation neglects the core acceleration due to the development of the laminar boundary layer.

That the acceleration term must be included is further substantiated by the fact that the total viscosities computed by equation 35 for the bellmouth inlet with Re = 15,000 are below the value of the molecular viscosity.

This effect was also observed at the high Reynolds number. Thus, no reliable figures for the eddy viscosity in the bellmouth inlet region can be obtained from this investigation.

Radial Heat Flux

As shown in Appendix A, the function

$$\Phi = \int_0^{r_*} U\, r_* \frac{\partial \Theta}{\partial Z}\, d\, r_*$$

is proportional to the radial heat flux. The function is listed for runs 1 through 18 in Table II.

The radial heat flux for run 4, computed as outlined in Appendix A, is shown in figure 40. For the region $0 < y^+ < 10$, the heat flux is approximately equal to that at the wall. For y^+ greater than 10, the variation of heat flux with radius is very nearly linear. Thus the assumption made by Martinelli and others[39] of constant radial heat flux near the wall and a linear distribution in the turbulent core appears to be a good one. Of course, if the thermal boundary layer has not merged, the heat flux diminishes to zero at the edge of the boundary layer.

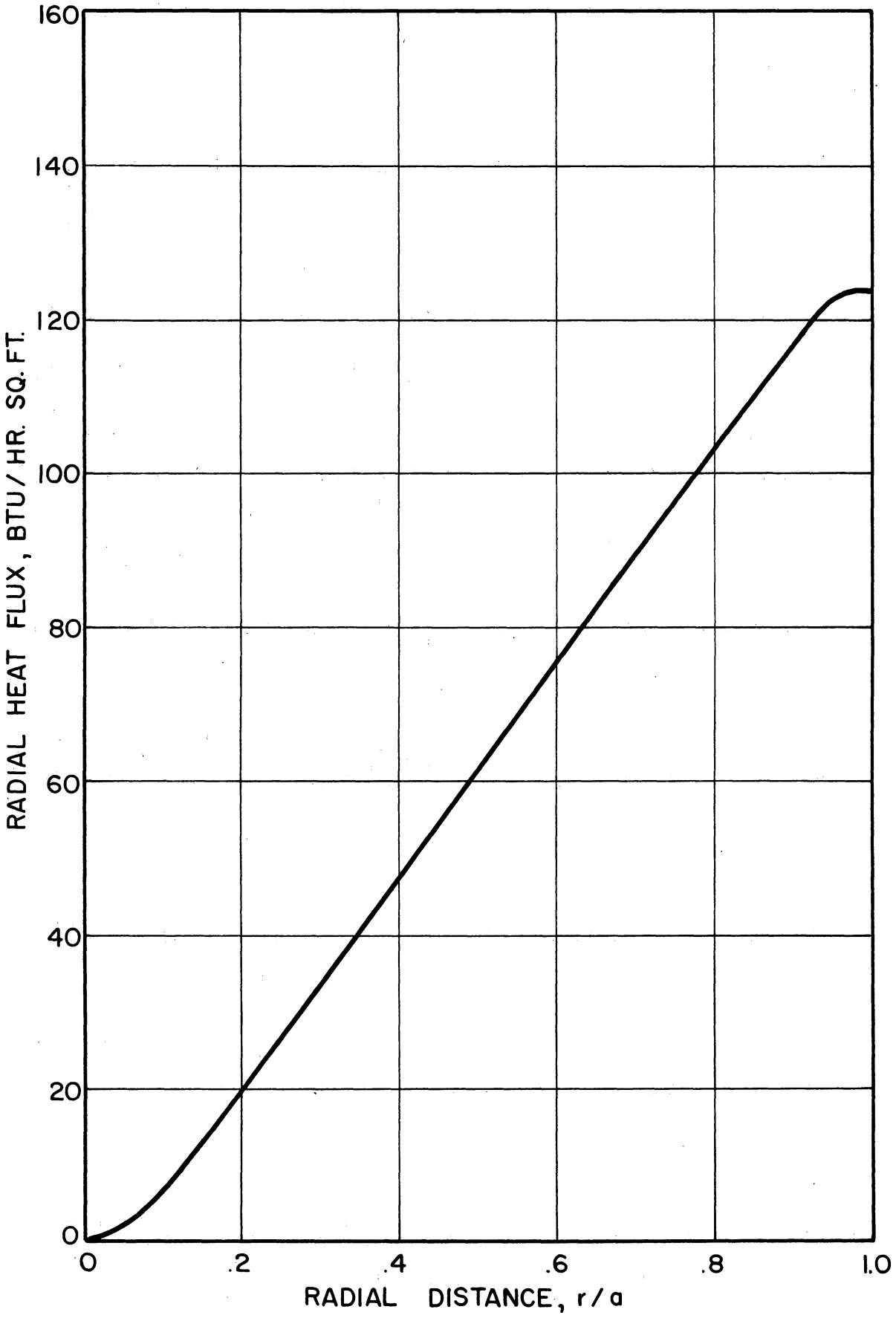

Figure 40. Radial Heat Flux Distribution for Run 4.

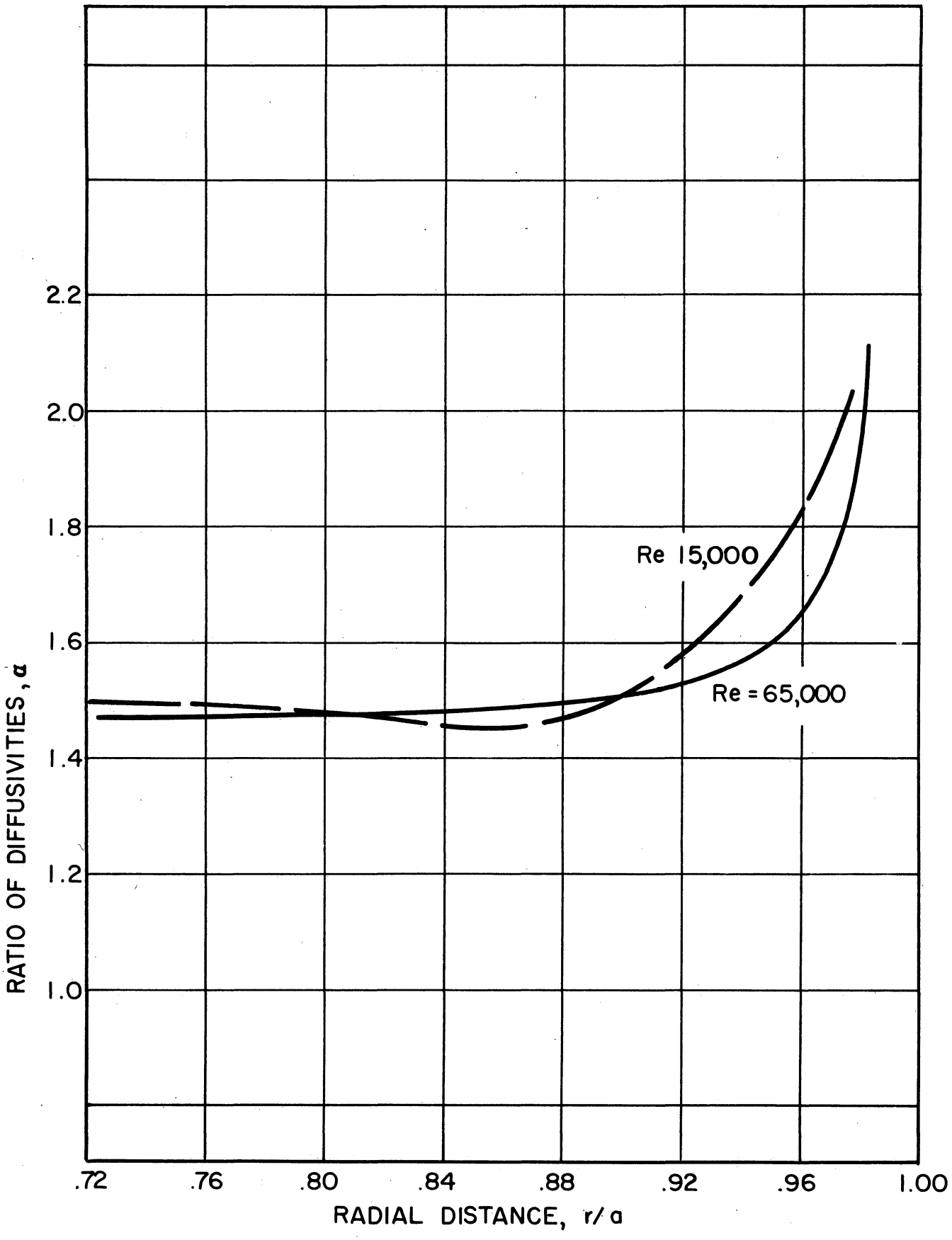

Figure 41. Variation with Radius of the Ratio $\alpha = \frac{\epsilon_c}{\epsilon_\nu}$ for the Long Tube Entrance

CONCLUSIONS

1) Significant differences in heat and momentum transfer in the inlet region are caused by the two initial velocity distributions studied in this investigation.

2) These differences are due to variations in the velocity gradient in the boundary layers developing downstream from the inlet. In addition, the bellmouth produces an initially laminar boundary layer with resulting reductions in heat transfer rate and pressure drop.

3) At a Reynolds number of 15,000, acceleration effects account for about 70 percent of the pressure drop directly downstream from the bellmouth entrance.

4) For both initial velocity distributions studied, the thermal boundary layer had merged and the Nusselt number reached within 3 percent of its asymptotic value within ten diameters after the start of heating.

5) For fully developed turbulent flow, the eddy diffusivities for heat and momentum transfer in the thermal inlet region vary with radius and Reynolds number, but not length. The ratio ϵ_c/ϵ_ν varies with radius and slightly with Reynolds number. For the region $.5 < r/a < .9$, the range of variation is from about 1.4 to 1.6. The ratio increases sharply near the wall.

6) Eddy conductivities in the bellmouth inlet region are very low directly downstream from the inlet because of the presence of a laminar boundary layer. The conductivities gradually increase with distance downstream.

7) To accurately calculate eddy viscosities in the bellmouth inlet region, one must include acceleration effects due to the developing hydrodynamic boundary layer. Neglect of these effects results in negative eddy diffusivities.

8) The assumption of constant radial heat flux in the laminar sub-layer and the buffer layer, and a linear heat flux distribution in the turbulent core, is good, except possibly very close to the entrance.

9) Theoretical analyses which postulate the same distribution of eddy conductivity in developing thermal boundary layers as for fully developed ones are valid for the case of fully developed hydrodynamic boundary layers in the thermal entrance region, but may be subject to large error when the hydrodynamic and thermal boundary layers develop simultaneously.

10) For fully developed thermal boundary layers, the longitudinal temperature gradient at any radius is approximately equal to the longitudinal gradient of the mixed mean temperature, at points very close to the wall. This relationship is not true when thermal boundary layers are not fully developed.

APPENDIX A

CALCULATION OF EDDY DIFFUSIVITIES

APPENDIX A

CALCULATION OF EDDY DIFFUSIVITIES

The equations used in computing the eddy diffusivities for heat and momentum are derived below and the method of computing the diffusivities outlined.

Eddy Viscosities

The momentum equation in the x direction for laminar flow in a pipe inlet is[18]

$$u \frac{\partial u}{\partial x} + v \frac{\partial u}{\partial r} = - \frac{g_c}{\rho} \frac{\partial p}{\partial x} + \nu \left(\frac{\partial^2 u}{\partial r^2} + \frac{1}{r} \frac{\partial u}{\partial r} + \frac{\partial^2 u}{\partial x^2} \right) \qquad (33)$$

From boundary layer theory the third term in the brackets may be neglected. Assuming that eddy and molecular diffusivities may be directly added, equation (33) written for turbulent flow is

$$u \frac{\partial u}{\partial x} + v \frac{\partial u}{\partial r} = - \frac{g_c}{\rho} \frac{\partial p}{\partial x} + \frac{1}{r} \frac{\partial}{\partial r} \left[r (\nu + \epsilon_\nu) \frac{\partial u}{\partial r} \right] \qquad (34)$$

where the diffusivities for momentum have been placed inside the derivative sign since ϵ_ν is a function of radius.

For fully developed flow $\frac{\partial u}{\partial x}$ and v are equal to zero and equation (34) reduces to

$$\frac{1}{\rho} \frac{\partial p}{\partial x} = \frac{1}{r} \frac{\partial}{\partial r} \left[r \, (\nu + \epsilon_\nu) \frac{\partial u}{\partial r} \right] \qquad (35)$$

Integrating, with ρ considered constant,

$$\nu + \epsilon_\nu = \frac{g_c}{\rho} \frac{\partial p}{\partial x} \frac{r}{2} \Big/ \frac{\partial u}{\partial r} \qquad (36)$$

Using the relation $\frac{\partial p}{\partial x} = \frac{2}{r} \tau_w$ and the linear shear stress law for fully developed flow, it may be shown that equation (36) is the same as equation (10), the defining equation for eddy viscosity in fully developed flow. Introducing the dimensionless variables r_* and U, equation (36) becomes

$$\nu + \epsilon_\nu = \frac{1}{2} \frac{g_c}{\rho} \frac{\partial p}{\partial x} \frac{(r_o)^2}{u_m} \frac{r_*}{\frac{\partial U}{\partial r_*}} \tag{37}$$

Eddy viscosities for the long tube entrance were computed from equation (37).

The expression for eddy viscosity in the hydrodynamic entrance region is obtained by integration of equation (34):

$$\nu + \epsilon_\nu = \frac{\int_0^r r\, u \frac{\partial u}{\partial x}\, dr + \int_0^r r\, v \frac{\partial u}{\partial r}\, dr + \frac{g_c}{\rho} \frac{\partial p}{\partial x} \frac{r^2}{2}}{r \frac{\partial u}{\partial r}} \tag{38}$$

The analysis under Pressure Drop in Chapter V of the relative magnitude of pressure drop due to wall skin friction and that due to momentum changes in the inlet region indicates that the sum of the two integrals in equation (38) is appreciable with respect to the $\frac{dp}{dx}$ term. The evaluation of both of the integrals involves a knowledge of the longitudinal velocity gradient, which appears explicitly in the first integral and implicitly in the second since v is obtained from the continuity equation

$$\frac{\partial u}{\partial x} + \frac{1}{r} \frac{\partial (vr)}{\partial r} = 0 \tag{39}$$

The evaluation of longitudinal velocity gradients from experimental velocity profiles, especially near the edge of the hydrodynamic boundary layer, is very difficult, since the order of magnitude of the changes in velocity at corresponding radii between two adjacent traverses is of the same order of magnitude as the experimental error. This problem is further complicated by the fact that it was necessary to make separate runs for each X/D investigated. Since increases in core velocity between adjacent profiles due to deceleration in the boundary layer were on the order of one percent, differences in flow rate of one percent between runs would be sufficient to yield a zero or even negative longitudinal velocity profile in the core.

Because of these difficulties it was decided not to compute the values of the integrals for all cases. The eddy viscosities reported in Table II for the bellmouth were computed using only the $\frac{dp}{dx}$ term. This is equivalent to using a linear distribution of shear stress with radius, which is rigorously correct only for fully developed flow. The assumption is worst right at the inlet and progressively better at greater X/D's.

To estimate the magnitude of the maximum error caused by this approximation, the two integrals in equation (38) were evaluated at an X/D of 1.5 for Re = 15,000. Integrating the continuity equation (39), one obtains

$$r\,v\Big]_0^r = \int_0^r r\,\frac{\partial u}{\partial x}\,dr \qquad (40)$$

The integral was evaluated graphically, using the estimated values of $\frac{\partial u}{\partial x}$ shown in figure 34. The value of the integral must be zero at both

$r = 0$ and $r = r$, since v is zero at the wall. This condition was fulfilled by the graphical integration, indicating that the values used for $\frac{\partial u}{\partial x}$ were reasonable.

Values of the three terms on the right side of equation (40) are tabulated as a function of r in Table III. It is seen that although the first term may be neglected except very close to the wall, the second term may be as much as 1-1/3 times as great as the $\frac{dp}{dx}$ term. Thus values of eddy viscosity computed by neglecting momentum transfer due to boundary layer development are not reliable in the region close to the inlet.

Table III also lists values of radial velocity at several radii for the bellmouth entrance at an X/D of 1.5 and Reynolds number of 15,000. Axial velocities at corresponding points are included for comparison. The largest ratio of radial to axial velocity found was .0037 at r_* of about .85.

Eddy Conductivities

The equation for eddy conductivity for fully developed flow is obtained by integration of equation (16):

$$\frac{k}{\rho C_p} + \epsilon_c = \frac{\int_0^r u\, r \frac{\partial t}{\partial x}\, dr}{r \frac{\partial t}{\partial r}} \qquad (41)$$

As mentioned previously this equation neglects axial conduction, heating due to pressure changes, and frictional dissipation. Introducing the dimensionless variables U, Θ, and r_*, equation (41) becomes

$$\frac{k}{\rho C_p} + \epsilon_c = \frac{u_m \, a \int_0^{r_*} r_* \, U \, \frac{d\Theta}{dZ} \, d r_*}{r_* \, \frac{d\Theta}{dr_*}} \qquad (42)$$

This relation was used for computing eddy conductivities in the thermal inlet region following the long tube entrance.

For the bellmouth entrance a term must be added to equation (41) to account for radial transfer of heat by convection due to the development of the hydrodynamic boundary layers:

$$\frac{k}{\rho C_p} + \epsilon_c = \frac{\int_0^r u \, r \, \frac{\partial t}{\partial x} \, dr + \int_0^r v \, r \, \frac{\partial t}{\partial r} \, dr}{r \, \frac{\partial t}{\partial r}} \qquad (43)$$

Using the radial velocities from Table III the magnitude of the radial flow term in equation (43) was estimated at X/D = 1.5. It was found that the maximum error introduced by neglect of this term was 11 percent. The percentage error decreases with distance downstream. The radial convection term was therefore neglected in computing eddy conductivities for the bellmouth. This assumption introduced only small errors except possibly for the first X/D.

Radial Heat Flux

The radial heat flux at any radius in a tube is given by

$$q(r) = \frac{\rho \, C_p \int_0^r r \, \frac{\partial ut}{\partial x} \, dr}{r} \qquad (44)$$

For constant u (fully developed flow), the u may be taken out of the derivative. Then, introducing U, r_*, and Θ, equation (44) becomes:

$$q(r) = \frac{\rho C_p (t_w - t_o) u_m \int_0^{r_*} r_* U \frac{\partial \Theta}{\partial Z} dr_*}{r_*}$$

$$= \frac{\rho C_p (t_w - t_o) u_m \Phi}{r_*} \qquad (45)$$

The radial heat flux is therefore proportional to the integral Φ, which appears in the expression for eddy conductivity and is tabulated in Table II.

If the flow is not fully developed, a slight error is introduced by computing radial heat fluxes from equation (45), since u is not now a constant and should be left inside the differential sign.

APPENDIX B

Table I. Gross Values for Heat Transfer Runs

Table II. Point Values for Temperature and Velocity Traverses

Table III. Momentum Terms in the Entrance Region for Bellmouth Entrance. X/D = 1.5 Re = 15,000

Figure 35. Calibration for Chromel-Constantan Thermocouples

TABLE I. GROSS VALUES FOR HEAT TRANSFER RUNS

Run	$\frac{X}{D}$	Re	W	ΔT	q	h	Nu
			LONG TUBE ENTRANCE				
1	.453	15,000	66.6	24.5	207	8.45	69.4
2	1.13	14,780	66.0	26.7	174	6.53	53.7
3	4.12	14,860	66.4	25.0	147	5.87	47.8
4	9.97	14,700	65.8	21.1	121	5.72	46.6
5	.453	64,100	285.0	22.6	551	24.4	201.0
6	1.13	64,200	287.0	28.9	601	20.8	172.0
7	4.12	63,800	284.0	24.6	462	18.7	154.0
8	9.97	64,900	290.0	22.9	390	17.0	140.0
			BELLMOUTH ENTRANCE				
9	.453	14,830	66.0	25.9	149	5.74	47.2
10	1.13	14,820	66.1	27.3	119	4.37	35.9
11	1.75	14,800	66.0	27.4	98.3	3.59	29.5
12	4.12	14,910	66.3	29.1	78.9	2.71	22.4
13	9.97	14,820	66.2	27.5	79.1	2.88	23.7
14	.453	63,900	284.0	20.1	387	20.4	167.0
15	1.13	65,500	291.0	27.7	535	19.3	159.0
16	1.75	64,200	286.0	26.0	456	17.9	146.0
17	4.12	65,300	290.0	29.8	546	18.3	150.0
18	9.97	65,350	290.0	22.1	388	17.6	144.0

TABLE II. POINT VALUES FOR TEMPERATURE AND VELOCITY TRAVERSES

Run 1 — u_b = 20.7 ft/sec — t_w = 104.01°F

Long Tube Entrance — u^* = 1.22 ft/sec — t_b = 79.60°F

Heated L/D = .453 — $\left(\frac{\partial\Theta}{\partial Z}\right)_b$ = .0130 — ρ = .0707 lb/cu ft

Re = 15,000 — t_o = 79.35°F — $k/\rho C_p$ = .000251 sq ft/sec

y in.	r in.	$\frac{r}{a}$	t °F	Θ	$\frac{\partial\Theta}{\partial\frac{r}{a}}$	$10^2\frac{\partial\Theta}{\partial Z}$	u ft/sec	U	$10^3\,\Phi$	$\frac{\epsilon_c}{\nu}$	$\frac{\partial U}{\partial\frac{r}{a}}$	$\frac{\epsilon_\nu}{\nu}$	$\frac{\epsilon_c}{\epsilon_\nu}$	y^+	u^+
.7533	.0067	.0088	79.35	0	0	0	25.2	1.000	0		.002	74.3		439	20.6
.638	.122	.161	79.35	0	0	0	25.1	.996	0		.075	35.7		372	20.5
.588	.172	.226	79.35	0	0	0	25.1	.996	0		.120	31.2		343	20.5
.538	.222	.292	79.36	0	0	0	24.8	.983	0		.170	28.4		314	20.3
.488	.272	.358	79.35	0	0	0	24.5	.972	0		.224	26.3		285	20.0
.438	.322	.424	79.35	0	0	0	24.2	.961	0		.275	25.4		255	19.8
.388	.372	.489	79.35	0	0	0	23.5	.933	0		.330	24.4		226	19.2
.338	.422	.555	79.35	0	0	0	23.0	.914	0		.386	23.6		197	18.8
.288	.472	.621	79.35	0	0	0	22.5	.892	0		.443	23.0		168	18.4
.238	.522	.687	79.35	0	.002	.005	21.4	.851	0		.505	22.3		139	17.5
.188	.572	.753	79.37	.0008	.025	.02	20.6	.818	.005	1.03	.578	21.3		110	16.9
.163	.597	.786	79.46	.0045	.052	.025	20.1	.800	.008	.367	.620	20.7		95.0	16.5
.138	.622	.818	79.55	.0081	.105	.140	19.6	.778	.025	1.28	.670	19.9		80.5	16.0
.113	.647	.851	79.65	.0122	.197	.700	18.8	.755	.100	4.18	.772	17.8		65.9	15.4
.088	.672	.884	79.76	.0166	.375	2.19	18.1	.717	.395	9.78	1.08	13.0		51.3	14.8
.078	.682	.897	79.91	.0227	.493	2.83	17.7	.702	.590	11.2	1.30	10.8	1.04	45.4	14.4
.068	.692	.910	80.09	.0300	.780	3.47	17.1	.680	.835	9.66	1.55	9.03	1.07	39.6	14.0
.058	.702	.924	80.46	.0450	1.255	4.13	16.6	.658	1.16	7.98	2.03	6.78	1.18	33.8	13.6
.048	.712	.937	80.91	.0633	1.92	4.72	15.8	.627	1.51	6.44	2.88	4.57	1.41	28.0	12.9
.038	.722	.950	81.85	.101	3.30	5.27	14.6	.579	1.88	4.17	4.54	2.58	1.61	22.1	11.9
.033	.727	.957	82.53	.129	4.25	5.53	13.6	.540	2.08	3.34	5.73	1.86	1.79	19.2	11.1
.028	.732	.963	83.10	.152	5.32	5.70	12.7	.503	2.26	2.67	6.92	1.38	1.93	16.3	10.3
.023	.737	.970	84.15	.195	6.90	5.86	11.5	.456	2.45	1.96	8.62	.920	2.13	13.4	9.40
.018	.742	.976	85.56	.252	8.59	5.90	10.1	.399	2.60	1.43	10.5	.590	2.42	10.5	8.22
.013	.747	.983	87.48	.330	11.50	5.88	7.78	.309	2.72	.775	13.4	.256	3.03	7.58	6.36
.011	.749	.986	88.15	.357	13.40	5.83	7.01	.278	2.77	.490	14.7	.152	3.22	6.42	5.73
.009	.751	.988	89.02	.392	14.70	5.79	6.10	.242	2.80	.327	15.7	.075	4.36	5.24	4.98
.008	.752	.989	89.30	.406	15.6	5.77	5.52	.219	2.81	.229	16.0	.057	4.02	4.66	4.51
.007	.753	.991	89.96	.430	18.1	5.68	5.06	.201	2.83	.057	16.5	.027	2.11	4.08	4.13
.006	.754	.992	90.41	.448	20.5	5.63	4.54	.180	2.84	0	16.7	.015		3.50	3.71
.005	.755	.993	90.95	.470	23.0	5.52	3.96	.157	2.85		16.8	.01		2.92	3.24
.004	.756	.9947	91.85	.507	28.5	5.25	3.92							2.33	3.11

TABLE II. (Cont.)

Run 2 — u_b = 20.5 ft/sec — t_w = 109.7°F

Long Tube Entrance — u^* = 1.21 ft/sec — t_b = 83.02°F

Heated L/D = 1.13 — $\left(\frac{\partial \Theta}{\partial Z}\right)_b$ = .00993 — ρ = .0711 lb/cu ft

Re = 14,780 — t_o = 82.17°F — $k/\rho C_p$ = .000250 sq ft/sec

y in.	r in.	$\frac{r}{a}$	t °F	Θ	$\frac{d\Theta}{d\frac{r}{a}}$	$10^2 \frac{d\Theta}{dZ}$	u, ft/sec	U	$10^3 \Phi$	$\frac{\epsilon_c}{\nu}$	$\frac{dU}{d\frac{r}{a}}$	$\frac{\epsilon_\nu}{\nu}$	$\frac{\epsilon_c}{\epsilon_\nu}$	y^+	u^+
.760	0	0	82.15	0	0	0	25.91	1.000	0		0			435	21.4
.734	.026	.0342	82.15	0	0	0	25.91	1.000	0		.020	26.9		420	21.4
.684	.076	.1000	82.15	0	0	0	25.81	.996	0		.056	28.1		391	21.3
.634	.126	.1658	82.15	0	0	0	25.70	.992	0		.095	27.5		363	21.3
.584	.176	.2316	82.17	0	.0001	0	25.60	.988	0		.132	27.6		334	21.2
.534	.226	.2974	82.20	.00108	.002	.0020	25.20	.973	0		.172	27.2		305	20.8
.484	.276	.3632	82.22	.00181	.005	.0040	25.00	.965	0		.213	26.8		277	20.7
.434	.326	.4290	82.25	.00290	.007	.0060	24.40	.942	.0020	5.06	.258	26.1	.193	248	20.2
.384	.376	.4948	82.27	.00363	.010	.010	24.01	.927	.0035	5.35	.310	25.0	.214	220	19.9
.334	.426	.5606	82.30	.00472	.015	.025	23.43	.904	.010	9.94	.365	24.1	.412	191	19.4
.284	.476	.6264	82.30	.00472	.019	.048	22.70	.876	.020	14.8	.425	23.1	.640	162	18.7
.234	.526	.6922	82.34	.00617	.025	.078	21.81	.842	.041	21.3	.442	24.6	.865	134	18.0
.184	.576	.7580	82.40	.00835	.034	.180	21.07	.813	.087	31.0	.580	20.3	1.53	105	17.4
.159	.601	.7909	82.43	.00944	.050	.430	20.50	.791	.146	34.1	.640	19.2	1.77	91.0	16.9
.134	.626	.8238	82.51	.0124	.095	.920	19.98	.771	.278	26.1	.718	17.7	1.46	76.7	16.5
.114	.646	.8501	82.79	.0225	.238	1.43	19.45	.751	.480	21.0	.86	15.1	1.39	65.2	16.1
.094	.666	.8765	83.23	.0385	.575	1.87	18.75	.724	.760	15.8	1.18	11.1	1.42	53.8	15.5
.074	.686	.9028	83.91	.0632	.948	2.36	17.75	.685	1.12	10.9	1.60	8.20	1.33	42.3	14.6
.054	.706	.9291	84.94	.101	1.95	2.76	16.56	.639	1.53	6.59	2.93	4.17	1.58	30.9	13.7
.034	.726	.9554	87.00	.175	4.22	2.89	13.91	.537	1.96	3.17	5.35	1.92	1.65	19.5	11.5
.024	.736	.9686	88.98	.247	7.05	2.91	11.56	.446	2.15	1.53	8.65	.725	2.11	13.7	9.56
.019	.741	.9752	90.55	.304	8.80	2.90	9.49	.366	2.23	1.01	11.15	.325	3.11	10.9	7.85
.014	.746	.9817	92.17	.363	10.60	2.88	7.18	.277	2.29	.632	13.50	.185	3.42	8.01	5.94
.010	.750	.9870	93.94	.428	12.80	2.86	5.34	.206	2.32	.288				5.72	4.42
.007	.753	.9909	95.20	.473	15.00	2.82	4.04	.156	2.34	.045				4.00	3.34
.006	.754	.9923	95.79	.495	16.05	2.60	3.61	.139	2.35	0				3.43	2.99
.005	.755	.9936	96.26	.512	16.95	2.15	3.46			0				2.86	2.86
.004	.756	.9949	96.64	.526	18.25		3.41			0				2.29	2.74

TABLE II. (Cont.)

Run 3

Long Tube Entrance

Heated L/D = 4.15

Re = 14,860

u_b = 20.5 ft/sec

u^* = 1.21 ft/sec

$\left(\frac{\partial\Theta}{\partial Z}\right)_b$ = .00841

t_o = 83.78°F

t_w = 110.8°F

t_b = 85.8°F

ρ = .0714 lb/cu ft

$k/\rho C_p$ = .000251 sq ft/sec

y in.	r in.	$\frac{r}{a}$	t °F	Θ	$\frac{\partial\Theta}{\partial\frac{r}{a}}$	$10^2\frac{\partial\Theta}{\partial Z}$	u ft/sec	U	$10^3\,\Phi$	$\frac{\epsilon_c}{\nu}$	$\frac{\partial U}{\partial\frac{r}{a}}$	$\frac{\epsilon_\nu}{\nu}$	$\frac{\epsilon_c}{\epsilon_\nu}$	y^+	u^+
.7595	.0005	.00066	83.78	0	0	0	25.3	1.000	0		0			438	20.8
.6785	.0815	.1073	83.78	0	.008	0	25.1	.992	0		.066	26.5		391	20.7
.5785	.1815	.2389	83.79	.00037	.025	.02	24.6	.974	0		.149	26.1		333	20.3
.4785	.2815	.3705	83.93	.00555	.052	.049	24.0	.951	.007	1.94	.232	26.0		276	19.8
.3785	.3815	.5021	84.20	.0155	.105	.375	23.0	.910	.033	4.38	.315	25.9		218	19.0
.2785	.4815	.6337	84.75	.0359	.185	.740	21.8	.863	.250	18.4	.405	25.4		160	18.0
.2285	.5315	.6995	85.12	.0496	.255	.956	21.0	.832	.540	26.7	.470	24.1	1.11	132	17.4
.1785	.5815	.7653	85.73	.0722	.416	1.22	20.3	.802	.970	26.9	.565	21.9	1.23	103	16.7
.1535	.6065	.7982	86.16	.0880	.500	1.37	19.8	.784	1.23	27.1	.630	20.4	1.33	88.4	16.3
.1285	.6315	.8311	86.68	.107	.582	1.48	19.2	.760	1.52	27.5	.730	18.2	1.52	74.0	15.9
.1035	.6565	.8640	87.21	.127	.840	1.52	18.6	.736	1.84	22.1	.870	13.6	1.63	59.6	15.3
.0785	.6815	.8969	88.06	.158	1.11	1.52	17.7	.702	2.16	18.6	1.25	11.1	1.67	45.2	14.6
.0585	.7015	.9232	88.98	.193	1.69	1.51	16.4	.649	2.41	12.8	2.20	6.10	2.10	33.7	13.5
.0435	.7165	.9429	90.13	.235	2.50	1.49	15.1	.596	2.59	8.65	3.75	3.25	2.66	25.1	12.4
.0285	.7315	.9627	91.75	.295	4.37	1.39	12.3	.485	2.73	4.50	7.33	1.22	3.69	16.4	10.1
.0185	.7415	.9758	94.04	.380	6.80	1.24	9.24	.366	2.80	3.61	11.0	.500		10.7	7.62
.0135	.7465	.9824	95.25	.425	8.10	1.09	6.86	.272	2.82	2.80	13.2	.258		7.78	5.66
.0095	.7505	.9877	96.47	.470	9.27	1.02	5.38	.213	2.83	1.36	15.1	.105		5.47	4.44
.0075	.7525	.9903	97.16	.495	10.20	.850	4.54	.180	2.83	1.10	16.1	.04		4.32	3.75
.0065	.7535	.9916	97.52	.509	10.65	.810	4.00	.158	2.83	.991	16.5	.015		3.74	3.30
.0055	.7545	.9929	97.90	.523	13.5	.740	3.64	.136	2.84	.492	16.7	.005		3.17	3.00
.0045	.7555	.9942	98.44	.543			3.42							2.59	2.82
.0035	.7565	.9956	99.20	.571			3.24							2.02	2.67

TABLE II. (Cont.)

Run 4 — u_b = 21.0 ft/sec — t_w = 108.48°F

Long Tube Entrance — u^* = 1.24 ft/sec — t_o = 87.35°F

Heated L/D = 9.97 — $\left(\frac{\partial \Theta}{\partial Z}\right)_b$ = .00757 — ρ = .0693 lb/cu ft

Re = 14,700 — t_o = 83.49°F — $k/\rho C_p$ = .000258 sq ft/sec

y in.	r in.	$\frac{r}{a}$	t °F	Θ	$\frac{d\Theta}{d\frac{r}{a}}$	$10^3\frac{d\Theta}{dZ}$	u ft/sec	U	$10^3\ \Phi$	$\frac{\epsilon_c}{\nu}$	$\frac{dU}{d\frac{r}{a}}$	$\frac{\epsilon_\nu}{\nu}$	$\frac{\epsilon_c}{\epsilon_\nu}$	y^+	u^+
.7076	.0524	.06896	84.40	.0364	.017	5.64	25.2	1.000	.018	142	.032	35.7		403	20.4
.6326	.1274	.1677	84.49	.0400	.056	6.03	25.1	.996	.080	77.7	.079	35.2		360	20.3
.5576	.2024	.2664	84.72	.0492	.105	6.43	24.7	.980	.210	68.3	.130	33.9	2.01	317	20.0
.4826	.2774	.3651	85.01	.0608	.154	6.86	24.2	.961	.410	66.4	.181	33.4	1.98	275	19.6
.4076	.3524	.4638	85.66	.0868	.206	7.32	23.6	.937	.690	65.7	.240	32.0	2.05	232	19.1
.3326	.4274	.5625	86.26	.111	.263	7.80	23.0	.914	1.05	63.8	.302	30.8	2.07	189	18.6
.2826	.4774	.6283	86.73	.129	.312	8.14	22.4	.890	1.33	60.8	.348	29.8	2.04	161	18.1
.2326	.5274	.6941	87.30	.153	.392	8.49	21.9	.869	1.65	54.5	.412	27.8	1.96	132	17.7
.1826	.5774	.7599	88.06	.183	.560	8.82	21.0	.832	2.01	42.2	.500	24.9	1.70	104	17.0
.1326	.6274	.8257	89.31	.233	.795	9.19	20.2	.800	2.39	32.0	.630	21.4	1.49	75.4	16.3
.1076	.6524	.8586	90.02	.261	.932	9.34	19.6	.778	2.60	28.3	.780	17.8	1.59	61.2	16.0
.0828	.6774	.8915	91.00	.300	1.12	9.50	18.9	.748	2.79	23.5	1.14	12.4	1.90	47.0	15.2
.0576	.7024	.9244	92.02	.341	1.75	9.60	17.0	.673	3.00	15.4	2.09	6.55	2.35	32.8	13.7
.0426	.7174	.9441	93.23	.390	2.80	9.57	15.6	.619	3.12	9.25	3.97	3.06	3.20	24.2	12.6
.0326	.7274	.9573	94.24	.430	4.02	9.35	13.8	.549	3.19	6.06	6.65	1.45	4.17	18.6	11.2
.0276	.7324	.9638	95.05	.463	4.75	9.22	12.6	.500	3.22	4.86	8.55	.92		15.7	10.2
.0226	.7374	.9704	95.91	.497	5.67	8.95	11.0	.435	3.24	3.85	11.05	.498		12.9	8.86
.0176	.7424	.9770	96.86	.535	6.76	8.60	8.88	.352	3.26	2.99	13.5	.232		10.0	7.18
.0126	.7474	.9836	98.19	.588	7.90	7.90	6.50	.258	3.27	2.32	15.4	.089		7.17	5.25
.0096	.7504	.9875	99.03	.622	8.80	7.00	5.29	.210	3.28	1.92	16.2	.039		5.46	4.28
.0076	.7524	.9902	99.59	.644	9.65	6.00	4.41	.175	3.28	1.61	16.5	.025		4.32	3.57
.0066	.7534	.9915	99.91	.657	10.20	5.80	4.00	.158	3.28	1.45	16.7	.012		3.76	3.22
.0056	.7544	.9928	100.26	.671	10.95	5.30	3.72	.148	3.28	1.25	16.9	0		3.19	3.00
.0046	.7554	.9941	100.64	.686	12.10	4.80	3.65	.145				0		2.62	2.94
.0036	.7564	.9954	101.33	.714			3.80	.151				0		2.05	3.06
.0031	.7569	.9961	102.67	.768								0			

TABLE II. (Cont.)

Run 5 — u_b = 88.3 ft/sec — t_w = 104.46°F

Long Tube Entrance — u^* = 4.42 ft/sec — t_b = 81.85°F

Heated L/D = .453 — $\left(\frac{\partial\Theta}{\partial Z}\right)_b$ = .00957 — ρ = .0713 lb/cu ft

Re = 64, 100 — t_o = 81.48°F — $k/\rho C_p$ = .000250 sq ft/sec

y in.	r in.	$\frac{r}{a}$	t °F	Θ	$\frac{\partial\Theta}{\partial\frac{r}{a}}$	$10^2\frac{\partial\Theta}{\partial Z}$	u ft/sec	U	$10^3\,\Phi$	$\frac{\epsilon_c}{\nu}$	$\frac{\partial U}{\partial\frac{r}{a}}$	$\frac{\epsilon_\nu}{\nu}$	$\frac{\epsilon_c}{\epsilon_\nu}$	y^+	u^+
.638	.022	.0289	81.44	0	0	0	110	1.000	0		0				
.538	.122	.1605	81.46	0	0	0	109	.999	0		.022	373			
.488	.272	.3579	81.50	.00087	0	0	108	.986	0		.122	149		1030	24.6
.438	.322	.4237	81.48	0	0	.010	107	.976	.0004		.177	122		925	24.3
.388	.372	.4894	81.49	.00044	0	.019	105	.961	.0037		.244	102		818	23.9
.338	.422	.5552	81.49	.00044	.005	.032	103	.942	.0120	176	.325	86.4	2.04	713	23.4
.288	.472	.6211	81.49	.00044	.013	.050	101	.918	.0267	133	.414	75.6	1.76	608	22.8
.238	.522	.6868	81.54	.00261	.026	.072	97.6	.887	.0510	116	.510	67.8	1.71	502	22.1
.188	.572	.7526	81.59	.00479	.047	.108	93.3	.848	.0870	101	.630	60.1	1.68	396	21.1
.138	.622	.8184	81.64	.00696	.079	.250	88.7	.806	.160	97.3	.765	53.7	1.81	291	20.0
.113	.647	.8513	81.67	.00827	.123	.510	85.8	.780	.240	91.2	.890	47.9	1.91	238	19.4
.088	.672	.8842	81.77	.0126	.222	.930	82.2	.747	.390	80.2	1.12	39.3	2.04	186	18.6
.068	.692	.9105	81.93	.0196	.435	1.60	78.5	.714	.620	63.0	1.43	31.6	1.99	143	17.7
.048	.712	.9368	82.35	.0379	.980	2.80	74.0	.673	1.00	43.1	1.77	26.1	1.65	101	16.7
.038	.722	.9500	82.74	.0548	1.55	3.60	71.5	.650	1.27	33.8	1.90	24.6	1.37	80.3	16.2
.028	.732	.9632	83.36	.0818	2.55	4.30	68.1	.619	1.57	24.5	2.85	16.3	1.50	59.1	15.4
.023	.737	.9697	83.77	.0997	3.48	4.63	65.7	.597	1.75	19.7	3.80	12.1	1.63	48.6	14.9
.018	.742	.9763	84.40	.127	5.02	4.87	61.6	.569	1.92	14.5	5.55	8.01	1.81	37.9	13.9
.013	.747	.9829	85.30	.166	8.25	4.97	57.5	.523	2.10	9.04	9.00	4.60	1.96	27.4	13.0
.011	.749	.9855	85.88	.191	10.4	4.95	54.6	.496	2.16	7.09	11.4	3.43	2.07	23.2	12.3
.009	.751	.9882	86.60	.223	14.7	4.50	51.0	.464	2.22	4.70	17.0	1.97	2.39	19.0	11.5
.008	.752	.9895	87.21	.249	17.7	4.20	48.3	.439	2.26	3.75	21.3	1.38	2.72	16.9	10.9
.007	.753	.9908	87.75	.273	20.5	3.30	45.0	.409	2.27	3.05	28.0	.81	3.76	14.8	10.2
.006	.754	.9921	88.35	.299	22.4	2.75	39.6	.360	2.28	2.67				12.7	8.96
.005	.755	.9934	89.06	.330	42.5	2.40			2.29	.736					
.004	.756	.9947	90.24	.381		1.90									
.0035	.7565	.9954	91.79	.449											

TABLE II. (Cont.)

Run 6

Long Tube Entrance

Heated L/D = 1.13

Re = 64,200

u_b = 87.2 ft/sec

u^* = 4.36 ft/sec

$\left(\frac{\partial \Theta}{\partial Z}\right)_b$ = .00742

t_o = 84.24°F

t_w = 113.65°F

t_b = 84.74°F

ρ = .0717 lb/cu ft

$k/\rho C_p$ = .000249 sq ft/sec

y in.	r in.	$\frac{r}{a}$	t °F	Θ	$\frac{\partial \Theta}{\partial \frac{r}{a}}$	$10^2 \frac{\partial \Theta}{\partial Z}$	u ft/sec	U	$10^3 \Phi$	$\frac{\epsilon_c}{\nu}$	$\frac{\partial U}{\partial \frac{r}{a}}$	$\frac{\epsilon_\nu}{\nu}$	$\frac{\epsilon_c}{\epsilon_\nu}$	y^+	u^+
.7385	.0215	.02829	84.24	0	0	0	105	1.000	0		0				
.6885	.0715	.09408	84.24	0	0	0	104	.990	0		.011	431			
.6385	.1215	.1599	84.24	0	0	0	104	.989	0		.023	352			
.5885	.1715	.2257	84.21	0	.001	.0008	104	.987	0		.038	300			
.5385	.2215	.2914	84.31	.00238	.002	.0035	103	.984	.001	66.0	.058	253			
.4885	.2715	.3572	84.31	.00238	.0025	.0075	103	.980	.002	85.3	.086	209		1030	23.8
.4385	.3215	.4230	84.28	.00136	.0045	.0165	102	.967	.005	101.0	.129	165		927	23.6
.3885	.3715	.4888	84.29	.00170	.006	.0400	101	.963	.013	172.0	.190	129	1.33	819	23.3
.3385	.4215	.5546	84.31	.00238	.009	.104	100	.947	.036	280.0	.270	103	2.72	714	23.0
.2885	.4715	.6204	84.31	.00238	.013	.182	97.8	.926	.086	415.0	.372	83.3		608	21.5
.2385	.5215	.6862	84.30	.00204	.018	.280	94.6	.896	.175	624.0	.490	69.8		503	21.7
.1885	.5715	.7520	84.42	.00612	.026	.403	90.5	.857	.315	624.0	.620	60.4		398	20.8
.1635	.5965	.7849	84.45	.00714	.040	.480	88.3	.836	.415	514.0	.692	56.3		345	20.3
.1385	.6215	.8178	84.52	.00900	.082	.608	85.8	.812	.520	301.0	.780	52.1		292	19.7
.1185	.6415	.8441	84.59	.0119	.1035	.780	83.5	.791	.640	218.0	.847	49.3		250	19.2
.0985	.6615	.8704	84.70	.0157	.195	1.14	81.0	.767	.810	185.0	1.01	42.6		208	18.6
.0785	.6815	.9867	84.92	.0231	.608	1.61	77.9	.738	1.05	74.0	1.23	35.9	2.06	166	17.9
.0585	.7015	.9230	85.47	.0418	.940	2.08	73.5	.696	1.36	59.9	1.66	27.2	2.22	123	16.9
.0385	.7215	.9493	86.58	.0796	1.95	2.80	68.6	.650	1.77	35.6	2.35	21.1	1.69	81.2	15.8
.0285	.7315	.9625	87.52	.112	2.88	2.89	65.1	.616	2.00	26.5	3.10	14.7	1.81	60.2	14.9
.0235	.7365	.9691	88.12	.132	3.70	2.89	62.5	.592	2.11	21.2	4.30	10.4	2.04	49.7	14.4
.0185	.7415	.9757	88.97	.161	5.40	2.80	58.9	.558	2.22	14.8	6.55	6.53	2.26	39.1	13.5
.0135	.7465	.9822	90.23	.204	8.93	2.30	53.2	.504	2.31	8.65	10.3	3.82	2.26	28.5	12.2
.0105	.7495	.9862	91.55	.249	12.6	1.65	48.4	.458	2.35	5.76	14.5	2.44	2.36	22.2	11.1
.0085	.7515	.9888	92.62	.285	15.6	1.50	43.6	.413	2.36	4.39	20.0	1.50	2.93	17.9	10.0
.0065	.7535	.9915	94.05	.334	21.2	1.14	36.5	.346	2.38	2.88	30.2	.66	4.37	13.7	8.37
.0055	.7545	.9928	94.96	.365	26.0	.940	32.0	.303	2.38	2.07	36.0	.39	5.24	11.6	7.34
.0045	.7555	.9941	95.07	.368	31.2	.820	26.5	.251	2.38	1.49	45.0	.12		9.50	6.07
.0035	.7565	.9954	96.32	.411		.550	21.0	.199						7.38	4.82

TABLE II. (Cont.)

Run 7

Long Tube Entrance

Heated L/D = 4.15

Re = 63,800

u_b = 84.5 ft/sec

u* = 4.22 ft/sec

$\left(\frac{\partial\Theta}{\partial Z}\right)_b$ = .00638

t_o = 80.40°F

t_w = 106.69°F

t_b = 82.05°F

ρ = .0742 lb/cu ft

$k/\rho C_p$ = .000240 sq ft/sec

y in.	r in.	$\frac{r}{a}$	t °F	Θ	$\frac{\partial\Theta}{\partial\frac{r}{a}}$	$10^2 \frac{\partial\Theta}{\partial Z}$	u ft/sec	U	$10^3\ \Phi$	$\frac{\epsilon_c}{\nu}$	$\frac{\partial U}{\partial\frac{r}{a}}$	$\frac{\epsilon_\nu}{\nu}$	$\frac{\epsilon_c}{\epsilon_\nu}$	y^+	u^+
.7595	.0005	.00066	80.53	0	0	0	102.3	1.000	0		0				
.6795	.0805	.1059	80.40	0	.0025	.011	102.1	.998	0		.029	192			
.5795	.1805	.2375	80.46	.00228	.010	.0355	101.4	.991	0		.083	152			
.4795	.2805	.3690	80.51	.00418	.024	.104	98.2	.960	.030	130	.149	129	1.01	1070	23.3
.3795	.3805	.5007	80.61	.00799	.059	.196	94.5	.924	.111	143	.234	111	1.29	797	22.4
.2795	.4805	.6322	80.96	.0213	.158	.355	90.4	.884	.295	112	.355	92.8	1.21	587	21.4
.2295	.5305	.6980	81.32	.0350	.234	.523	87.6	.856	.450	104	.430	84.7	1.23	482	20.8
.1795	.5805	.7638	81.79	.0529	.345	.820	84.5	.826	.718	103	.535	74.2	1.39	377	20.0
.1545	.6055	.7967	82.21	.0689	.425	1.03	82.4	.806	.910	101	.605	68.4	1.48	325	19.5
.1295	.6305	.8296	82.58	.0829	.543	1.22	81.5	.797	1.16	96.9	.700	61.6	1.57	272	19.3
.1045	.6555	.8625	83.06	.101	.691	1.38	78.2	.763	1.44	90.9	.835	53.4	1.70	220	18.5
.0795	.6805	.8954	83.78	.129	.960	1.47	74.6	.729	1.74	75.5	1.025	45.0	1.68	167	17.7
.0595	.7005	.9217	84.52	.157	1.30	1.47	71.8	.702	1.99	61.2	1.24	38.2	1.60	125	17.0
.0445	.7155	.9415	85.37	.189	1.75	1.43	69.1	.675	2.18	48.6	1.52	31.7	1.53	93.5	16.4
.0295	.7305	.9612	86.41	.229	2.51	1.31	65.1	.636	2.35	35.2	2.95	16.2	2.19	62.0	15.4
.0195	.7405	.9743	87.47	.269	4.18	1.20	59.3	.580	2.45	21.1	5.60	8.17	2.58	41.0	14.1
.0145	.7455	.9809	88.39	.304	6.07	1.11	55.4	.542	2.50	14.3	9.00	4.73	3.02	30.5	13.1
.0115	.7485	.9849	89.09	.331	8.05	1.06	51.4	.486	2.52	10.5	12.1	3.28	3.20	24.2	12.2
.0095	.7505	.9875	89.78	.357	9.90	.93	47.1	.460	2.53	8.27	14.8	2.52	3.28	20.0	11.2
.0075	.7525	.9901	90.45	.382	12.7	.71	42.6	.416	2.54	6.13	18.6	1.81	3.38	15.8	10.1
.0065	.7535	.9915	90.83	.397	14.8	.63	39.4	.385	2.54	5.08	21.4	1.44	3.53	13.7	9.33
.0055	.7545	.9928	91.49	.422	18.3	.55	36.7	.359	2.54	3.80	25.8	1.025	3.71	11.6	8.69
.0045	.7555	.9941	92.18	.448	21.5	.48	33.6	.328	2.55	3.04				9.45	7.96
.0035	.7565	.9954	92.89	.475			30.4							7.35	7.20

TABLE II.. (Cont.)

Run 8 — u_b = 89.35 ft/sec — t_w = 107.49°F

Long Tube Entrance — u^* = 4.46 ft/sec — t_b = 84.55°F

Heated L/D = 9.97 — $\left(\frac{\partial\Theta}{\partial Z}\right)_b$ = .00543 — ρ = .0718 lb/cu ft

Re = 64,900 — t_o = 81.81°F — $k/\rho C_p$ = .000248 sq ft/sec

y in.	r in.	$\frac{r}{a}$	t °F	Θ	$\frac{\partial\Theta}{\partial\frac{r}{a}}$	$10^3\frac{\partial\Theta}{\partial Z}$	u ft/sec	U	$10^4\,\Phi$	$\frac{\epsilon_c}{\nu}$	$\frac{\partial U}{\partial\frac{r}{a}}$	$\frac{\epsilon_\nu}{\nu}$	$\frac{\epsilon_c}{\epsilon_\nu}$	y^+	u^+
.7325	.0275	.03618	81.88	0	.0048	0	109.8	1.000			.012	158			
.6825	.0775	.1020	81.82	0	.016	0	109.8	1.000			.035	153			
.6325	.1275	.1678	81.81	0	.033	0	109.7	.993			.062	143			
.5825	.1775	.2336	81.88	.00273	.052	.32	108.2	.986	.038	14.1	.094	131	.108		
.5325	.2275	.2993	82.00	.0074	.072	.48	107.7	.981	.118	21.0	.131	120	.175		
.4825	.2775	.3651	82.07	.0101	.0975	.68	105.9	.965	.257	28.1	.175	110	.255	1025	23.8
.4325	.3275	.4309	82.37	.0218	.126	1.01	104.6	.952	.460	33.1	.222	102	.325	920	23.5
.3825	.3775	.4967	82.56	.0292	.162	1.44	102.8	.936	.800	39.2	.271	96.1	.408	813	23.1
.3325	.4275	.5625	82.87	.0413	.215	1.92	100.4	.915	1.33	43.4	.330	89.4	.487	707	22.5
.2825	.4775	.6283	83.31	.0584	.287	2.44	98.0	.893	2.10	46.1	.395	84.2	.547	601	22.0
.2325	.5275	.6941	83.85	.0794	.385	2.90	94.8	.864	3.11	45.9	.473	76.7	.599	494	21.3
.1825	.5775	.7599	84.58	.108	.535	3.27	90.6	.826	4.40	43.0	.554	71.7	.599	388	20.4
.1575	.6025	.7928	85.08	.127	.627	3.42	88.8	.810	5.10	40.2	.598	69.3	.579	335	19.9
.1325	.6275	.8257	85.66	.150	.752	3.54	86.9	.791	5.82	36.5	.648	66.4	.549	282	19.5
.1075	.6525	.8586	86.38	.178	.895	3.64	84.2	.767	6.61	33.3	.720	62.2	.537	229	18.9
.0825	.6775	.8915	87.18	.209	1.08	3.74	81.4	.742	7.40	29.5	.860	53.8	.548	176	18.3
.0575	.7025	.9243	88.15	.247	1.40	3.80	75.9	.691	8.21	24.1	1.35	35.3	.683	122	17.1
.0425	.7175	.9441	88.99	.280	1.70	3.84	73.4	.669	8.70	20.3	1.80	26.8	.757	90.4	16.5
.0325	.7275	.9572	89.59	.303	2.10	3.82	70.6	.643	8.99	16.4	2.60	18.5	.887	69.2	15.8
.0225	.7375	.9704	90.53	.340	3.06	3.78	66.1	.602	9.30	11.0	4.30	10.9	1.01	47.8	14.8
.0175	.7425	.9770	91.11	.362	4.75	3.72	62.3	.568	9.45	6.69	6.60	6.84	.978	37.2	14.0
.0125	.7475	.9836	92.24	.406	8.65	3.64	56.1	.511	9.57	3.04	11.60	3.50	.868	26.6	12.6
.0095	.7505	.9875	93.27	.446	12.30	3.55	50.1	.456	9.62	1.73	18.60	1.81	.957	20.2	11.2
.0075	.7525	.9901	94.21	.483	16.30	3.47	44.1	.402	9.68	.956	26.0	1.02	.937	16.0	9.89
.0065	.7535	.9915	94.84	.507	20.0	3.42	39.1	.356	9.70	.520	30.5	.72	.720	13.8	8.77
.0055	.7545	.9928	95.61	.537	24.9	3.37	34.6	.315	9.70	.139	35.4	.485	.287	11.7	7.77
.0045	.7555	.9941	96.53	.573		3.35	29.4	.268	9.71					9.58	6.62
.0040	.7560	.9947	97.15	.597											

TABLE II. (Cont.)

Run 9 — u_b = 20.4 ft/sec

Bellmouth Entrance — $\left(\frac{\partial\Theta}{\partial Z}\right)_b$ = .00887 — t_b = 82.25°F

Heated L/D = .453 — t_o = 81.88°F — ρ = .0716 lb/cu ft

Re = 14,830 — t_w = 108.15°F — $k/\rho C_p$ = .000249 sq ft/sec

y in.	r in.	$\frac{r}{a}$	t °F	Θ	$\frac{\partial\Theta}{\partial\frac{r}{a}}$	$\frac{\partial\Theta}{\partial Z}$	u ft/sec	U	$10^3\,\Phi$	$\frac{\epsilon_c}{\nu}$	$\frac{\partial U}{\partial\frac{r}{a}}$	$\frac{\epsilon_\nu}{\nu}$	$\frac{\epsilon_c}{\epsilon_\nu}$		
.7600	0	0	81.88	0	0	0	22.1	1.00	0		0				
.7345	.0255	.0336	81.88	0	0	0	22.1	1.00	0		0				
.6845	.0755	.0993	81.88	0	0	0	22.1	1.00	0		0				
.5845	.1755	.2309	81.88	0	0	0	22.1	1.00	0		0				
.4845	.2755	.3625	81.88	0	0	0	22.1	1.00	0		0				
.3845	.3755	.4941	81.89	.00038	0	0	22.1	1.00	0		0				
.3345	.4255	.5599	81.89	.00038	0	0	22.1	1.00	0		0				
.2845	.4755	.6257	81.91	.00114	0	0	22.1	1.00	0		0				
.2345	.5255	.6915	81.91	.00114	.005	0	22.1	1.00	0		0				
.1845	.5755	.7572	82.00	.00457	.022	0	22.1	1.00	0		0				
.1345	.6255	.8230	82.05	.00647	.057	0	22.1	.996	0		.15				
.0845	.6755	.8888	82.22	.0130	.143	.0002	21.2	.958	0		1.87				
.0645	.6955	.9151	82.34	.0175	.520	.016	19.3	.876	.17	1.48	4.60	1.13	1.31		
.0595	.7005	.9217	82.51	.0240	.945	.023	18.7	.845	.27	1.08	5.75	1.13	.957		
.0545	.7055	.9283	82.73	.0324	1.58	.032	17.6	.797	.415	.864	6.70	.98	.882		
.0495	.7105	.9349	83.06	.0450	2.57	.041	16.4	.744	.58	.523	7.65	.62	.844		
.0445	.7155	.9415	83.54	.0632	3.80	.051	15.1	.685	.78	.328	8.55	.46	.713		
.0395	.7205	.9480	84.35	.0940	5.25	.062	13.8	.623	1.01	.205	9.45	.33	.622		
.0345	.7255	.9546	85.47	.137	6.84	.076	12.4	.559	1.31	.192	10.5	.19	1.01		
.0295	.7305	.9612	87.00	.195	8.48	.108	10.8	.490	1.63	.180	11.4	.11	1.64		
.0245	.7355	.9678	88.68	.258	10.14	.126	9.21	.417	1.95	.179	12.2	.03			
.0195	.7405	.9743	90.58	.331	11.85	.099	7.29	.330	2.23	.126	12.6	0			
.0145	.7455	.9809	92.66	.410	13.89	.077	5.02	.227	2.39	0	12.9	0			
.0095	.7505	.9875	94.80	.492	16.39	.050	3.61	.163	2.47	0	13.0	0			
.0075	.7525	.9901	95.74	.528	17.60	.040	2.96	.134	2.49	0	13.0	0			
.0055	.7545	.9928	96.62	.561	19.60	.028	2.46	.111	2.50	0	13.0	0			
.0045	.7555	.9941	97.18	.582	20.7	.023	2.37	.107	2.50	0	13.0	0			
.0035	.7565	.9954	97.68	.601	21.8	.018				0		0			
.0030	.7570	.9961	97.96	.612	22.5	.015				0		0			

TABLE II. (Cont.)

Run 10 u_b = 20.32 ft/sec

Bellmouth Entrance $\left(\frac{\partial\Theta}{\partial Z}\right)_b$ = .00674 t_b = 81.12°F

Heated L/D = 1.13 t_o = 80.66°F ρ = .0718 lb/cu ft

Re = 14,820 t_w = 108.43°F $k/\rho C_p$ = .000249 sq ft/sec

y in.	r in.	$\frac{r}{a}$	t °F	Θ	$\frac{\partial\Theta}{\partial\frac{r}{a}}$	$10\frac{\partial\Theta}{\partial Z}$	u ft/sec	U	$10^3\,\Phi$	$\frac{\epsilon_c}{\nu}$	$\frac{\partial U}{\partial\frac{r}{a}}$	$\frac{\epsilon_\nu}{\nu}$	$\frac{\epsilon_c}{\epsilon_\nu}$		
.760	.000	0	80.67	0	0	0	21.8	1.00	0		0				
.549	.211	.2776	80.66	0	0	0	21.8	1.00	0		0				
.349	.411	.5408	80.66	0	0	0	21.8	1.00	0		0				
.199	.561	.7382	80.62	0	0	0	21.8	1.00	0		.025				
.149	.611	.8040	80.62	0	0	.005	21.6	.991	.005		.25				
.124	.636	.8368	80.67	.00036	.043	.025	21.3	.978	.038	7.09	.64	12.8	.553		
.099	.661	.8697	80.81	.0054	.254	.109	20.6	.945	.210	6.26	1.55	4.92	1.27		
.084	.676	.8895	81.00	.0122	.620	.199	19.7	.904	.435	4.96	2.85	2.29	2.16		
.074	.686	.9026	81.38	.0260	1.26	.275	18.6	.852	.688	3.46	4.13	1.30	2.66		
.069	.691	.9092	81.65	.0378	1.68	.325	17.9	.820	.839	3.00	5.00	.920	3.26		
.064	.696	.9158	81.99	.0479	2.23	.383	17.1	.786	1.00	2.52	6.00	.610	4.13		
.059	.701	.9224	82.44	.0641	2.92	.452	16.3	.748	1.21	2.18	7.15	.360	6.06		
.054	.706	.9290	83.09	.0875	3.70	.534	15.5	.712	1.43	1.91	8.25	.181	10.55		
.049	.711	.9355	83.84	.115	4.57	.645	14.4	.662	1.68	1.72	9.15	.067			
.044	.716	.9421	84.87	.152	5.50	.798	13.0	.594	1.96	1.59	10.0	0			
.039	.721	.9487	86.18	.199	6.47	.950	11.6	.530	2.26	1.51	10.23	0			
.034	.726	.9553	87.81	.258	7.47	.965	10.0	.459	2.56	1.42	10.25	0			
.029	.731	.9618	89.04	.302	8.50	.840	8.52	.391	2.81	1.29	10.25	0			
.024	.736	.9684	90.88	.368	9.66	.700	7.02	.322	2.99	1.11	10.25	0			
.019	.741	.9750	92.43	.424	10.97	.550	5.60	.257	3.11	.874	10.25	0			
.014	.746	.9816	94.20	.488	12.6	.410	4.16	.191	3.17	.597	10.25	0			
.011	.749	.9855	95.64	.540	13.8	.323	3.10	.142	3.20	.430	10.25	0			
.009	.751	.9882	95.76	.544	14.8	.257	2.72	.125	3.21	.306	10.25	0			
.007	.753	.9908	96.28	.562	16.5	.203	2.34	.107	3.22	.079	10.25	0			

TABLE II. (Cont.)

Run 11 $u_b = 20.5$ ft/sec

Bellmouth Entrance $\left(\frac{\partial \Theta}{\partial Z}\right)_b = .00548$ $t_b = 84.53°F$

Heated L/D = 1.75 $t_o = 83.78°F$ $\rho = .0712$ lb/cu ft

Re = 14,800 $t_w = 111.92°F$ $k/\rho C_p = .000250$ sq ft/sec

y in.	r in.	$\frac{r}{a}$	t °F	Θ	$\frac{\partial \Theta}{\partial \frac{r}{a}}$	$10^2 \frac{\partial \Theta}{\partial Z}$	u ft/sec	U	$10^3 \Phi$	$\frac{\epsilon_c}{\nu}$	$\frac{\partial U}{\partial \frac{r}{a}}$	$\frac{\epsilon_\nu}{\nu}$	$\frac{\epsilon_c}{\epsilon_\nu}$		
.758	.002	.00263	83.93	0	0	0	22.1	1.000	0		0				
.549	.211	.2777	83.76	0	0	0	22.1	1.000	0		0				
.349	.411	.5409	83.78	0	0	0	22.1	1.000	0		0				
.249	.511	.6725	83.77	0	0	0	22.1	1.000	0		0				
.199	.561	.7383	83.78	0	0	0	22.1	1.000	0		.02				
.179	.581	.7646	83.78	0	.021	.11	22.1	1.000	.015	6.21	.130	56.9			
.169	.591	.7776	83.78	0	.041	.16	22.06	.999	.027	5.45	.205	36.4			
.159	.601	.7909	83.85	.00249	.074	.24	22.0	.996	.045	4.86	.300	24.9			
.149	.611	.8041	83.86	.00284	.114	.36	21.9	.991	.000076	5.33	.420	17.9			
.139	.621	.8172	83.90	.00426	.165	.53	21.8	.985	.00012	5.80	.570	12.8			
.129	.631	.8304	83.97	.00675	.237	.77	21.5	.975	.000192	6.50	.765	9.70	.67		
.119	.641	.8436	84.12	.0121	.342	1.12	21.3	.965	.00031	7.31	1.03	7.08	2.04		
.109	.651	.8567	84.24	.0164	.498	1.60	21.1	.954	.00053	8.71	1.60	4.27	2.04		
.099	.661	.8699	84.46	.0242	.775	2.20	20.4	.924	.00075	7.66	2.40	2.57	2.99		
.089	.671	.8830	84.87	.0387	1.34	2.95	19.6	.886	.00104	5.72	3.33	1.61	3.55		
.079	.681	.8962	85.51	.0615	2.08	3.85	18.5	.837	.00139	4.60	4.37	.920	5.00		
.069	.691	.9094	86.48	.0960	3.13	4.63	17.1	.772	.00180	3.70	5.47	.640	5.78		
.059	.701	.9225	87.86	.145	4.37	4.98	15.1	.681	.00221	3.00	6.65	.360	8.33		
.049	.711	.9357	89.86	.216	5.66	4.35	13.2	.598	.00258	2.49	7.95	.160			
.039	.721	.9488	92.32	.303	7.02	3.47	10.9	.493	.00285	1.99	8.92	.0170			
.029	.731	.9620	95.08	.392	8.63	2.63	7.95	.360	.00303	1.48	9.35	0			
.024	.736	.9686	96.27	.444	9.60	2.17	6.66	.301	.00308	1.20	9.47	0			
.019	.741	.9752	97.47	.487	10.7	1.76	5.20	.235	.00311	.940	9.58	0			
.014	.746	.9817	98.68	.530	12.2	1.32	3.80	.172	.00312	.633	9.62	0			
.009	.751	.9883	100.28	.586	13.3	.85					9.62	0			
.007	.753	.9909	100.80	.605	13.9	.70					9.62	0			
.005	.755	.9936	100.99	.612	14.7	.50					9.62	0			

TABLE II. (Cont.)

Run 12 u_b = 29.2 ft/sec

Bellmouth Entrance $\left(\frac{\partial\Theta}{\partial Z}\right)_b$ = .00407 t_b = 82.48°F

Heated L/D = 4.12 t_o = 81.20°F ρ = .0713 lb/cu ft

Re = 14,910 t_w = 111.59°F $k/\rho C_p$ = .000250 sq ft/sec

y in.	r in.	$\frac{r}{a}$	t °F	Θ	$\frac{\partial\Theta}{\partial\frac{r}{a}}$	$10^3\frac{\partial\Theta}{\partial Z}$	u ft/sec	U	$10^3\,\Phi$	$\frac{\epsilon_c}{\nu}$	$\frac{\partial U}{\partial\frac{r}{a}}$	$\frac{\epsilon_\nu}{\nu}$	$\frac{\epsilon_c}{\epsilon_\nu}$		
.761	.000	0	81.19	0	0	0	22.9	1.00	0		0				
.679	.081	.1066	81.20	0	0	0	22.9	1.00	0		0				
.579	.181	.2381	81.20	0	0	0	22.9	1.00	0		0				
.479	.281	.3698	81.20	0	0	0	22.9	1.00	0		0				
.379	.381	.5014	81.22	.00066	.0025	.005	22.9	1.00	0		0				
.279	.481	.6330	81.34	.00461	.0135	1.65	22.90	.998	.060	58.7	.04				
.229	.531	.6988	81.35	.00494	.0350	2.85	22.75	.992	.157	53.5	.20	28.9	1.85		
.204	.556	.7317	81.40	.00658	.087	3.55	22.49	.980	.235	30.2	.38	15.4	1.96		
.179	.581	.7646	81.66	.0151	.237	4.27	22.12	.964	.330	14.0	.58	10.3	1.36		
.154	.606	.7975	81.89	.0227	.460	5.25	21.58	.941	.440	8.78	.89	6.65	1.32		
.129	.631	.8304	82.50	.0428	.850	6.56	20.70	.902	.588	5.65	1.61	3.40	1.66		
.104	.651	.8567	83.44	.0737	1.45	7.80	19.21	.839	.725	3.49	2.22	2.30	1.52		
.079	.681	.8961	85.81	.152	2.57	8.60	17.09	.745	.965	2.08	3.30	1.29	1.61		
.059	.701	.9225	88.23	.231	3.48	8.07	14.70	.641	1.10	1.43	6.00	.275	5.20		
.044	.716	.9423	91.45	.337	4.20	6.75	11.02	.480	1.19	1.07	8.30	0			
.029	.731	.9620	94.31	.431	4.97	3.95	7.25	.316	1.20	.648	8.30	0			
.019	.741	.9752	96.41	.501	5.63	2.25	4.74	.207	1.22	.407	8.30	0			
.012	.746	.9817	97.65	.541	6.15	1.47	3.51	.153	1.22	.242	8.30	0			
.011	.749	.9857	98.30	.563	6.70	1.12	2.69	.117	1.22	.101	8.30	0			
.009	.751	.9883	98.90	.582	7.50	.90	2.23	.0970	1.22	0	8.30	0			
.008	.752	.9896	99.20	.592	8.00	.79	1.97	.0859	1.22	0	8.30	0			
.007	.753	.9909	99.55	.603	8.45	.65	1.71	.0745	1.22	0	8.30	0			
.005	.755	.9936	100.4	.632	10.05	.48	1.20	.0523	1.22	0	8.30	0			
.004	.756	.9949	100.75	.676	10.73	.32				0		0			

TABLE II. (Cont.)

Run 13 $u_b = 20.5$ ft/sec

Bellmouth Entrance $\left(\frac{\partial \Theta}{\partial Z}\right)_b = .00413$ $t_b = 84.20°F$

Heated L/D = 9.97 $t_o = 81.62°F$ $\rho = .0714$ lb/cu ft

Re = 14,820 $t_w = 111.7°F$ $k/\rho C_p = .000249$ sq ft/sec

y in.	r in.	$\frac{r}{a}$	t °F	Θ	$\frac{\partial \Theta}{\partial \frac{r}{a}}$	$10^3 \frac{\partial \Theta}{\partial Z}$	u ft/sec	U	$10^3\ \Phi$	$\frac{\epsilon_c}{\nu}$	$\frac{\partial U}{\partial \frac{r}{a}}$	$\frac{\epsilon_\nu}{\nu}$	$\frac{\epsilon_c}{\epsilon_\nu}$		
.683	.077	.1013	82.27	.0216	.0025	1.88	23.4	1.00	.014	480	0				
.583	.177	.2329	82.45	.0276	.0145	1.95	23.4	1.00	.052	133	0				
.483	.277	.3645	82.55	.0309	.0240	2.12	23.4	1.00	.130	128	0				
.383	.377	.4961	82.66	.0346	.0430	2.43	23.4	.999	.260	105	.030				
.283	.477	.6277	82.91	.0429	.0940	2.84	23.1	.988	.455	65.8	.188	31.6	2.06		
.233	.527	.6935	83.11	.0495	.175	3.12	22.6	.969	.583	40.3	.347	18.6	2.17		
.183	.577	.7593	83.64	.0672	.327	3.48	22.0	.940	.730	24.0	.620	11.0	2.18		
.133	.627	.8251	84.42	.0931	.630	3.86	20.7	.885	.910	13.7	1.31	5.16	2.65		
.108	.652	.8580	85.64	.134	.985	4.02	19.2	.819	1.00	8.74	1.78	3.73	2.35		
.083	.677	.8909	86.84	.174	1.88	4.13	17.5	.748	1.12	4.29	2.54	1.44	2.98		
.063	.697	.9172	88.75	.237	3.00	4.19	15.7	.670	1.17	2.19	3.76	1.35	1.62		
.043	.717	.9436	92.35	.357	4.31	4.16	12.5	.535	1.24	1.16	7.40	.22			
.033	.727	.9567	94.29	.421	5.02	4.10	9.86	.421	1.26	.790	9.16	0			
.028	.732	.9633	95.34	.456	5.38	4.06	8.18	.349	1.26	.629	9.41	0			
.023	.737	.9699	96.55	.496	5.78	3.98	6.97	.297	1.27	.491	9.55	0			
.018	.742	.9765	97.72	.535	6.20	3.87	5.11	.218	1.28	.360	9.60	0			
.013	.747	.9831	99.00	.577	6.67	3.60	3.80	.162	1.28	.224	9.60	0			
.010	.750	.9870	99.76	.603	7.04	3.20	2.82	.120	1.29	.145	9.60	0			
.008	.752	.9896	100.4	.623	7.33	2.95	2.31	.0986	1.29	.0782	9.60	0			
.007	.753	.9909	100.7	.635	7.52	2.60	2.02	.0862	1.29	.0446	9.60	0			
.005	.755	.9936	101.3	.6536	8.07	2.20	1.44	.0615	1.29		9.60	0			
.0035	.7565	.9956	102.0	.6766	8.65	1.55						0			

TABLE II. (Cont.)

Run 14

Bellmouth Entrance

Heated L/D = .453

Re = 63,900

u_b = 86.2 ft/sec

$\left(\frac{\partial \Theta}{\partial Z}\right)_b$ = .00731

t_o = 80.02°F

t_w = 100.40°F

t_b = 80.27°F

ρ = .0727 lb/cu ft

$k/\rho C_p$ = .000244 sq ft/sec

y in.	r in.	$\frac{r}{a}$	t °F	Θ	$\frac{\partial \Theta}{\partial r}_a$	$10^2 \frac{\partial \Theta}{\partial Z}$	u ft/sec	U	$10^3\ \Phi$	$\frac{\epsilon_c}{\nu}$	$\frac{\partial U}{\partial r}_a$				
.7585	0	0	79.98	0	0	0	90.1	1.00	0		0				
.6825	.0775	.1020	80.01	0	0	0	90.1	1.00	0		0				
.5825	.1775	.2336	80.00	0	0	0	90.1	1.00	0		0				
.4825	.2775	.3652	80.03	0	0	0	90.1	1.00	0		0				
.3825	.3775	.4968	80.02	0	0	0	90.1	1.00	0		0				
.2825	.4775	.6284	80.02	0	0	0	90.1	1.00	0		0				
.1825	.5775	.7600	80.03	.00049	0	0	90.1	1.00	0		0				
.1325	.6275	.8258	80.09	.00343	.022	0	90.1	1.00	0		.101				
.1075	.6525	.8587	80.15	.00638	.077	0	89.3	.991	0		.255				
.0875	.6725	.8850	80.18	.00785	.0160	.01	88.7	.986	.0005		.515				
.0775	.6825	.8982	80.25	.0113	.219	.055	88.1	.978	.0032		.775				
.0675	.6925	.9113	80.32	.0147	.305	.225	86.8	.963	.0185	.800	1.16				
.0575	.7025	.9245	80.41	.0191	.455	.675	84.6	.940	.070	4.18	1.59				
.0475	.7125	.9377	80.59	.0280	.945	1.72	83.0	.920	.195	6.03	2.60				
.0375	.7225	.9508	80.92	.0442	1.52	3.45	79.0	.877	.470	9.52	4.35				
.0275	.7325	.9640	81.42	.0687	2.68	4.92	71.4	.792	.945	10.9	7.35				
.0175	.7425	.9771	82.81	.137	7.60	5.13	60.3	.669	1.42	4.97	12.3				
.0125	.7475	.9837	84.17	.204	12.2	4.91	51.8	.575	1.61	3.10	16.8				
.0075	.7525	.9903	86.11	.299	18.5	4.25	39.7	.441	1.76	1.77	24.6				
.0055	.7545	.9929	87.15	.350	23.2	3.73	33.6	.373	1.80	1.18	28.0				
.0035	.7565	.9956	89.20	.450	39.0	2.70	28.1	.312	1.82	1.38	33.0				
.0025	.7575	.9969	90.06	.493	54.0	2.10	24.1	.268	1.84	0	35.4				
.0015	.7585	.9982	91.65	.571						0					

TABLE II. (Cont.)

Run 15 u_b = 83.0 ft/sec

Bellmouth Entrance $\left(\frac{\partial\Theta}{\partial Z}\right)_b$ = .00676 t_b = 80.74°F

Heated L/D = 1.13 t_o = 80.34°F ρ = .0738 lb/cu ft

Re = 65,500 t_w = 108.45°F $k/\rho c_p$ = .000242 sq ft/sec

y in.	r in.	$\frac{r}{a}$	t °F	Θ	$\frac{\partial\Theta}{\partial\frac{r}{a}}$	$10^2 \frac{\partial\Theta}{\partial Z}$	u ft/sec	U	$10^3\ \Phi$	$\frac{\epsilon_c}{\nu}$	$\frac{\partial U}{\partial\frac{r}{a}}$				
.762	.002	0	80.34	0	0	0	95.8	1.00	0		0				
.499	.261	.3435	80.32	0	0	0	95.8	1.00	0		0				
.349	.411	.5409	80.32	0	0	0	95.8	1.00	0		0				
.299	.461	.6067	80.32	0	0	0	95.8	1.00	0		0				
.224	.536	.7054	80.31	0	0	0	95.8	1.00	0		0				
.199	.561	.7383	80.32	0	0	.01	95.6	.998	0		.020				
.174	.586	.7712	80.32	0	0	.02	95.1	.991	0		.068				
.149	.611	.8041	80.34	0	0	.05	94.7	.987	0		.152				
.124	.636	.8370	80.34	0	.050	.08	94.1	.981	.031	24.7	.334				
.099	.661	.8699	80.36	.00071	.23	.35	92.5	.965	.085	13.8	.635				
.074	.686	.9028	80.37	.0139	.57	1.15	90.0	.939	.28	18.1	1.25				
.049	.711	.9357	81.53	.0423	1.51	2.20	84.6	.883	.73	17.0	2.80				
.034	.726	.9554	82.71	.0843	3.15	3.02	77.0	.803	1.16	12.3	4.70				
.024	.736	.9686	84.18	.137	5.05	3.14	69.8	.727	1.46	9.18	6.60				
.019	.741	.9752	85.16	.172	6.35	3.12	65.2	.680	1.60	7.75	7.90				
.014	.746	.9817	86.30	.212	8.65	3.06	60.0	.626	1.72	5.73	9.80				
.011	.749	.9857	87.62	.259	11.0	2.94	56.0	.584	1.80	4.44	12.8				
.009	.751	.9883	88.33	.284	12.8	2.88	51.7	.539	1.84	3.69	17.4				
.008	.752	.9896	88.80	.301	13.8	2.83	50.1	.523	1.86	3.36	19.8				
.007	.753	.9909	89.30	.319	15.1	2.70	46.0	.479	1.87	2.96	22.6				
.006	.754	.9923	89.95	.342	18.5	2.50	43.7	.456	1.89	2.18	27.0				
.005	.755	.9936	90.71	.369	23.0	2.36	41.0	.427	1.90	1.50	30.4				

TABLE II. (Cont.)

Run 16 u_b = 86.8 ft/sec

Bellmouth Entrance $\left(\frac{\partial\Theta}{\partial Z}\right)_b$ = .00620 t_b = 85.40°F

Heated L/D = 1.75 t_o = 84.89°F ρ = .073 lb/cu ft

Re = 64,200 t_w = 111.41°F $k/\rho C_p$ = .000246 sq ft/sec

y in.	r in.	$\frac{r}{a}$	t °F	Θ	$\frac{\partial\Theta}{\partial\frac{r}{a}}$	$10^2\frac{\partial\Theta}{\partial Z}$	u ft/sec	U	$10^3\,\Phi$	$\frac{\epsilon_c}{\nu}$	$\frac{\partial U}{\partial\frac{r}{a}}$				
.757	.003	.00395	84.89	0	0	0	95.3	1.00	0		0				
.549	.211	.2777	84.86	0	0	0	95.3	1.00	0		0				
.349	.411	.5409	84.87	0	0	0	95.3	1.00	0		0				
.249	.511	.6725	84.88	0	0	.045	95.3	1.00	.014		0				
.199	.561	.7383	84.88	0	0	.11	94.5	.992	.047		0				
.174	.586	.7712	84.89	0	-.013	.18	94.3	.990	.082	287	.032				
.149	.611	.8041	84.95	.00226	.052	.335	93.5	.986	.150	125	.194				
.129	.631	.8304	84.97	.00302	.133	.60	93.1	.978	.242	75.8	.321				
.109	.651	.8567	85.12	.00867	.285	.95	92.2	.968	.410	57.4	.525				
.089	.671	.8830	85.40	.0192	.565	1.33	90.2	.947	.665	45.3	.895				
.079	.681	.8962	85.64	.0283	.765	1.57	88.7	.932	.830	41.0	1.18				
.069	.691	.9094	85.95	.0400	.858	1.80	87.4	.918	1.01	40.2	1.54				
.059	.701	.9225	86.32	.0539	1.26	2.04	85.7	.900	1.22	35.2	2.00				
.049	.711	.9357	86.85	.0739	1.62	2.28	82.3	.864	1.46	32.2	2.70				
.039	.721	.9488	87.44	.0962	2.20	2.46	77.6	.815	1.70	27.0	3.70				
.029	.731	.9620	88.50	.136	3.25	2.52	72.8	.764	1.94	20.2	5.30				
.024	.736	.9686	89.13	.160	4.35	2.51	69.0	.725	2.06	15.5	6.15				
.019	.741	.9752	90.16	.195	5.85	2.44	64.8	.686	2.16	11.6	8.25				
.014	.746	.9817	91.18	.239	7.80	2.30	57.8	.606	2.27	8.61	11.4				
.011	.749	.9857	92.16	.274	9.50	2.18	53.0	.557	2.32	7.06	14.6				
.009	.751	.9883	92.79	.298	11.2	2.08	49.0	.515	2.36	5.86	18.6				
.007	.753	.9909	93.66	.331	13.7	1.84	44.0	.462	2.39	4.61	23.0				
.006	.754	.9923	94.16	.349	16.6	1.72	41.0	.430	2.40	3.58	28.0				
.005	.755	.9936	95.03	.382	24.7	1.64	36.6	.384	2.40	1.94	39.2				

TABLE II. (Cont.)

Run 17

Bellmouth Entrance

Heated L/D = 4.12

Re = 65,300

u_b = 87.0 ft/sec

$\left(\frac{\partial\Theta}{\partial Z}\right)_b$ = .00619

t_o = 81.28 °F

t_w = 112.63 °F

t_b = 82.87 °F

ρ = .0739 lb/cu ft

$k/\rho C_p$ = .000241 sq ft/sec

y in.	r in.	$\frac{r}{a}$	t °F	Θ	$\frac{\partial\Theta}{\partial\frac{r}{a}}$	$10^2 \frac{\partial\Theta}{\partial Z}$	u ft/sec	U	$10^3\,\Phi$	$\frac{\epsilon_c}{\nu}$	$\frac{\partial U}{\partial\frac{r}{a}}$				
.7595	.0005	.00066	81.22	0	0	0	92.9	1.00	0	0	0				
.6775	.0825	.01086	81.22	0	0	0	92.9	1.00	0	0	0				
.5775	.1825	.2402	81.22	0	0	0	92.9	1.00	0	0	0				
.4775	.2825	.3718	81.28	0	.003	.024	92.9	1.00	0	0	0				
.4275	.3325	.4376	81.31	.00096	.0045	.060	92.9	1.00	.008	139	.005				
.3775	.3825	.5034	81.32	.00128	.017	.12	92.9	1.00	.039	157	.035				
.3275	.4325	.5692	81.34	.00191	.036	.21	92.9	1.00	.095	160	.082				
.2775	.4825	.6350	81.51	.00734	.074	.34	92.9	1.00	.202	148	.149				
.2525	.5075	.6679	81.60	.0102	.107	.43	91.1	.981	.285	137	.181				
.2275	.5325	.7008	81.73	.0143	.156	.55	90.5	.974	.390	122	.225				
.2025	.5575	.7337	81.92	.0204	.239	.74	89.7	.965	.550	107	.275				
.1775	.5825	.7666	82.23	.0303	.350	1.01	88.8	.956	.745	94.7	.336				
.1525	.6095	.8021	82.72	.0459	.490	1.40	87.6	.943	1.06	91.6	.445				
.1275	.6325	.8324	83.35	.0660	.640	1.68	86.1	.927	1.40	89.6	.625				
.1025	.6575	.8653	84.01	.0871	.860	1.86	83.0	.893	1.87	85.4	.970				
.0775	.6825	.8982	85.02	.119	1.25	1.90	79.6	.856	2.34	70.5	1.40				
.0575	.7025	.9245	86.32	.161	1.69	1.85	75.7	.814	2.69	57.2	1.75				
.0275	.7325	.9640	88.85	.241	2.99	1.65	66.9	.720	3.24	36.9	4.30				
.0225	.7375	.9706	89.54	.263	3.62	1.59	63.7	.685	3.31	30.4	6.10				
.0175	.7425	.9771	90.36	.290	4.85	1.52	60.7	.653	3.38	22.6	9.35				
.0125	.7475	.9837	91.68	.332	7.70	1.43	52.7	.567	3.42	13.7	14.6				
.0075	.7525	.9903	93.76	.398	14.1	1.30	41.6	.448	3.47	6.84	25.4				
.0065	.7535	.9916	94.42	.419	16.1	1.28	38.2	.411	3.47	5.88	31.2				
.0055	.7545	.9929	95.13	.442	18.0	1.24	34.0	.366	3.48	5.07	35.8				
.0045	.7555	.9942	95.89	.466	18.8	1.21	30.8	.331	3.48	4.83					
.0035	.7565	.9956	96.20	.476		1.14	26.9	.290	3.49						

TABLE II. (Cont.)

Run 18

Bellmouth Entrance

Heated L/D = 9.97

Re = 65,350

u_b = 87.7 ft/sec

$\left(\frac{\partial\Theta}{\partial Z}\right)_b$ = .00539

t_o = 81.32°F

t_w = 106.99°F

t_b = 84.90°F

ρ = .0738 lb/cu ft

$k/\rho C_p$ = .000242 sq ft/sec

y in.	r in.	$\frac{r}{a}$	t °F	Θ	$\frac{\partial\Theta}{\partial\frac{r}{a}}$	$10^3\frac{\partial\Theta}{\partial Z}$	u ft/sec	U	$10^3\,\Phi$	$\frac{\epsilon_c}{\nu}$	$\frac{\partial U}{\partial\frac{r}{a}}$				
.732	.028	.0368	81.45	.00506	.0075	1.8	99.8	1.00	.0024	341	.001				
.632	.128	.1684	81.65	.0129	.043	2.39	100.0	1.00	.0325	62.5	.018				
.532	.228	.3000	81.89	.0222	.101	3.28	99.6	.998	.12	146	.042				
.432	.328	.4316	82.30	.0382	.178	4.45	98.2	.984	.31	149	.095				
.382	.378	.4974	82.66	.0522	.227	5.12	97.6	.978	.45	147.	.15				
.332	.428	.5632	83.10	.0693	.285	5.71	96.6	.968	.63	144.	.235				
.282	.478	.6290	83.63	.0900	.368	6.24	94.3	.945	.85	135	.330				
.232	.528	.6948	84.36	.118	.477	6.71	92.0	.922	1.12	124.	.445				
.182	.578	.7606	85.26	.154	.615	7.15	88.7	.889	1.42	111	.600				
.157	.603	.7935	85.86	.177	.703	7.30	86.8	.869	1.60	104	.690				
.132	.628	.8264	86.46	.200	.810	7.51	84.8	.850	1.76	94.9	.805				
.107	.653	.8593	87.25	.231	.940	7.68	81.9	.821	1.94	86.8	.945				
.082	.678	.8922	88.05	.262	1.14	7.81	79.0	.792	2.11	74.4	1.15				
.062	.698	.9186	88.90	.295	1.34	7.92	75.5	.757	2.26	65.6	1.38				
.047	.713	.9383	89.62	.323	1.60	7.97	72.9	.730	2.37	55.8	1.85				
.032	.728	.9580	90.64	.363	2.08	7.95	68.2	.683	2.47	43.4	3.03				
.027	.733	.9646	91.05	.379	2.49	7.90	66.3	.664	2.50	36.2	3.80				
.022	.738	.9712	91.46	.395	3.19	7.80	63.4	.635	2.54	28.1	5.00				
.017	.743	.9778	92.16	.422	4.45	7.55	60.7	.608	2.56	19.9	7.30				
.012	.748	.9844	93.05	.457	7.30	7.24	54.5	.546	2.59	11.6	13.8				
.010	.750	.9870	93.68	.482	9.80	7.00	49.4	.495	2.60	8.33	18.6				
.008	.752	.9896	94.45	.512	13.05	6.80	43.7	.438	2.61	5.80	24.2				
.007	.753	.9909	95.01	.533	14.7	6.55	40.8	.409	2.61	5.06	26.0				
.006	.754	.9923	95.47	.551	16.6	6.35	37.2	.373	2.62	4.33	31.4				
.005	.755	.9936	96.04	.573	18.5	6.20	32.9	.330	2.62	3.74	35.5				
.004	.756	.9949	96.45	.589											
.0035	.7565	.9956	96.65	.597											

TABLE III. MOMENTUM TERMS IN THE ENTRANCE REGION

r	$\frac{-10^4 \int_0^r r\, v \frac{\partial u}{\partial r}}{r \frac{\partial u}{\partial r}}$	$\frac{10^4 \int_0^r r\, u \frac{\partial u}{\partial x}\, dr}{r \frac{\partial u}{\partial r}}$	$\frac{10^4 \frac{g_c}{\rho} \frac{\partial p}{\partial x} \frac{r}{2}}{\frac{\partial u}{\partial r}}$	-v	u
in.	ft^2/sec	ft^2/sec	ft^2/sec	ft/sec	ft/sec
.76	1.66		5.26	0	0
.74	1.65	2.68	5.12	.0081	5.72
.72	1.52	3.06	5.17	.019	11.5
.69	1.59	8.48	9.27	.057	17.7
.66	1.61	30.5	23.5	.074	20.6
.64	1.72	65.3	49.7	.079	21.3
.62	1.53	128	93.7	.079	21.7
.60	1.18	241	174	.078	21.9
.58	.98	179	408	.075	22.0
.40				.049	22.0
.20				.017	22.0

Bellmouth Entrance X/D = 1.5 Re = 15,000

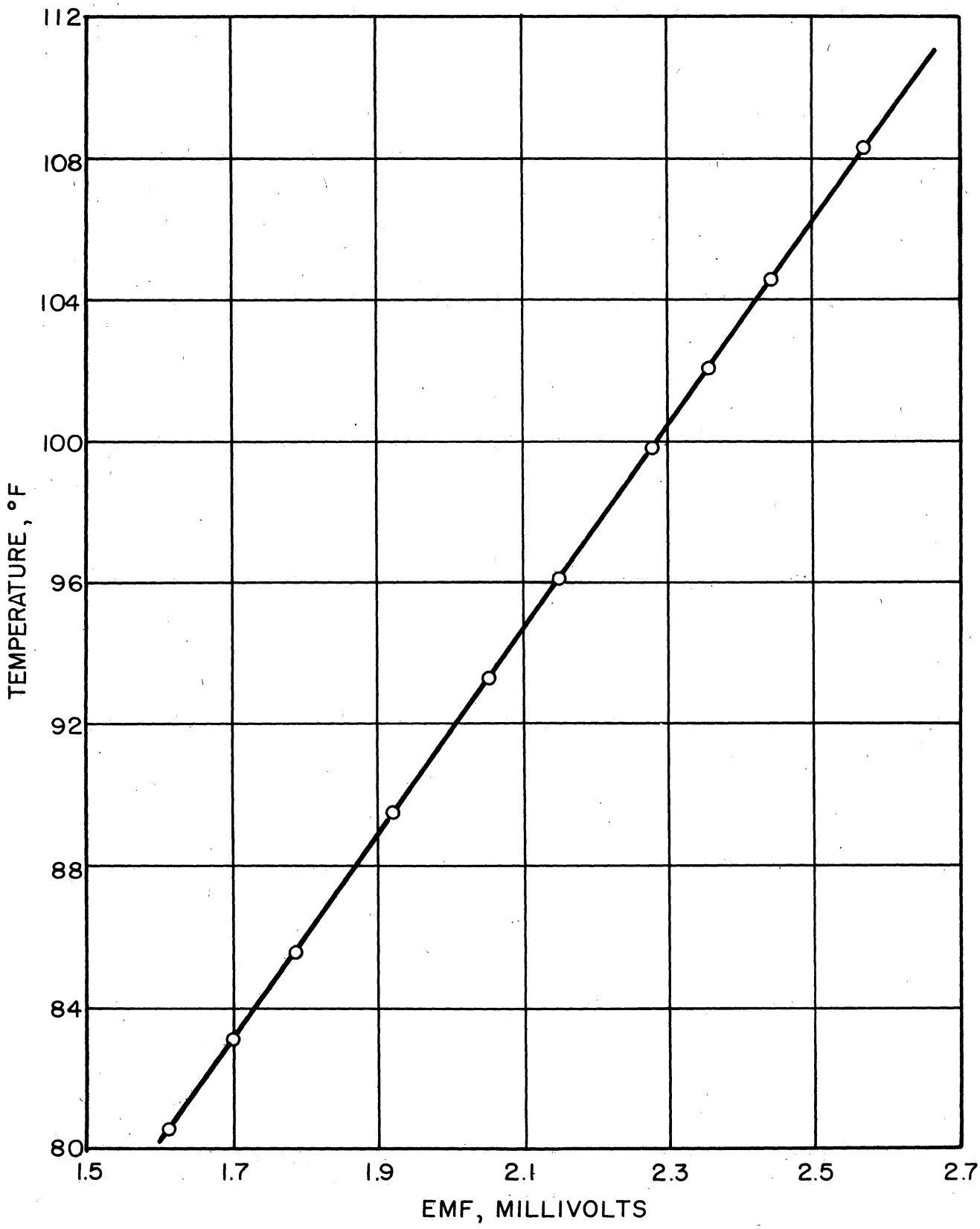

Figure 35. Calibration for Chromel-Constantan Thermocouples

BIBLIOGRAPHY

1. Aladyev, I. T., "Experimental Determination of Local and Mean Coefficients of Heat Transfer for Turbulent Flow in Pipes," NACA TM 1356 (1954)

2. Al-Arabi, M. and V. C. Davies, "Heat Transfer Between Tubes and a Fluid Flowing Through Then with Varying Degrees of Turbulence Due to Entrance Conditions," Chartered Mechanical Engineer 2 150-151 (1955)

3. Bakhmeteff, B. A., "The Mechanics of Turbulent Flow," Princeton University Press (1936)

4. Berry, V. J., "Non-Uniform Heat Transfer to Fluids Flowing in Conduits," Appl. Sci. Res., Sec. A, 4, 61-75 (1953)

5. Boelter, L. M. K., G. Young, and H. W. Iversen, "An Investigation of Aircraft Heaters-XXVII-Distribution of Heat Transfer in the Entrance Section of a Circular Tube," NACA TN 1451 (1948)

6. Burbach, T. H., "Stroemungswiderstand und Waermeübergang in Rohren," Leipzig (1930)

7. Cholette, A., "Heat Transfer, Local and Average Coefficients for Air Flowing Inside Tubes," C. E. P. 44 81-88 (1948)

8. Corcoran, W. H., and B. H. Sage, "Role of Eddy Conductivity in Thermal Transport," A. I. Ch. E. Journal 2 251-258 (1956)

9. Corcoran, W. H., F. Page, W. G. Schlinger, and B. H. Sage, "Temperature Gradients in Turbulent Gas Streams," Ind. Eng. Chem., 44 410-430 (1952)

10. Deissler, R. G., "Analytical and Experimental Investigation of Adiabatic Turbulent Flow in Smooth Tubes," NACA TN 2138 (1950)

11. Deissler, R. G., "Analysis of Turbulent Heat Transfer, Mass Transfer, and Friction in Smooth Tubes at High Prandtl and Schmidt Numbers," NACA TN 3145 (1954)

12. Deissler, R. G., "Turbulent Heat Transfer and Friction in the Entrance Regions of Smooth Passages," Trans. A.S.M.E. 77 1221-1233 (1955)

13. Dittus, F. W. and L. M. K. Boelter, University of California, Pubs. Eng., 2 443 (1930)

14. Eagle, A. and Ferguson, R. M., Proc. Roy. Soc. London (A) 127, 540 (1930)

15. Eckert, E. R. G., "Introduction to the Transfer of Heat and Mass," Mc-Graw Hill, New York (1950)

16. Elias, F., Zeitschr. f. angew. Math. u. Mech., 9 434 (1929)

17. General Electric Company "Tables of Thermocouple Characteristics," Bulletin GET-1415A p.7.

18. Goldstein, S. (Editor), "Modern Developments in Fluid Dynamics," Clarendon Press, Oxford (1950)

19. Graetz, L. "Uber die Waremleitungsfähigkeit von Flussigkeiten," Ann. Physik, 18, (1883) 25, 337 (1885)

20. Hartnett, J. P., "Experimental Determination of the Thermal Entrance Length for the Flow of Water and of Oil in Circular Pipes," Trans. A.S.M.E. 8 1211-1220 (1955)

21. Hausen, H., Z. Ver. Deut. Inc., Beiheft Verfahrenstechnik, No. 4, 91-98 (1943)

22. Hirschfelder, J. O., R. B. Bird, and E. L. Spotz, "Viscosity and Other Physical Properties of Gases and Gas Mixtures," Trans. A.S.M.E. 71 921-937 (1949)

23. Hoffman, H. W., "Turbulent Forced Convection in Circular Tubes Containing Molten Sodium Hydroxide," 1953 Heat Transfer and Fluid Mechanics Institute, Preprints of Papers, p.83, Stanford University Press, Stanford, California (1952)

24. Hottel, H. C. and A. J. Kalitinsky, J. Appl. Mech., 12, A 25-32 (1945)

25. Isakoff, S. E. and T. B. Drew, "Heat and Momentum Transfer in Turbulent Flow of Mercury," General Discussion on Heat Transfer, 405-409, Institution of Mechanical Engineers, London(1951). Also Ph D Thesis of Isakoff, University Microfilms, Ann Arbor, Michigan, Microfilm No. 4200

26. Jakob, M., "Heat Transfer," Vol. I, John Wiley and Sons Inc., New York (1949)

27. Jenkins, R., "Variation of Eddy Conductivity with Prandtl Modulus and its Use in Prediction of Turbulent Heat Transfer Coefficients," Heat Transfer and Fluid Mechanics Institute Preprints, 147-158, Stanford University Press, Stanford, California (1951)

28. Johns Hopkins University, Aerodynamics Handbook Staff, "Hankbook of Supersonic Aerodynamics," Navord Report 1488 (Vol. 5) U. S. Bureau of Ordinance (1953)

29. Johnson, H. A., J. P. Hartnett, and W. J. Clabaugh, "Heat Transfer to Molten Lead-Bismuth Eutectic in Turbulent Pipe Flow," 1952 Heat Transfer and Fluid Mechanics Institute, Preprints of Papers, p.5, Stanford University Press, Stanford, California (1952)

30. Knudsen, J. G. and D. L. Katz, "Fluid Dynamics and Heat Transfer," Engineering Res. Bul. No. 37, University of Michigan, Ann Arbor (1953)

31. Kovásznay, L. S. G., "Development of Turbulence-Measuring Equipment," NACA TN 2839 (1953)

32. Kuethe, A. M., and J. D. Schetzer, "Foundations of Aerodynamics," John Wiley and Sons, Inc., New York (1950)

33. Latzko, H., "Heat Transfer in a Turbulent Liquid or Gas Stream,: NACA TM 1068 (1944); Translated from Zeitschrift für angewandte Mathematick und Mechanik, 1, No. 4 (1921)

34. Laufer, J., "The Structure of Turbulence in Fully Developed Pipe Flow," NACA TN 2954 (1953)

35. Laufer, J., "Some Recent Measurements in a Two Dimensional Turbulent Channel," J. Aero. Sci., 17, 277-287 (1950)

36. Levy, S., "Heat Conduction Methods in Forced Convection Flow," A.S.M.E. Preprint of Paper No. 54-A-142 (1955)

37. Lorenz, H., Zeitshr.für Techn. Phys., 15 376 (1934)

38. Lyon, R. N., "Liquid Metal Heat Transfer Coefficients," Chem. Eng. Progress, 47, 75-79 (1951)

39. Martinelli, R. C., "Heat Transfer to Molten Metals," Trans. A.S.M.E. 69, 947-959 (1947)

40. McAdams, W. H., "Heat Transmission," 220-251, Mc Graw-Hill Book Co., New York (1954)

41. Ibid., p. 309-316

42. Moody, L. F., "Friction Factors for Pipe Flow," Trans. A.S.M.E., 66, 671 (1944)

43. Nikuradse, J., "Gestzmässigkeiten der Turbulenten Strömung in Glotten Röhren," V.D.I. Forschungsheft, 356 (1932)

44. Nusselt, W., Forschung a.d. Geb. d. Ingenieurwes. 2 309; (1931)

45. Poppendiek, H. F., and W. B. Harrison "Thermal Entrance-Region Heat Transfer in Liquid-Metal Systems," C.E.P. Symposium Series No. 17, Vol. 51 (1955)

46. Prandtl, Ludwig, "Essentials of Fluid Dynamics," Hafner Publishing Company, New York (1952)

47. Prandtl, L., "Uber die Ausgebildete Turbulenz," Proceedings of the Second International Congress for Applied Mechanics, 62-74, Zurich, Switzerland (1926)

48. Reichardt, H., "Heat Transfer Through Turbulent Friction Layers," NACA TM 1047 (1943)

49. Reynolds, Osborne, "On the Extent and Action of the Heating Surface of Steam Boilers," Proceedings of the Manchester Literary and Philosophical Society, 14, (1874) Also "Scientific Papers of Osborne Reynolds" Cambridge University Press (1900)

50. Ross, D., "Turbulent Flow in Smooth Pipes, A Reanalysis of Nikuradse's Experiments," Ordnance Research Laboratory, Pennsylvania State College (Sept. 1952)

51. Rothfus, R. R., and C. C. Monrad "Correlation of Turbulent Velocities for Tubes and Parallel Plates," Ind. Eng. Chem., 47, 1144-1149 (1955)

52. Sanders, V. D., M. S. Thesis, University of California, (1946)

53. Sehiller, L., "Stromung in Rohren," in Wien-Harms Handbuch der Experimentalphysik, Vol. IV 14, p. 48, Akademische Verlagsgesellschaft, Leipzig, (1931)

54. Schlinger, W. G., N. T. Hsu, S. D. Cavers, and B. H. Sage "Temperature Gradients in Turbulent Gas Streams," Ind. Eng. Chem., 45, 864-870 (1953)

55. Seban, R. A. and T. T. Shimazki, "Temperature Distributions for Air Flowing Turbulently in a Smooth Heated Pipe" General Discussion on Heat Transfer, 122-126, Institution of Mechanical Engineers, London (1951)

56. Seban, R. A. and T. T. Shimazki, "Heat Transfer to a Fluid Flowing Turbulently in a Smooth Pipe with Walls at Constant Temperature," Trans. A.S.M.E., 73, 803-808 (1951)

57. Shapiro, A. H., R. Siegel, and S. J. Kline, "Friction Factor in the Laminar Entry Region of A Smooth Tube," Proceedings of the Second U. S. National Congress of Applied Mechanics, 733-741, Amer. Soc. Mech. Engr., (1955)

58. Sheppard, W. A., "Temperature Distributions for Various Heated Fluids Flowing Turbulently in a Circular Tube," M. S. Thesis, University of California, Berkeley, Calif., May, (1946)

59. Sleicher, C. A., "Heat Transfer in a Pipe with Turbulent Flow and Arbitrary Wall-Temperature Distribution," Ph. D. Thesis in Chemical Engineering, Univ. of Mich., Ann Arbor (1955)

60. Stearns, R. F., R. M. Jackson, R. R. Johnson, C. A. Larson, "Flow Measurement with Orifice Meters," D. Van Nostrand Company, New York (1951)

61. Taylor, G. I., Proc. Roy. Soc. (A) 135, 70 (1932)

62. Weissberg, Harold L., "Velocity and Pressure Distributions in Turbulent Pipe Flow with Uniform Wall Suction," USAEC K 1187 Physics (March, 1951).

63. Willis, J. E., "Australian Council for Aeronatutics Report" ACA-19 (1945)